# VALIDATION OF DEPTH-AVERAGED MIXING LENGTH TURBULENCE MODEL FOR UNIFORM CHANNEL FLOWS

A THESIS SUBMITTED TO
THE GRADUATE SCHOOL OF NATURAL AND APPLIED SCIENCES
OF
THE MIDDLE EAST TECHNICAL UNIVERSITY

BY

ÇAĞRI HASAN KARAMAN

IN PARTIAL FULFILLMENT OF THE REQUIREMENTS
FOR
THE DEGREE OF MASTER OF SCIENCE
IN
CIVIL ENGINEERING

AUGUST 2014

Approval of the thesis:

**VALIDATION OF DEPTH AVERAGED MIXING LENGTH TURBULENCE MODEL FOR UNIFORM CHANNEL FLOWS**

submitted by **ÇAĞRI HASAN KARAMAN** in partial fulfillment of the requirements for the degree of **Master of Science in Civil Engineering Department, Middle East Technical University** by,

Prof. Dr. Canan ÖZGEN ____________________
Dean, **Graduate School of Natural and Applied Sciences**

Prof. Dr. Ahmet Cevdet YALÇINER ____________________
Head of Department, **Civil Engineering**

Prof. Dr. İsmail AYDIN
Supervisor, **Civil Engineering Dept., METU** ____________________

**Examining Committee Members:**

Prof. Dr. Zafer BOZKUŞ ____________________
**Civil Engineering Dept., METU**

Prof. Dr. İsmail AYDIN ____________________
**Civil Engineering Dept., METU**

Assoc. Prof. Utku KANOĞLU ____________________
**Engineering Sciences Dept., METU**

Assoc. Prof. Mete Köken ____________________
**Civil Engineering Dept., METU**

Assist. Prof. Dr. Müsteyde Banuda KOÇYİĞİT ____________________
**Civil Engineering Dept., Gazi University**

**Date:** *26.08.2014*

**I hereby declare that all information in this document has been obtained and presented in accordance with academic rules and ethical conduct. I also declare that, as required by these rules and conduct, I have fully cited and referenced all material and results that are not original to this work.**

Name, Last name: Çağrı Hasan Karaman

Signature :

# ABSTRACT

## VALIDATION OF DEPTH-AVERAGED MIXING LENGTH TURBULENCE MODEL FOR UNIFORM CHANNEL FLOWS

Karaman, Çağrı Hasan

M.S., Department of Civil Engineering

Supervisor: Prof. Dr. İsmail Aydın

August 2014, 97 pages

A one-dimensional depth averaged turbulence model based on volumetric mixing length definition is developed for shallow flows. Numerical solution of the model is done using finite volume method for steady, uniform closed duct flows to observe lateral momentum exchange over depth discontinuities. The model is verified by comparison to two-dimensional numerical solutions and to the experimental data available in the literature.

The model is then applied to uniform free surface flows in rectangular and compound channels. Comparisons with two-dimensional numerical solutions as well as experimental data taken from the literature indicated that depth integrated velocity and bed shear stresses are successfully predicted by the model with good accuracy.

**Keywords:** Mixing length, computational fluid dynamics, channel flow, turbulence model

# ÖZ

## DERİNLİK ENTEGRALLİ TÜRBÜLANS KARIŞIM UZUNLUĞU MODELİNİN ÜNİORM KANAL AKIMINDA DOĞRULANMASI


Karaman, Çağrı Hasan

Yüksek Lisans., İnşaat Mühendisliği Bölümü

Tez Yöneticisi: Prof. Dr. İsmail Aydın


Ağustos 2014, 97 sayfa


Sığ akımlar için hacimsel karışım uzunluğu tanımına dayalı 1-boyutlu derinlik entegralli türbülans modeli geliştirilmiştir. Yanal momentum değişimini gözlemlemek için kararlı, uniform kapalı kanal akımlarında modelin sayısal çözüm yapılarak 2-boyulu sayısal çözüm ve literatürde bulunan deney verileri ile model doğrulanmıştır.

Ardından, model dikdörtgen ve bileşik kesitli kanallarda serbest yüzeyli kanal akımlarına uygulanmıştır. İki boyutlu sayısal çözüm ve literatürden alınan deney verileriyle karşılaştırılarak derinlik entegralli hız ve cidar kayma gerilmesinin model tarafından başarıyla bulunduğu tespit edilmiştir.


**Anahtar Kelimeler:** Karışım uzunluğu, hesaplamalı akışkanlar mekaniği, kanal akımı, türbülans modeli

*For my family*

# ACKNOWLEDGMENTS

First and foremost, I express my most humble and sincere appreciation to my supervisor Prof. Dr. İsmail Aydin for his guidance, advice, understanding and inspiration throughout the research.

I dedicate this research to my beloved family for their endless love, trust, understanding and support.

I would also like to thank my manager Serdar Sürer in DHI Turkey for his support and understanding during my work in company. I wish to thank my friend Engin Koç for helping me in this research.

**TABLE OF CONTENTS**

## LIST OF FIGURES

### FIGURES

# LIST OF SYMBOLS

| | |
|---|---|
| $A$ | : Area |
| $b$ | : Width of side channel |
| $B$ | : Channel width |
| $C_f$ | : Bed friction parameter |
| $C_1, C_2, C_3$ | : Turbulence model constants |
| $C^+$ | : Constant |
| $C_p$ | : Constant defining pressure gradient |
| $E$ | : Empirical constant relating to the bottom roughness |
| $f_\mu$ | : Van Driest viscous damping function |
| $g$ | : Gravitational acceleration |
| $h$ | : Depth of side channel |
| $H$ | : Channel height |
| $k$ | : Turbulent kinetic energy |
| $l_m$ | : Mixing Length |
| $\bar{l}_m$ | : Depth averaged mixing length |
| $l_v$ | : Volumetric length scale |
| $n$ | : Darcy friction factor |
| $P$ | : Pressure |
| $p$ | : Pressure per unit mass |
| $r$ | : Distance from computational point to a point on the boundary |
| $R_e$ | : Reynolds number |

| | |
|---|---|
| $S$ | : Rates of strain |
| $t$ | : Time |
| $u$ | : Velocity component in $x$ – direction |
| $\bar{u}$ | : Depth averaged velocity in $x$ – direction |
| $u_{max}$ | : Maximum velocity in a computational cell |
| $U_{max}$ | : Maximum velocity in channel |
| $U_{mean}$ | : Mean velocity in channel |
| $\bar{u}_s$ | : Depth averaged velocity in computational cells closest to vertical walls |
| $\bar{u}_*$ | : Depth averaged shear velocity |
| $v$ | : Velocity component in $y$ - direction |
| $\bar{v}$ | : Depth averaged velocity in $y$ - direction |
| $w$ | : Velocity component in $z$ - direction |
| $x$ | : Streamwise direction parallel to channel bed |
| $y$ | : Lateral direction |
| $z$ | : Vertical direction normal to channel bed |
| $z_b$ | : Bottom of the channel |
| $z_s$ | : Upper symmetry boundary in channel |
| $\theta$ | : Channel bed angle |
| $\kappa$ | : Von Karman constant |
| $\lambda$ | : Free surface damping parameter |
| $\mu_e$ | : Dynamic effective viscosity of water |
| $\mu_t$ | : Dynamic turbulent viscosity of water |
| $\mu$ | : Dynamic viscosity of water |
| $\nu$ | : Kinematic viscosity of water |
| $\nu_t$ | : Kinematic turbulent viscosity of water |

$\nu_t$ : Kinematic effective viscosity of water

$\bar{\nu_e}$ : Depth integrated kinematic effective viscosity

$\xi$ : Vorticity component in the cross-stream plane

$\rho$ : Density of fluid

$\tau$ : Shear stress divided by density

$\tau_w$ : Wall shear stress

$\tau_{w,mean}$ : Mean wall shear stress in channel

$\tau_{wall}$ : Wall shear stress in parallel plate

$\tau_{v,w}$ : Vertical wall shear stress taken from 2D solution

$\bar{\tau}$ : Depth integrated shear stress

$\psi$ : Stream function

$\Omega$ : Vorticity vector

$\delta$ : Kronecker delta

**Superscripts**

$+$ **:** Dimensionless quantity

**Suberscripts**

$i$ : Directional index

$j$ : Directional index

$r$ : Normal to $r$ direction

# CHAPTER 1

# INTRODUCTION

## 1.1 General Description

Fluid mechanics has transformed into another area when Osborne Reynolds published his work of derivation of Reynolds Averaged Navier-Stokes (RANS) equations in 1894. Ludwig Prandtl of Gottingen, Germany published a paper in 1904 that flow over solid boundary can be considered in two parts. A region of fluid very close to the boundary where velocity is significantly influenced by viscosity which is boundary layer and rest of the flow which can be considered as inviscid (Monty, 2005). After these publications, advancements in fluid mechanics has gained greater pace. In the course of developments, turbulence has always been an unknown phenomenon. Although there are several advancements in modelling of the turbulence, scientists are unable to fully describe the complicated turbulent behavior of the fluid. For that reason, accurate representation of turbulent flow mechanisms in any flow section is of primary importance in turbulence modelling.

Rivers have always attracted human interest since it contributes civilization to grow from the aspect of irrigation, industry, household, wildlife habitat and fertility. However, a devastating effect of rivers which is flood always exists. Flood occurs in rivers when flow rate exceed carrying capacity of a river bed. Flood often damages homes, businesses and agriculture areas. People have been searching for ways to shun the devastating effects of floods by flow controlling and forecasting. Defenses such as levees, bunds, reservoirs and weirs are used to prevent rivers from bursting their banks. (Wright, 2000).

In the last century, with the rapid increase in urbanization, flood is a risk for people more than ever. At the same time advancements in fluid mechanics and computer science, provided improved forecasting tools for flood events giving time to prepare or evacuate before the flood comes. Once the flood is predicted, possible inundation areas should be known. This is done by numerically solving the Saint-Venant equations or depth integrated shallow flow equations in two-dimensions.

A flow can be characterized as shallow flow if the vertical dimension is much smaller than any typical horizontal scale. Shallow-water flows are nearly horizontal and simplification in mathematical formulation and numerical solution is done by assuming pressure distribution as hydrostatic. The flow is still three dimensional due to bottom friction however 3D effects are not essential since horizontal extent of the flow is much greater then vertical extent. Depth averaged form is sufficient to describe the flow which is two dimensional in horizontal plane (Vreugdenhil C. B., 1994). Sallow water model is being used in atmospheric flows, tidal flows, tidal mixing, residual currents, dam-break waves, coastal flows, tsunamis, lake flows and internal flows. Although shallow water model brings advantages, one of the drawbacks is its insensitivity to secondary flows in the channel.

Shallow flow equations are simplified type of Navier-Stokes equations derived by depth integrating. In a channel, width to depth ratio of 5 and more can be considered as shallow flow and equations are valid because secondary current effect vanishes.

## 1.2 Background

Most rivers constitute two parts due to its nature, main channel and flood plain. Prediction of flood in channels is difficult due to two stage domain. There are discontinuities resulting from hydraulic radius in main channel and flood plains. River engineers have analyzed flow in compound channels using subdivision techniques. This method is efficient overcoming the discontinuities in the domain but does not account turbulent interactions due to 3D nature of the flow (Sellin, Ervine, & Willetts, 1993). In order to solve shallow flow equations on any domain with a satisfactory representation of turbulence phenomena the Non-Linear Mixing Length Model (NMLM) (Aydin, 2009) will be considered.

### 1.2.1 Non-Linear Mixing Length Model (NMLM)

Advances in turbulence modelling provide different level of closures for turbulent stresses. Complex turbulent flows can be computed in detail by employing turbulence models involving solution of additional transport equations for turbulent quantities. However, these additional transport equations bring increased number of parameters, functions and constants to the model that increases computational effort and cost. Prandtl's mixing length theory is the simplest model to compute turbulent stresses (Aydın, 2004).

$$l_m = \kappa y f_\mu \tag{1-1}$$

where $\kappa$ is the von Karman constant, $y$ is the distance from the solid boundary and $f_\mu$ is van Driest viscous damping function. This mixing length definition performs well in boundary layer and has been used in many engineering applications. However, a drawback of the above definition of mixing length is that it is only appropriate for flat surfaces. Moreover, eddy mixing length is influenced by all boundary surfaces which can be seen from a point in the flow domain and not only from the closest boundary. For that reason, NMLM was introduced by (Aydin, 2009) to consider all solid boundaries on determination of the size of the mixing length at an internal point in the flow domain.

The NMLM is a nonlinear turbulence model for two dimensional uniform channel flow based on a three dimensional integral measure of boundary proximity. The model eliminates the need for solution of additional transport equations for the turbulence quantities for uniform channel flows.

Reynolds averaged momentum equation for steady, turbulent, fully developed uniform flow in x direction is written.

$$\frac{\partial u}{\partial t} + \frac{\partial (uv)}{\partial y} + \frac{\partial (uw)}{\partial z} = gsin\theta + \mathrm{v}\left(\frac{\partial^2 u}{\partial y^2} + \frac{\partial^2 u}{\partial z^2}\right) + \frac{\partial \tau_{yx}}{\partial y} + \frac{\partial \tau_{zx}}{\partial z} \tag{1-2}$$

Here, $u, v, w$ are the time mean velocities in x, y, z directions respectively, t is time, g is gravitational acceleration, $\nu$ is kinematic viscosity, $\tau$ is kinematic turbulent stress and $\theta$ is the angle between channel axis and horizontal plane.

Writing the stream wise vorticity transport equation and Poison equation for stream function in the cross plane:

$$\frac{\partial \xi}{\partial t} + \frac{\partial (v\xi)}{\partial y} + \frac{\partial (w\xi)}{\partial z} = v\left(\frac{\partial^2 \xi}{\partial y^2} + \frac{\partial^2 \xi}{\partial z^2}\right) + \frac{\partial^2 (\tau_{zz} - \tau_{yy})}{\partial y \partial z} + \frac{\partial^2 \tau_{yz}}{\partial y^2} - \frac{\partial^2 \tau_{yz}}{\partial z^2} \tag{1-3}$$

$$\frac{\partial^2 \psi}{\partial y^2} + \frac{\partial^2 \psi}{\partial z^2} = -\xi \tag{1-4}$$

Vorticity and velocity components are defined by

$$\xi = \frac{\partial w}{\partial y} - \frac{\partial v}{\partial z} \qquad v = \frac{\partial \psi}{\partial z} \qquad w = -\frac{\partial \psi}{\partial y} \tag{1-5}$$

When expressing turbulent stresses, quadratic products of the mean rate of strain $S_{ij}$ and mean vorticity $\Omega_{\mathrm{ij}}$ are retained that satisfy the required symmetry and contraction properties. Constitutive equations are expressed in terms of a mixing length resulting in elimination of turbulent turbulence viscosity.

$$
\begin{aligned}
\tau_{ij} = -\overline{u_i'u_j'} = l_m^2 \Big\{ &|\Omega| S_{ij} - C_1 \left( S_{ik}S_{jk} - \tfrac{1}{3} S_{kl}S_{kl}\delta_{ij} \right) \\
&- C_2 \left( S_{ik}\Omega_{jk} + S_{jk}\Omega_{ik} \right) - C_3 \left( \Omega_{ik}\Omega_{jk} - \tfrac{1}{3}\Omega_{kl}\Omega_{kl}\delta_{ij} \right) \Big\} \\
&- \tfrac{2}{3} k \delta_{ij}
\end{aligned}
\tag{1-6}
$$

$$S_{ij} = \frac{\partial u_i}{\partial x_j} + \frac{\partial u_j}{\partial x_i} \tag{1-7}$$

$$\Omega_{ij} = \frac{\partial u_i}{\partial x_j} - \frac{\partial u_j}{\partial x_i} \tag{1-8}$$

$$|\Omega| = \sqrt{\Omega_{12}^2 + \Omega_{13}^2 + \Omega_{23}^2} \tag{1-9}$$

Here $l_m$ = mixing length, $C_1, C_2, C_3$= constants $-0.42, 0.21, 0.42$ respectively , $k$ = turbulent kinetic energy, $\delta_{ij}$ is Kronecker delta. Model presented above can be applied to any flow geometry if mixing length is defined appropriately.

In a uniform channel with no variations in flow direction, time history of turbulence developments in the flow directions can be neglected. In this case, turbulence structure can be defined by local parameters such as geometry of cross section and local deformation kinetics. For this purpose, 'Volumetric Mixing Length' is introduced.

$$l_v = \pi \Big/ \int \lambda \frac{dA_r}{r^3} \tag{1-10}$$

$$l_m = \kappa l_v \tag{1-11}$$

where r is the distance from an internal computational point to a solid boundary area element dA, $dA_r$ is the projection of dA normal to r, and λ is a weighting parameter for boundary type and equals to 1 for solid boundaries. When Eq. (1-10) is integrated over solid boundaries, it gives an area weighted distance from the internal computational point to the solid boundary which is then taken as the eddy mixing length when multiplied by the von Karman constant. Thorough description of volumetric mixing length and evaluation of Eq. (1-10) over solid boundaries are given in the appendix 1.

### 1.2.2 Solution on Different Geometries

#### 1.2.2.1 Closed Duct Flows

Duct flow solution can be obtained by replacing gravity term in Eq.(1-2) with axial pressure gradient divided by density. Quarter of the domain is computed by defining symmetry boundary conditions at the interfaces. Mixing length distribution in a rectangular duct is given in Fig. (1-1) for width of the channel ($B$) to depth of the channel ($H$) ratio of 1 *(B/H=1)*.

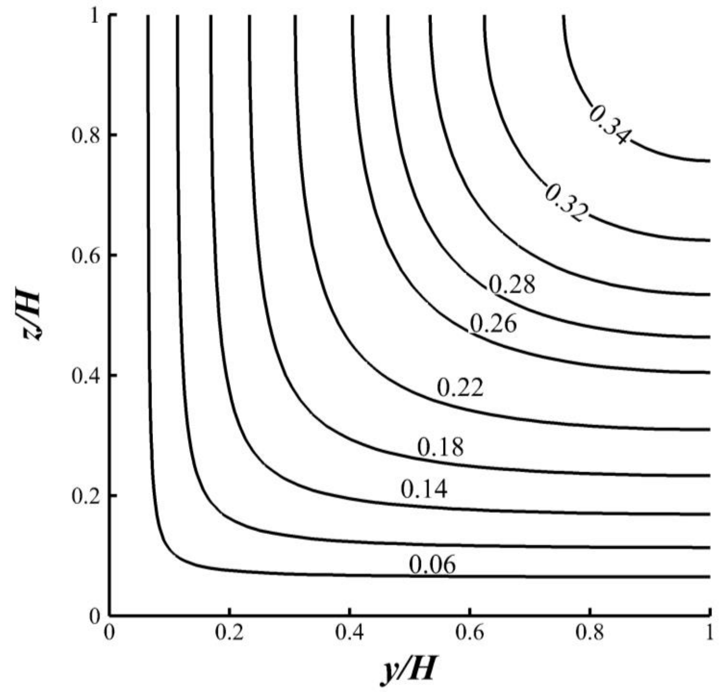


***Figure 1-1*** Mixing length distribution in rectangular duct for *B/H=1*, 2D NMLM solution

Ludwig Prandtl classified secondary flows into two categories. The secondary flow of Prandtl's first kind is defined as that induced by skewing of the mean flow in curved channels or meandering rivers. Such secondary flows exist either in the laminar or turbulent conditions. Prandtl's second kind of secondary flows, also called shear or turbulence-driven secondary flows, are those caused by the cross-sectional non-homogeneity of turbulence (Wang & Cheng, 2005).

In straight rectangular duct, secondary flow of second type occurs due to the presence of wall boundaries that causes turbulence anisotropy. The study of secondary flows in duct starts with (Launder & Ying, 1972) and was improved with the use of Direct Numerical Simulation (DNS) and Large Eddy Simulation (LES).

Secondary flow velocity can be up to 2-3 % of mean flow. However, in the regions closer to wall boundaries, secondary flow effects become dominant. Corner vortices formed by secondary flows obtained from NMLM solution are shown in Fig.(1-2) for width to depth ratio of 1 (*B/H = 1)* in a straight duct.

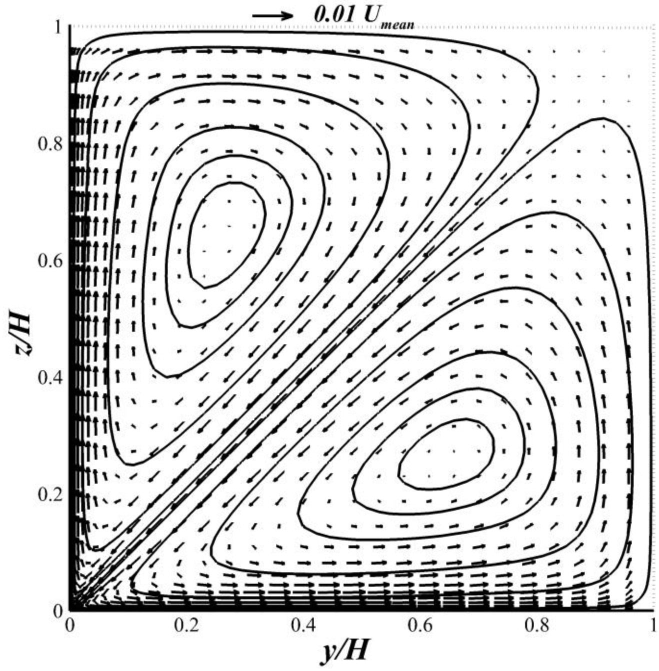


***Figure 1-2*** Secondary flows for *B/H=1(NMLM solution in rectangular duct)*

Contour lines of the computed velocity distribution in 2D space for a rectangular duct are given in Fig. (1-3) for width to depth ratio of 1. Bulking of axial velocity contour lines towards the corners is the result of secondary flows.

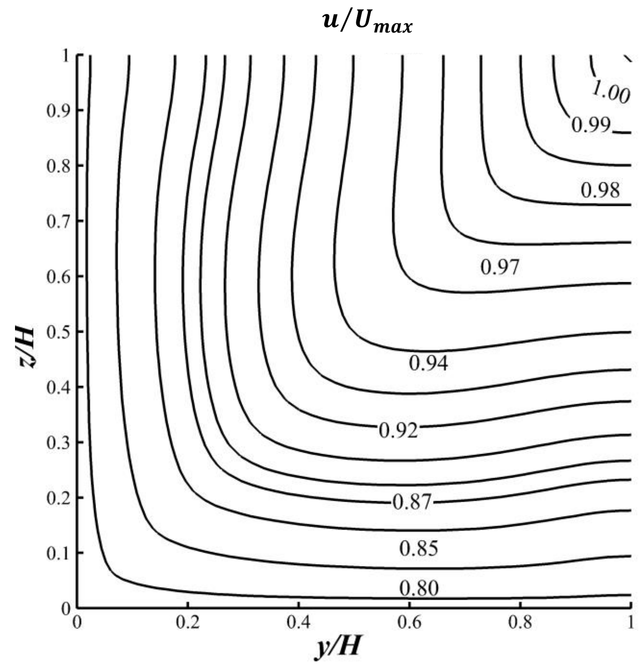


***Figure 1-3*** Velocity contours for *B/H=1(NMLM solution in rectangular duct)*

#### 1.2.2.2 Open Channel Flows

Volumetric mixing length model can be used in any type of cross section and in open channel flow which means that free surface exists. Free surface can be treated by using $\lambda$ parameter introduced in Eq.(1-10). Theoretically NMLM model treats free surface as a wall boundary, but $\lambda$ parameter damps the effect of this wall boundary and make it behave as free surface which means that reduced turbulent stresses near the surface. Mixing length distribution in an open channel with width to depth ratio of 5 (*B/H=5*) is given in Fig.(1-4).

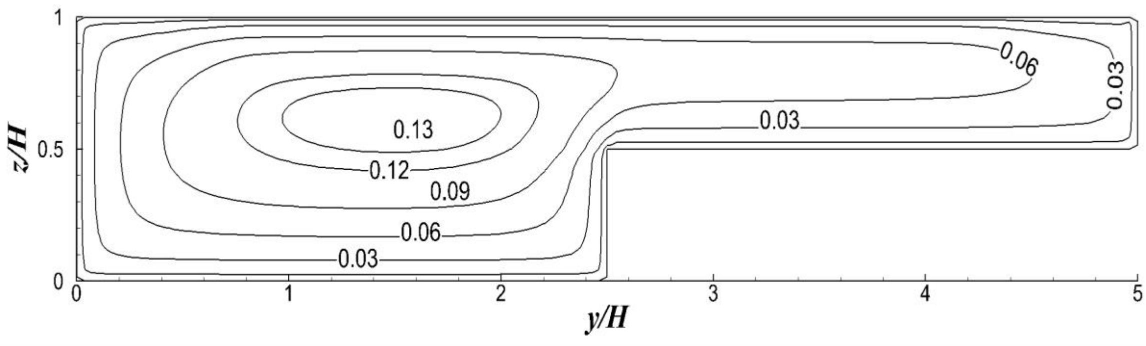


***Figure 1-4*** Mixing Length Distribution for *B/H=5* in a compound open channel

After solving the flow in open compound channel, secondary flows and velocity contours are given in Fig.(1-5) and Fig.(1-6) for the width to depth ratio of 5. *(B/H=5)*

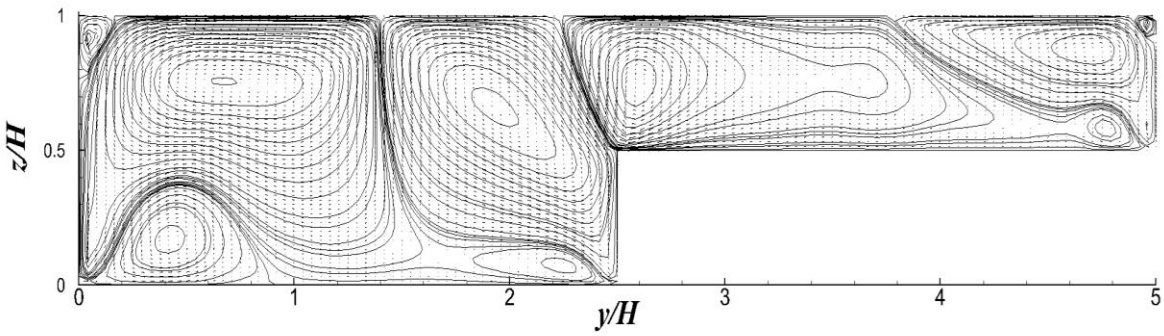


***Figure 1-5*** Secondary flow streamlines describing vortices in open channel for *B/H=5*

Accurate mixing length distribution can easily be computed in any domain. The turbulence model is simple and no transport equations are needed to be solved. Model is successful in producing secondary flows in uniform channel flow. It can be applied to closed-channel flows and open channel flows, however, contribution of free surface in calculation of mixing length should be put on more physical bases.

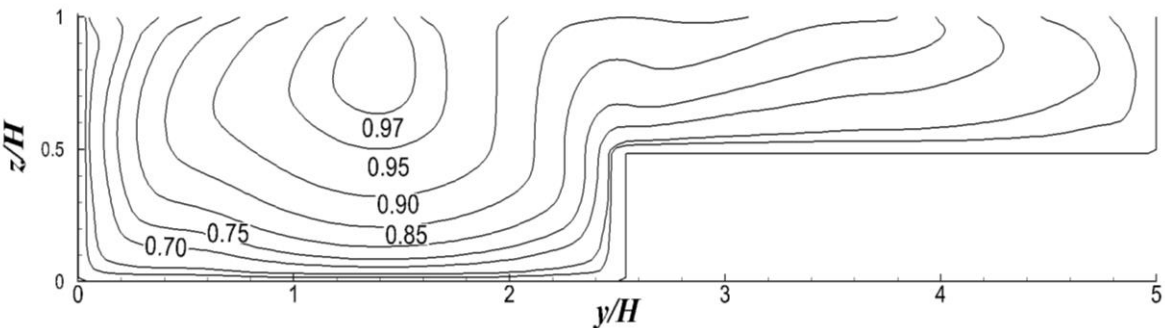


***Figure 1-6*** Axial velocity contours for *B/H=5*

## 1.3 Scope of the Work

Considering practical situations such as natural cross sections with irregular shape, river with flood plains, a canal with side berms, the primary flow is affected by lateral and vertical momentum transfer between regions of different depth (Knight & Demetriou, 1983). Two and three dimensional solutions are both difficult and expensive to investigate this momentum exchange and one dimensional solutions are needed for quick predictions of depth averaged velocity and wall shear stresses. In one dimensional (depth averaged) computation of river flow, understanding and modelling of turbulence mechanism is the critical step when lateral momentum exchange is significant. Due to the complicated 3D turbulent flow structures such as secondary currents originating from turbulence un-isotropy, interaction between main channel and flood plain is difficult to explain. There are different types of turbulence models introduced in the literature to model the flow such as k-ε and k-ω and variations of these. In k-ε or k-ω models, additional two transport equations are introduced to the model to be solved and this brings more numerical complexity. Only, turbulence models with nonlinear constitutive relations between the stresses and rates of strain are able to produce secondary currents. However, in one dimensional shallow water models, simplest formulations for turbulence should be preferred since the governing equations are simplified by integration in the vertical direction which automatically eliminates the possibility of modelling secondary flow structures.

The scope of present study is to investigate the horizontal transfer of linear momentum over lateral discontinuities in steady, uniform channel flow by using swallow flow equations. Nonlinear Mixing Length Model (NMLM) proposed by (Aydin, 2004 & 2009) is used to formulate the turbulent stresses. However, this model using a ‘volumetric mixing length’ definition was originally proposed for 2D uniform flows. In the present study, the volumetric mixing length (VML) is modified by depth integration to be used in one-dimensional shallow flow computation.

# CHAPTER 2

# 1D MODEL DEVELOPMENT

Navier-Stokes equations are the system of non-linear partial differential equations that describe conservation of mass and momentum. In shallow flows, the wave lengths in horizontal plane are large compared to the water-depth. This ensures that the flow everywhere can be regarded as having a direction parallel to the bottom, i.e. vertical acceleration can be neglected and a hydrostatic pressure variation along the vertical can be assumed (Environment, 2010).

In open channel flow, presence of free surface introduces difficulties in mathematical model because there is no fixed boundary. One way to overcome this problem for the time averaged velocities is to take the free surface boundary as a symmetry axis and treat it accordingly. However, such a simple treatment is not acceptable for turbulent fluctuations. The interaction with air can be non-negligible when surface velocity is above a limit value. Modelling of free surface effects in turbulence models is a challenging task requiring detailed experimental verification (Yue, Lin, & Patel, 2003) .

Main aim of this study is to develop an accurate formulation for turbulent shear stresses on vertical planes along the flow direction in computing depth averaged velocity field. At the beginning, the 2D NMLM (Aydin, 2009) will be used to obtain reference numerical solutions for the development and calibration of the turbulence formulation in depth averaged flow solution. In this development stage, closed conduit flows in rectangular ducts will be considered to avoid free surface effects.

Next, the depth averaged model will be tested in free surface flows with varying width to depth ratios of the channel.

## 2.1 Derivation of Depth Averaged Equations for Rectangular Duct Flow

To develop and test the depth integrated model, closed conduit flow in rectangular ducts will be studied first since the NMLM model can perform better in the absence of free surfaces. Uniform flow in x-direction in a long prismatic rectangular duct (Fig. 2-1) will be considered.

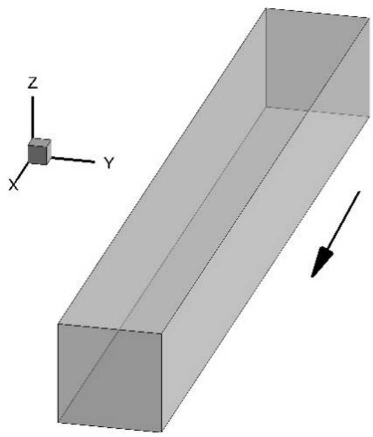


***Figure 2-1*** Coordinate axes and geometry of rectangular duct

Since the flow is uniform, flow variables other than pressure are independent of x. Flow in a section of the duct (Fig.2-2) is symmetrical about y and z-axes, thus velocity profiles in the four quadrants of the cross-section are identical. The two-dimensional flow then can be computed only in one quadrant with symmetry boundary conditions on the common boundaries. Depth averaged momentum equation can be obtained from the Reynolds averaged Navier Stokes equation in x direction;

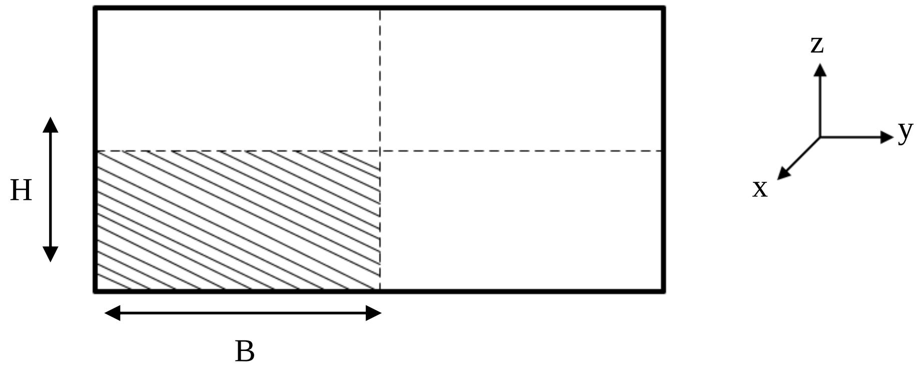


***Figure 2-2*** Cross Section of duct Flow

$$\frac{\partial u}{\partial t}+\frac{\partial u^2}{\partial x}+\frac{\partial uv}{\partial y}+\frac{\partial uw}{\partial z}=-\frac{1}{\rho}\frac{\partial p}{\partial x}+\frac{\partial \tau_{xx}}{\partial x}+\frac{\partial \tau_{xy}}{\partial y}+\frac{\partial \tau_{xz}}{\partial z} \tag{2-1}$$

Since the flow is uniform v and w velocity components are zero. For steady, uniform flow the above equation becomes;

$$0=-\frac{1}{\rho}\frac{\partial p}{\partial x}+\frac{\partial \tau_{xy}}{\partial y}+\frac{\partial \tau_{xz}}{\partial z} \tag{2-2}$$

Integrating this equation in z-direction between bottom of the channel and upper symmetry boundary gives;

$$0=\int_{z_b}^{z_s}-\frac{1}{\rho}\frac{\partial p}{\partial x}dz+\int_{z_b}^{z_s}\frac{\partial \tau_{xy}}{\partial y}dz+\int_{z_b}^{z_s}\frac{\partial \tau_{xz}}{\partial z}dz \tag{2-3}$$

For uniform flows pressure gradient is a constant. Therefore,

$$-\frac{1}{\rho}\frac{\partial p}{\partial x}=C_p \tag{2-4}$$

$$0=C_pH+\int_{z_b}^{z_s}\frac{\partial \tau_{xy}}{\partial y}dz+\int_{z_b}^{z_s}\frac{\partial \tau_{xz}}{\partial z}dz \tag{2-5}$$

Expanding terms in the above equation with Leibniz's rule;

$$\int_{z_b}^{z_s} \frac{\partial \tau_{xy}}{\partial y} dz = \frac{\partial}{\partial y} \int_{z_b}^{z_s} \tau_{xy}\, dz - \tau_{xy,s} \frac{\partial z_s}{\partial y} + \tau_{xy,b} \frac{\partial z_b}{\partial y} \tag{2-6}$$

$$\int_{z_b}^{z_s} \frac{\partial \tau_{xz}}{\partial z} dz = \tau_{xz,s} - \tau_{xz,b} \tag{2-7}$$

Rearranging;

$$0 = C_p H + \frac{\partial}{\partial y} \int_{z_b}^{z_s} \tau_{xy}\, dz - \tau_{xy,s} \frac{\partial z_s}{\partial y} + \tau_{xy,b} \frac{\partial z_b}{\partial y} + \tau_{xz,s} - \tau_{xz,b} \tag{2-8}$$

Taking into account that there is no variations in bed elevation, flow depth and $\tau_{xy}$ is considered constant throughout the depth;

$$0 = C_p H + \frac{\partial}{\partial y} \left( \bar{\tau}_{xy} H \right) - \tau_{xz,b} \tag{2-9}$$

where $\tau_{xz,b}$ is bottom shear stress. Rearranging equation (2-9) the differential equation to be solved numerically is obtained;

$$\frac{\partial}{\partial y} \left( \bar{\tau}_{xy} \right) - \frac{\tau_{xz,b}}{H} = -C_p \tag{2-10}$$

## 2.2 Determination of bottom shear stress

Determination of bottom shear stress will be an important issue in depth integrated computation since only depth integrated velocity will be available. Bottom shear stress is evaluated by using (Vreugdenhil C. B., 1994);

$$\tau_{xz,b} = C_f \bar{u} \sqrt{\bar{u}^2 + \bar{v}^2} \tag{2-11}$$

where $\bar{v}$ component of velocity is taken as zero for uniform flows and Eq.(2-11) becomes;

$$\tau_{xz,b} = C_f \bar{u}^2 \tag{2-12}$$

A search has been conducted in the literature and an empirical formula for bottom shear stress is obtained from (Pierce & Zimmerman, 1973)

$$C_f = \kappa^2 \left(\ln E R_e {C_f}^{0.5} - 1\right)^{-2} \tag{2-13}$$

where $\kappa$ is von Karman constant equals to 0.4, $E$ is an empirical constant relating to the bottom roughness and equals to 9 for smooth bottoms, $R_e$ is Reynolds number defined as $H\bar{u}/\nu$ , $H$ is flow depth , $\nu$ is kinematic viscosity and $\bar{u}$ is depth averaged velocity.

Before using this empirical formula it tested in simple case of flow between parallel plates. The numerical solution procedure for the flow between two wide parallel plates is described as follows.

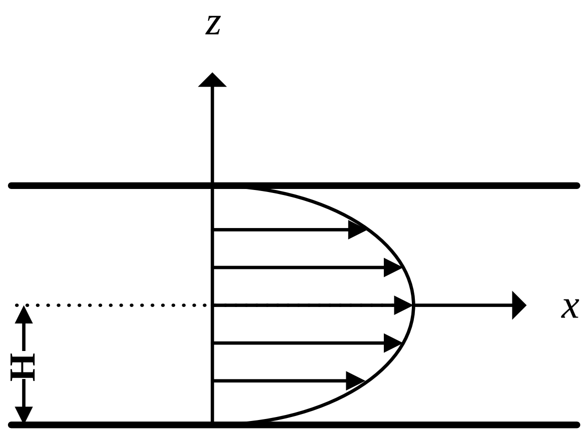


***Figure 2-3*** Infinitely long parallel plates

Writing Reynolds Averaged Navier-Stokes (RANS) equations in x-direction yields (Fig.2-3);

$$\frac{d}{dz}\left(\mu_e \frac{du}{dz}\right) = \frac{dP}{dx} \tag{2-14}$$

Discretization of this equation is performed by using finite difference method.

Grid clustering is done and smaller mesh size is used where nodes closer to the bottom boundary. Effective viscosity is calculated using mixing length theory which is;

$$\mu_e = \mu_t + \mu \tag{2-15}$$

$$\mu_t = \rho v_t \tag{2-16}$$

$$\nu_t = l_m^2 \frac{du}{dz} \tag{2-17}$$

Mixing length $l_m$ is calculated by using volumetric mixing length formulation given by Eqs (1-10) and (1-11).

Bottom shear stress is obtained from pressure gradient

$$\tau_{wall} = -\frac{dP}{dx} H \tag{2-18}$$

Average velocity is calculated after obtaining velocity distribution and $C_f$ value is calculated from;

$$C_f = \frac{\tau_{wall}}{\rho \bar{u}^2} \tag{2-19}$$

A comparison of $C_f$ values from Eq. (2-13) and numerical solution is performed and seen that Eq. (2-13) underestimates $C_f$ value at low Reynolds numbers. By trial and error, changing the superscript in Eq. (2-13), one can improve the expression. Original value of 0.5 is changed to 0.52 to fit Eq. (2-13) to the numerical solution.

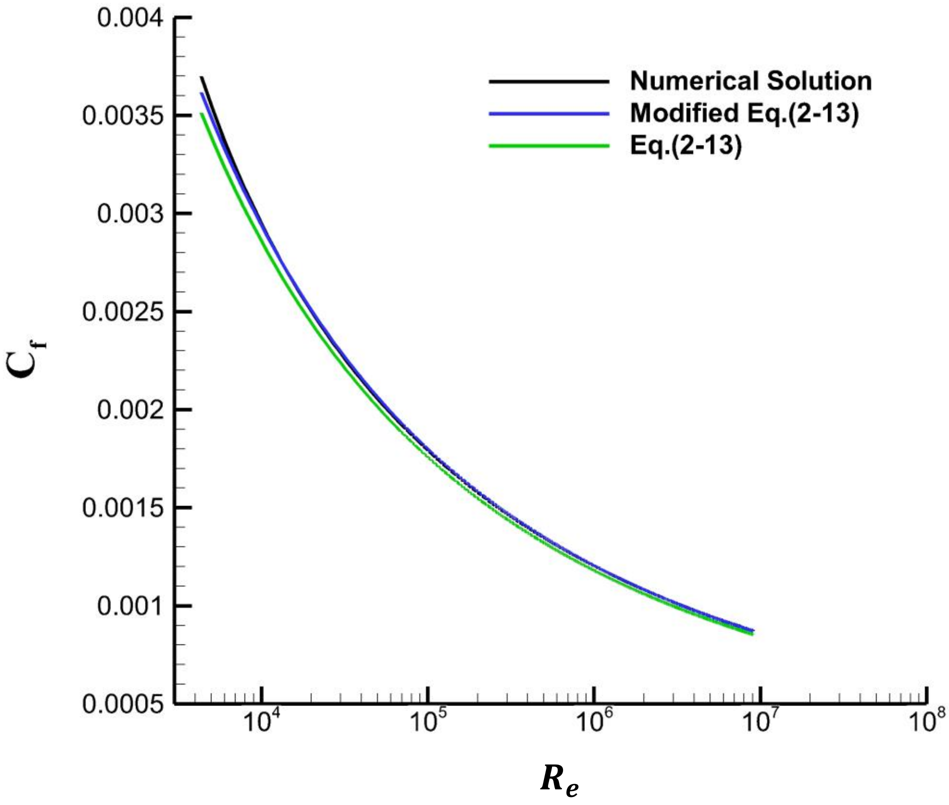


***Figure 2-4*** Variation of bottom friction coefficient with Reynolds Number

Fig. (2-4) shows that modified equation of $C_f$ overlaps with the numerical solution. Hence, Eq.(2-13) is modified as

$$C_f = \kappa^2 \left(\ln E R_e {C_f}^{0.52} - 1\right)^{-2} \tag{2-20}$$

## 2.3 Modelling of Turbulence

NMLM turbulence model is going to be applied to 1D model. However, originally the model was proposed for 2D flow domains. To be able to use the volumetric mixing length model in 1D flows, mixing length distribution in 2D domain should be integrated in the vertical direction. The two-dimensional solution uses a rectangular structured grid system with clustering near boundaries. A typical example is shown in Fig. (2-5). The computed mixing length contour lines for the same domain are shown in Fig. (2-6). The numbers on the contour lines indicate the mixing length in meters.

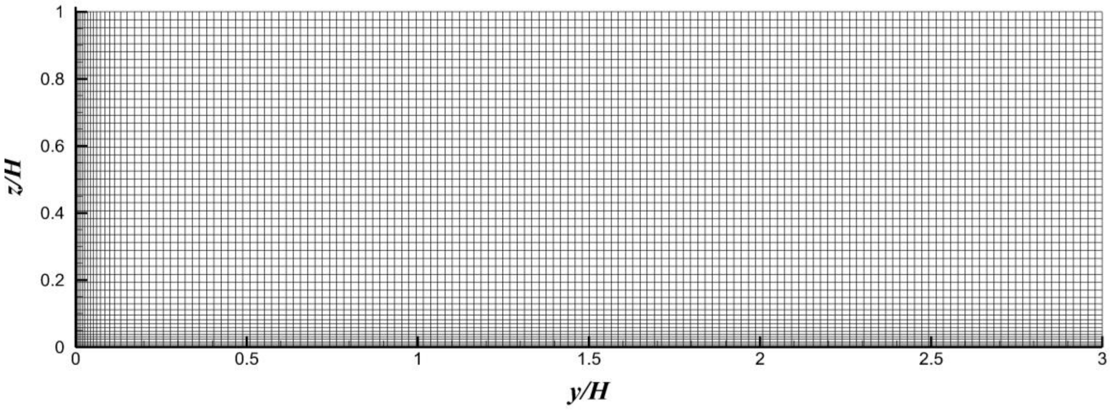


***Figure 2-5*** two-dimensional grid, *B/H=3*

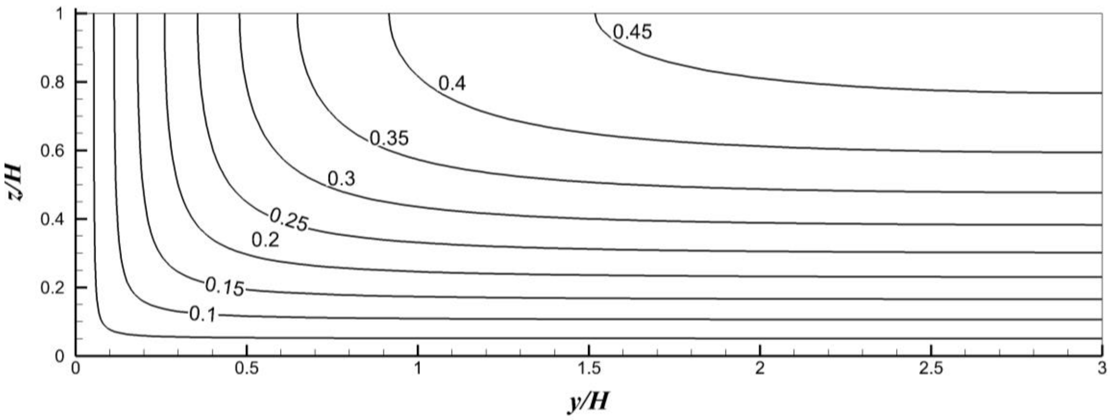


***Figure 2-6*** Two-dimensional mixing length distribution, *B/H=3*

In order to use volumetric mixing length in 1D model, depth averaging is performed by using the 2D mixing length distribution.

$$\overline{l_m} = \frac{1}{H}\int_0^H l_m \, dz \tag{2-21}$$

Depth averaged mixing length distribution over the channel width is given for width to depth ratio of 3 in Fig. (2-7). This calculated mixing length can be used in 1D model to solve turbulent stresses.

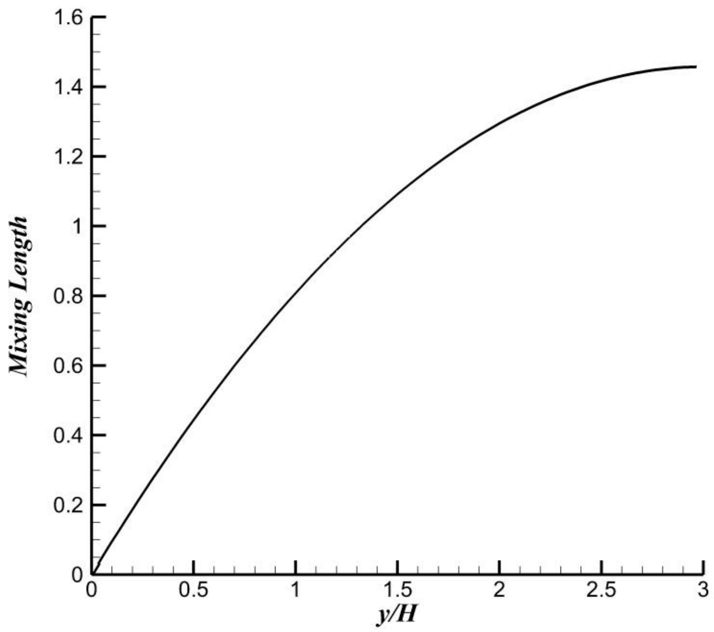


***Figure 2-7*** Depth averaged mixing length distribution, *B/H=3*

# CHAPTER 3

## DEPTH AVERAGED MODEL FOR UNIFORM DUCT FLOWS

Depth averaged 1D model developed in Chapter 2 will be applied to different closed duct flows. As mentioned before, closed duct flow is considered to test the turbulence model without the free surface effects. Test cases that will be considered are:

- Uniform flow in rectangular duct
- Uniform flow in compound duct
- Uniform flow in periodic compound duct

In each case, 1D model will be applied to the specific geometry by modifying shear stress and turbulence treatment. Numerical solutions will be done for 1D depth integrated model and compared to 2D solutions from the aspect of integrated velocity and wall shear stress distributions for different width to depth ratios.

## 3.1 Numerical solution

The governing equation Eq.(2-10) for the 1D case is discretized. The computational domain is divided into N number of vertical slices Fig. (3-1) and the dependent variable u is defined at the centroid of each element.

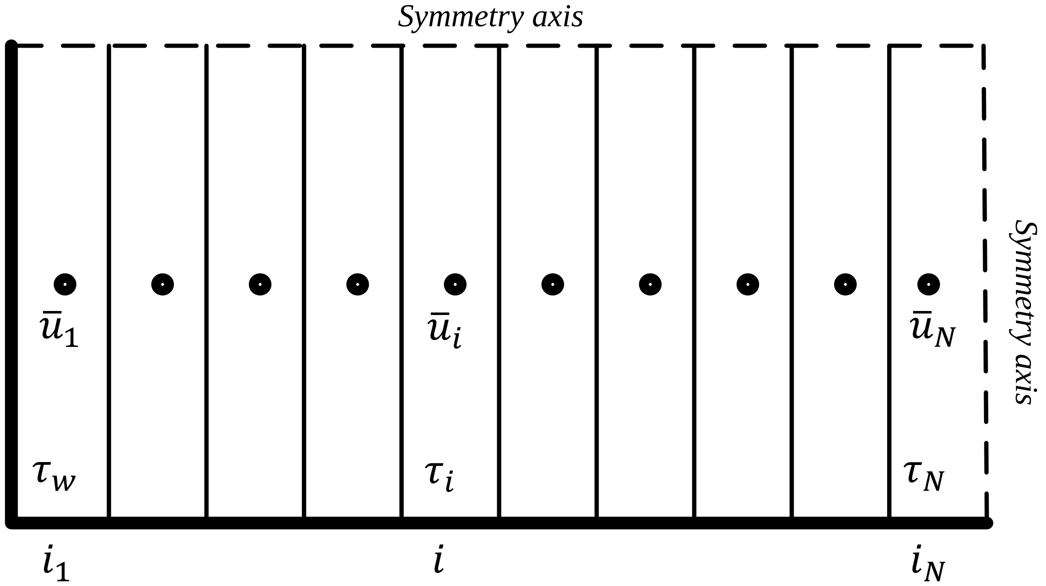


***Figure 3-1*** Computational domain

Eq. (2-10) is discretized with uniform cell spacing. Kinematic shear stresses are expressed in terms of kinematic effective viscosity and velocity gradient in y-direction.

$$\bar{\tau}_{xy} = \bar{\nu}_e \frac{d\bar{u}}{dy} \tag{3-1}$$

Using Eq. (2-12) and Eq. (3-1) in Eq. (2-10), the governing equation is written as;

$$\frac{\partial}{\partial y}\left(\bar{\nu}_e \frac{d\bar{u}}{dy}\right) - \frac{C_f \bar{u}^2}{H} = -C_p \tag{3-2}$$

Eq. (3-2) is discretized by second order central differences.

$$\frac{\bar{\tau}_{i+1} - \bar{\tau}_i}{\Delta y} = -C_p + \frac{C_{f_i}\bar{u}_i\bar{u}_i}{H} \tag{3-3}$$

$$\bar{\nu}_{e_{i+1}}\frac{\bar{u}_{i+1} - \bar{u}_i}{\Delta y} - \bar{\nu}_{e_i}\frac{\bar{u}_i - \bar{u}_{i-1}}{\Delta y} = \left[C_p + \frac{C_{f_i}\bar{u}_i\bar{u}_i}{H}\right]\Delta y \tag{3-4}$$

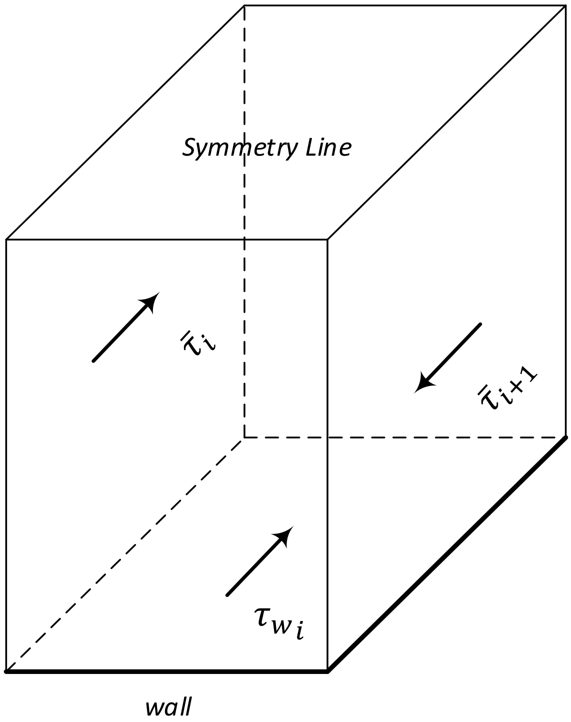


***Figure 3-2*** Forces on a single cell

Collecting similar terms yields;

$$\left(\frac{\bar{\nu}_{e_{i+1}}}{\Delta y}\right)\bar{u}_{i+1} + \left(-\frac{\bar{\nu}_{e_{i+1}}}{\Delta y} - \frac{\bar{\nu}_{e_i}}{\Delta y} - \frac{C_{f_i}\bar{u}_i}{H}\Delta y\right)\bar{u}_i + \left(\frac{\bar{\nu}_{e_i}}{\Delta y}\right)\bar{u}_{i-1} = C_p\Delta y \tag{3-5}$$

The above equation results in N number of linear equations when written for each internal computational cell. The set of linear equations can be written in the form of a tri-diagonal matrix for an implicit solution. Numerical solution is done by using

Thomas algorithm (Appendix B). Wall (no-slip) boundary condition on the left and symmetry boundary condition on the right ends are applied.

## 3.2 Uniform duct flow

The channel geometry and solution domain are shown in Figs. (2-1) and (2.2). Numerical solution is obtained for uniform duct flow by solving Eq. (3-5). Turbulence parameters and wall shear stress calculations are defined in the following sections.

### 3.2.1 Turbulence Model

Volumetric mixing length is used to represent turbulent stresses. Computational grid over 2D space in the cross-section is formed and volumetric mixing length is calculated at all grid points. Point values of the computed mixing length are averaged over the vertical in each computational cell to find the depth averaged values to be used in the 1D solution.

Firstly, wall shear stresses are taken from 2D solution since it is the reference solution and 1D model is enforced to predict these values.  By doing this, an unknown in Eq. (2-10) is excluded and only the turbulence stresses are remained to be solved. This gives the flexibility to investigate the appropriate mixing length values for the correct wall shear stresses over the bottom boundary.

After trial and error applications using different boundary considerations in mixing length computation and comparing velocity and shear stress distributions with 2D solution, it is found that in calculation of volumetric mixing length over 2D space, the horizontal solid boundaries should be excluded and vertical solid boundaries should be stretched to infinity. By doing this, the rectangular duct geometry is simply treated as if the flow takes place in between two parallel plates in the vertical for the depth integrated solutions.

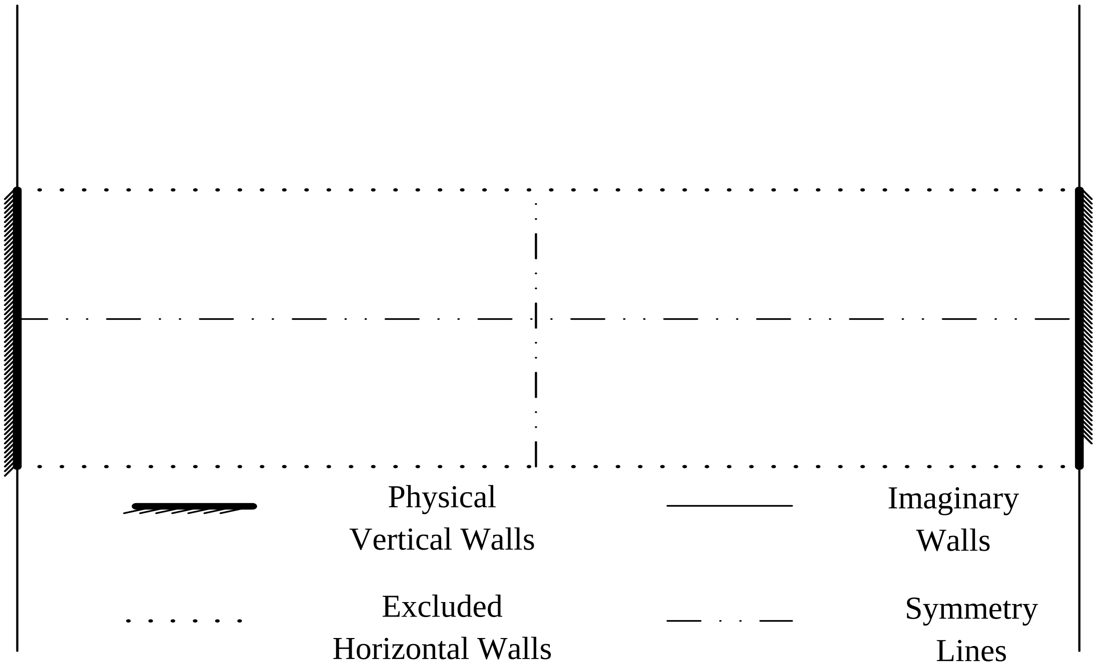


***Figure 3-3*** Depth averaged mixing length calculation in uniform duct flow

### 3.2.2 Wall Shear Stresses

Shear stresses on the bottom wall boundary are defined by using Eq. (2-20) in Section 2.3. The method simply calculates bottom wall shear stress by using average velocity and flow depth.

Shear stress on vertical side wall boundary is treated by the law of wall approach. Velocity at the centroid of the first computational element and it's distance to the side boundary are the two data to be used in the wall function to determine the wall shear velocity. Law of the wall is written as

$$u^{+} = \frac{1}{\kappa} ln y^{+} + C^{+} \tag{3-6}$$

where $C^{+}$ is constant equals to 5 , and the dimensionless parameters are defined as

$$u^{+} = \bar{u}/\bar{u}_{*} \qquad y^{+} = \frac{\bar{u}_{*} y}{\nu} \tag{3-7}$$

$\bar{u}_{*}$ is the shear velocity, ν is kinematic viscosity, $y$ is normal distance to the boundary. In order to have accurate solutions using the law of wall, the first computational point should be in the overlap region. By changing the distance of the first computational element to wall boundary, $y^+$ is controlled to be greater than 30.

### 3.2.3 Comparison with 2 Dimensional Solution

After completing the mixing length model, comparison with 2 dimensional solution is performed. Velocities, shear stress distributions in lateral direction and discharges are compared. Depth averaged volumetric mixing length evaluated by excluding the horizontal walls is used in the turbulence model and modified shear stress formulation (Eq. 2-20) is used to calculate shear stresses on the bed. Comparisons of different width to depth ratios for a pressure gradient of 10 N/m$^2$ are shown in Figs. (3-4 ~ 3-11).

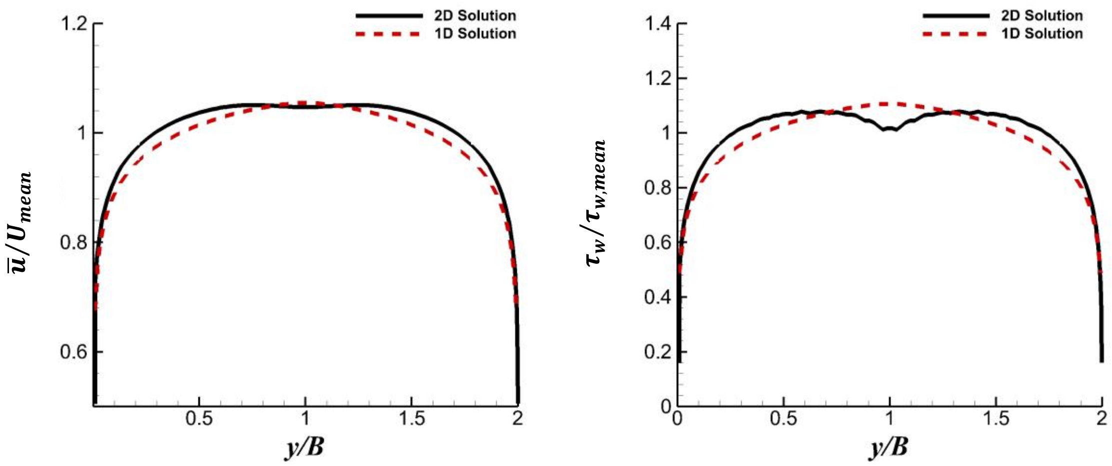


***Figure 3-4*** Velocity and shear stress comparison in rectangular duct, *B/H=1*

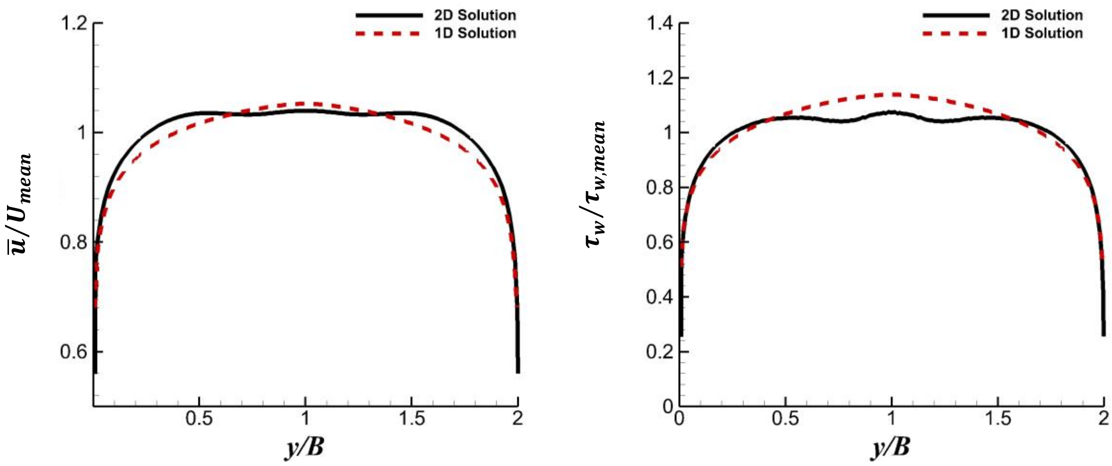


***Figure 3-5*** Velocity and shear stress comparison in rectangular duct, *B/H=2*

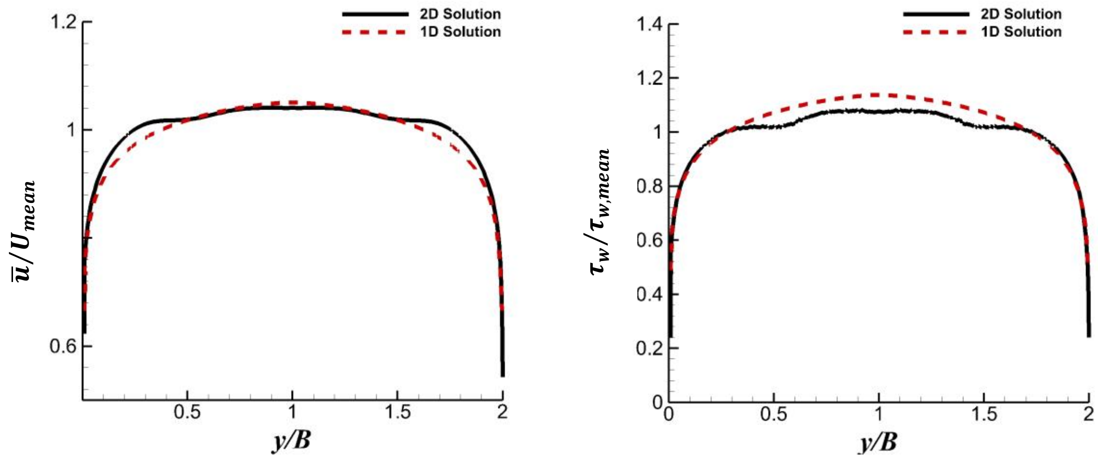


***Figure 3-6*** Velocity and shear stress comparison in rectangular duct, *B/H=3*

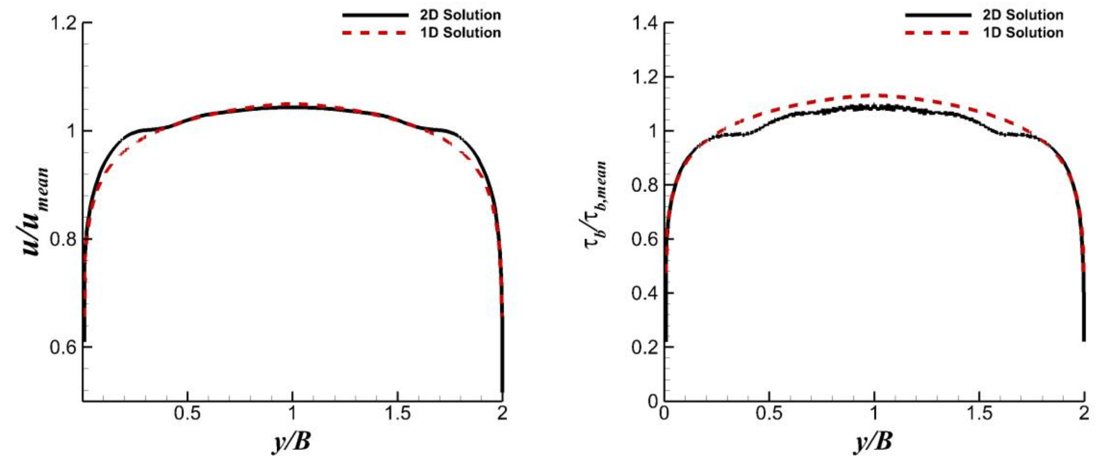


***Figure 3-7*** Velocity and shear stress comparison in rectangular duct, *B/H=4*

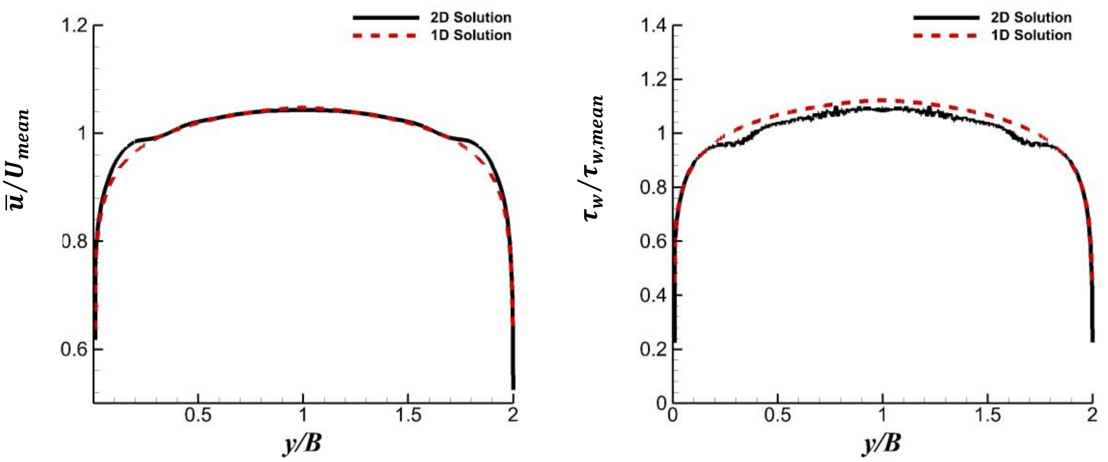


***Figure 3-8*** Velocity and shear stress comparison in rectangular duct, *B/H=5*

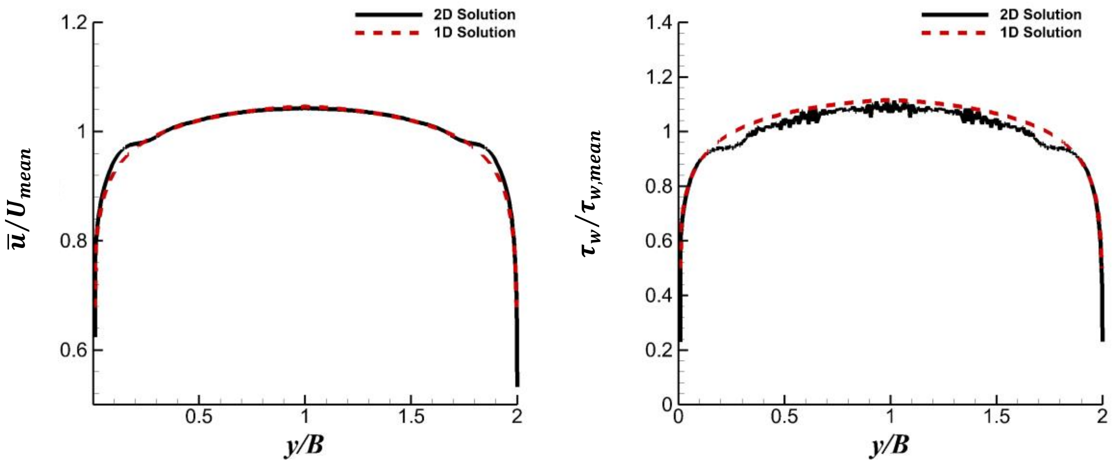


***Figure 3-9*** Velocity and shear stress comparison in rectangular duct, *B/H=6*

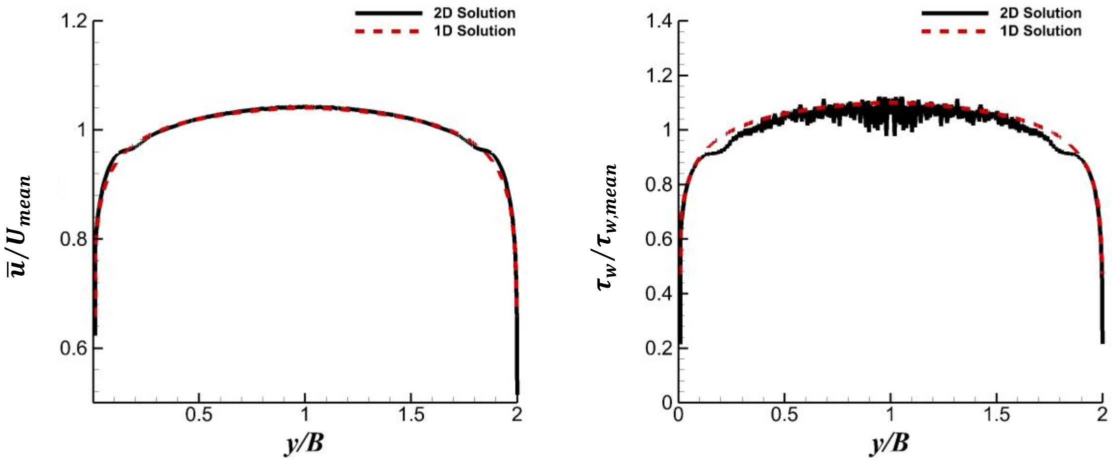


***Figure 3-10*** Velocity and shear stress comparison in rectangular duct, *B/H=8*

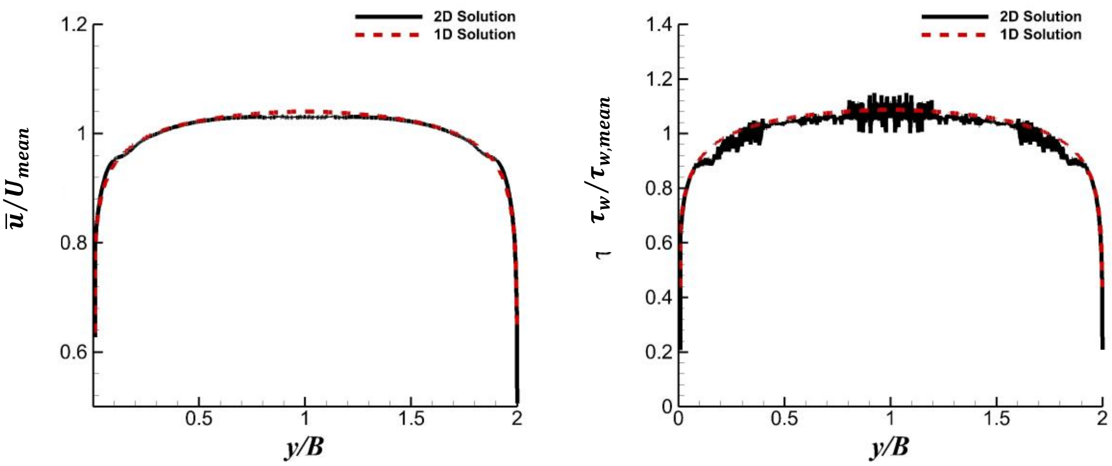


***Figure 3-11*** Velocity and shear stress comparison in rectangular duct, *B/H=10*

Comparisons show that model is successful in predicting the depth averaged velocity and bed shear stresses. In lower width to depth ratios, due to the secondary current effects, there are minor differences between the 1-D and 2-D solutions. However, as width to depth ratio increases, which means secondary current effect vanishes; 1-D model reproduces 2-dimensional solution almost identically.

To validate the model further, it is demonstrated that the solution is independent from the pressure gradient and the flow rate. To illustrate this, a variety of pressure gradients are used and compared with 2-dimensional solution for width to depth ratio of 3.

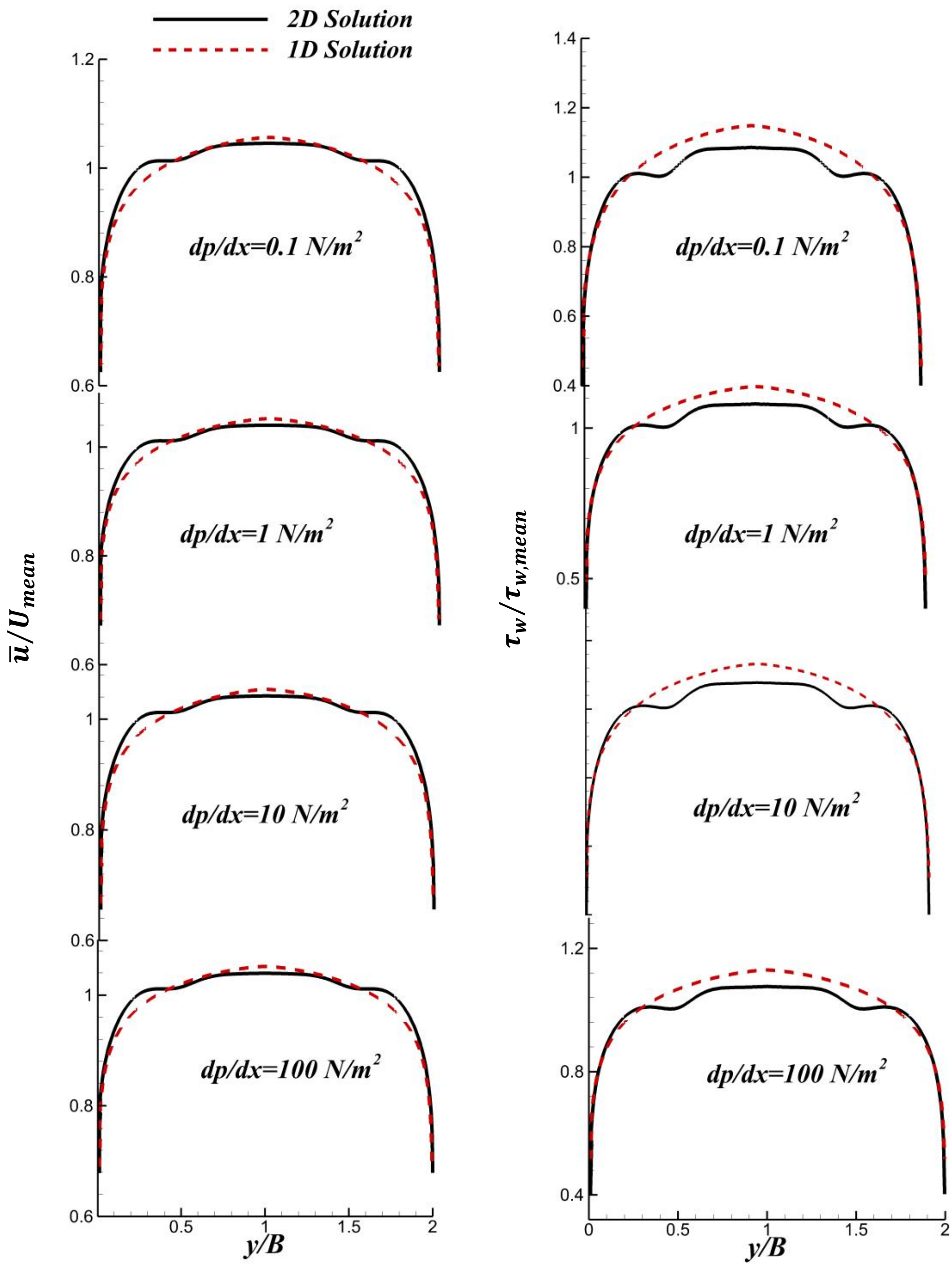


***Figure 3-12*** Velocity and shear stress comparison for different pressure gradients for *B/H=3*

Results indicated that, solution is independent of pressure gradient and gives successful results for variable pressure gradient and discharges.

### 3.3 Uniform Flow in Compound Duct

In the previous section it has been found that when calculating the mixing length, horizontal walls should be excluded. However, geometry in this case is different including discontinuities. Parallel plate approach has been proved to be working in rectangular duct. Adopting this approach to duct with level discontinuity is investigated. The generic cross-section geometry is given below as in Fig. (3-13).

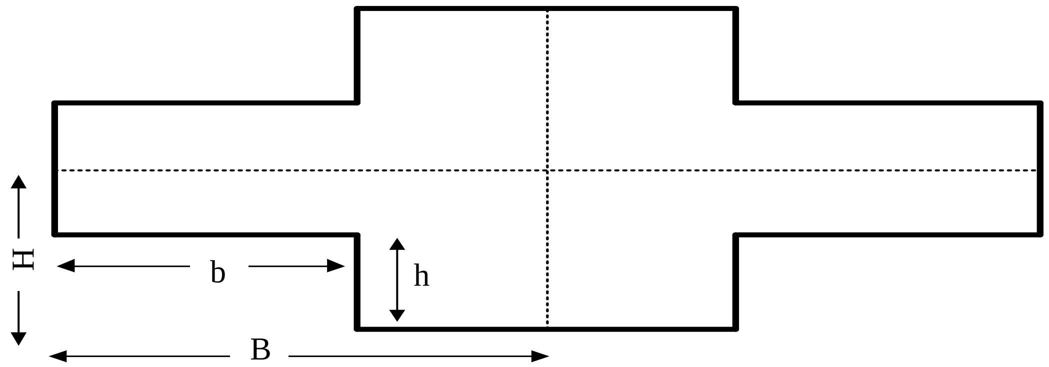


***Figure 3-13*** Compound duct geometry

#### 3.3.1 Turbulence Model

Same approach in uniform duct flow as described in Section 3.2 is applied. Computational grid over 2D domain is formed and mixing length distribution is calculated. In the development stage shear stresses again are taken from the 2D reference solution to leave mixing length as the only unknown parameter. It is known that from the previous section, when calculating mixing length, horizontal walls should not be included. After trial and error applications, different boundary considerations in mixing length computation and comparing velocity, shear stress distributions with 2D solution, it is found that in calculation of volumetric mixing length over 2D space, all vertical walls should be accounted for including the imaginary extensions to infinity.

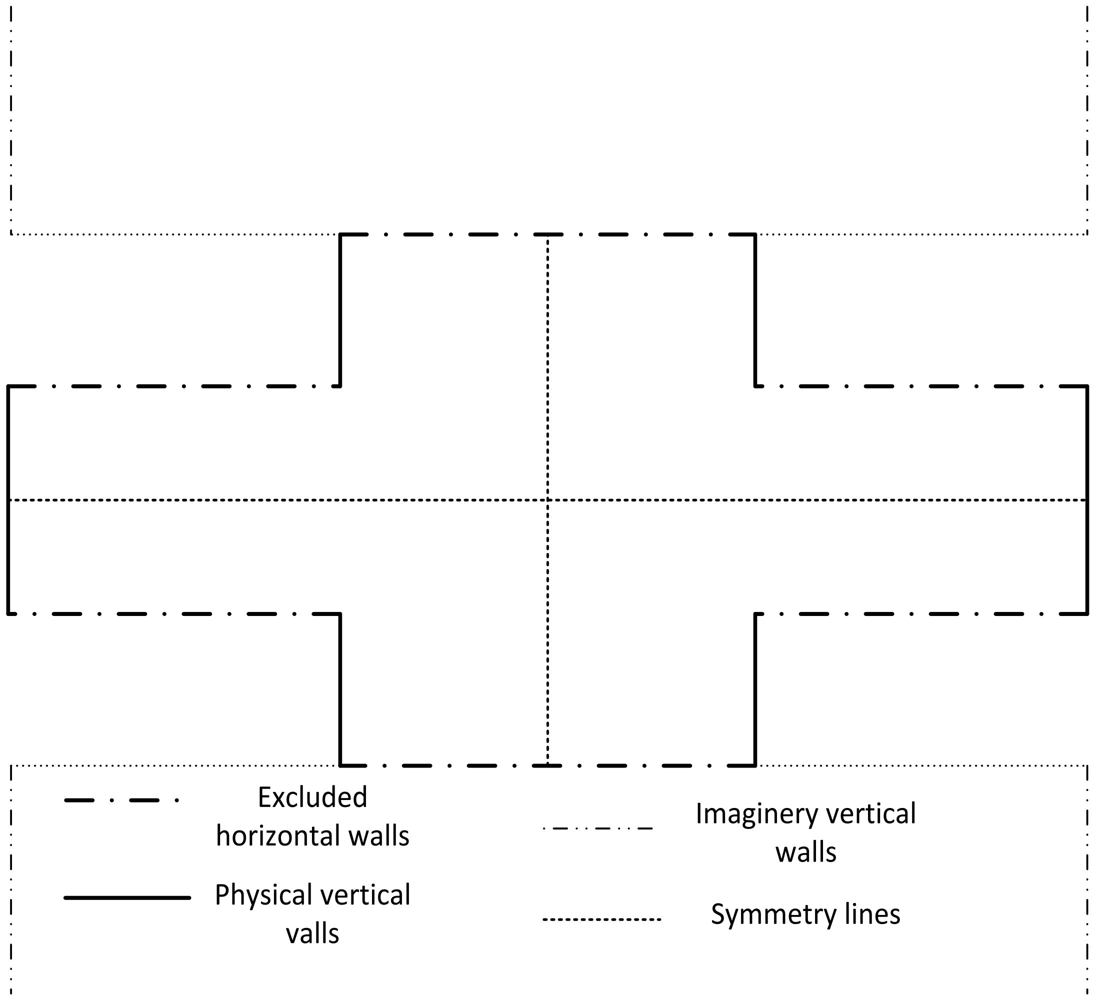


***Figure 3-14*** Mixing length calculation in uniform compound channel

As seen in the figure, outer vertical walls are stretched to infinity and horizontal walls are excluded. Channel is simply treated as composed of two parallel plates. Due to presence of the vertical walls over discontinuity, mixing length values around those points are additionally damped.

### 3.3.2 Wall shear stress

Wall shear stresses in horizontal extent are treated by using modified empirical function in Eq. (2-20) and vertical shear stresses are treated by using law of wall function controlling first computational node inside the overlap region. However, after trial and error application with 2D reference solution, it is seen that law of wall approach to estimate shear stresses on the vertical walls is not working properly as in the rectangular duct channel. Due to the turbulent interactions and secondary flows over the discontinuity, treatment of vertical wall boundary should be modified. For this reason, an approach has been developed to model shear stresses on vertical wall boundaries. On the discontinuity (the step), vertical wall shear stress is calculated by using depth averaged velocity. Fig. (3-15) shows the discretization over the discontinuity.

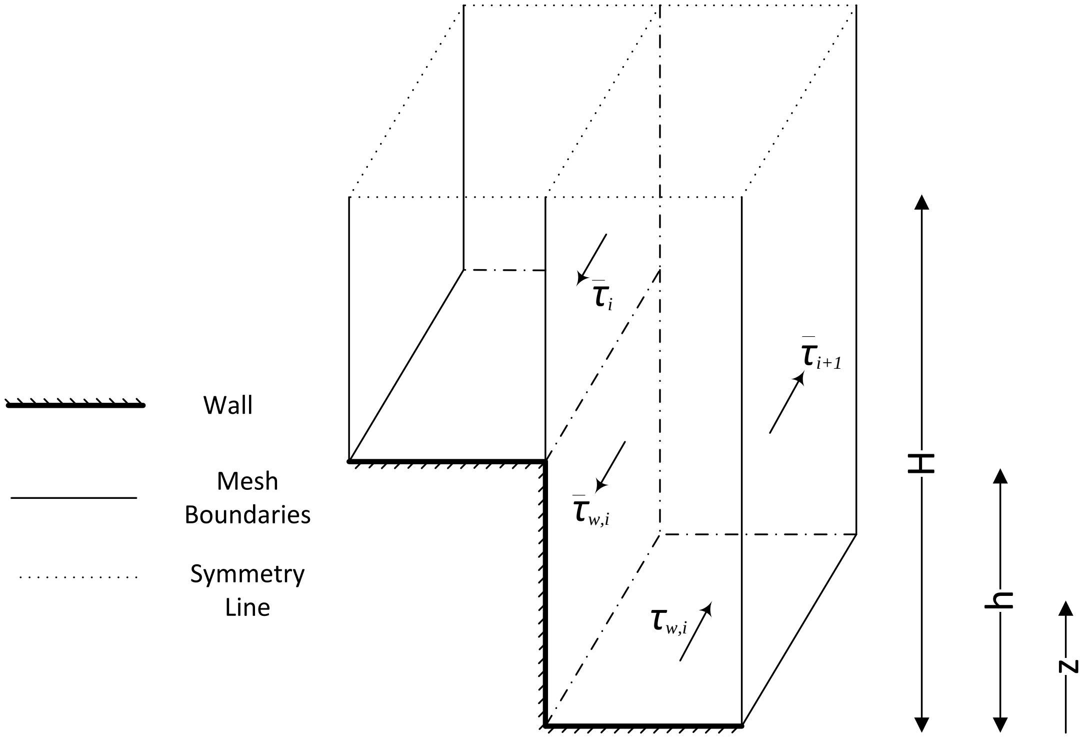


***Figure 3-15*** Discretization over the step

In this case, evaluating vertical wall shear stress using depth averaged velocity might introduce some errors because velocity is averaged for whole cell height from bottom to symmetry line which is *H*. However, to estimate wall shear stress on the vertical wall over the discontinuity, averaged velocity on the wall surface from bottom to height of vertical wall (*h)* should be considered. For this purpose, power law is used to estimate velocity distribution over the discontinuity (Kudela, 2012).

$$\frac{u}{u_{max}} = \left(\frac{z}{H}\right)^{1/n} \tag{3-8}$$

The purpose is to find velocity distribution in the cell over the depth. The only known value is averaged velocity and dividing average velocity by integral of $\left(\frac{z}{H}\right)^{1/n}$ from bottom to *H* gives maximum velocity in the cell.

$$u_{max} = \int_0^H u dz \Bigg/ \int_0^H \left(\frac{z}{H}\right)^{1/n} dz \tag{3-9}$$

And terms in Eq. (3-9) can be evaluated as;

$$\int_0^H u dz = H\bar{u} \qquad\qquad n = -2Log(\frac{2.51n}{R_e}) \tag{3-10}$$

$R_e$ is local Reynolds Number in the cell which is $H\bar{u}/v$.

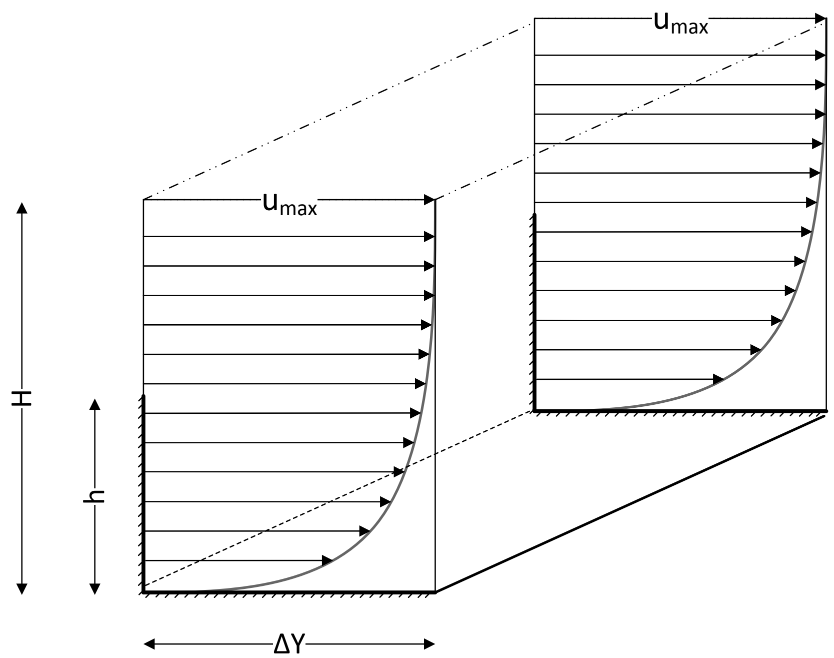


***Figure 3-16*** Velocity distribution in the step

Using the power law again in Eq.(3-8), velocity distribution in the step is found and depth averaging is performed from the bottom to height of step wall (*h*) to find the averaged velocity $u_s$ in the step zone.

After determining averaged velocity over the step, different sets of 2D solutions are performed for varying width (*B*) , depth (*H*), step width (*b*), step height (*h*) and pressure gradient ($C_p$). Shear stresses in the vertical walls are found and averaged in the direction of depth for each case. These exact values of vertical and horizontal shear stresses are used in 1D solutions to determine the friction relations.

In each 1D solution using 2D shear stresses, solution is performed and velocity distribution is found. Reynolds Number is calculated in computational cells closest to vertical walls. A dimensionless friction parameter is defined and determined in each 1D solution which is;

$$\frac{\tau_{v,w}}{\rho \bar{u}_s{}^2} \tag{3-11}$$

$\tau_{v,w}$ : Vertical wall shear stress taken from 2D solution

$\bar{u}_s$: Calculated depth averaged velocity in computational cells closest to vertical walls in 1D model using shear stresses from 2D solution

ρ : Density of the fluid

The dimensionless parameter introduced in Eq.(3-11) and Reynolds number in computational cells closest to vertical walls are noted in each case. Logarithm of Reynolds number $log(R_e)$ versus $\tau_{v,w}/\rho\bar{u}_s{}^2$ is plotted in Fig.(3-17) and a relation between the two parameters is obtained by using linear regression.

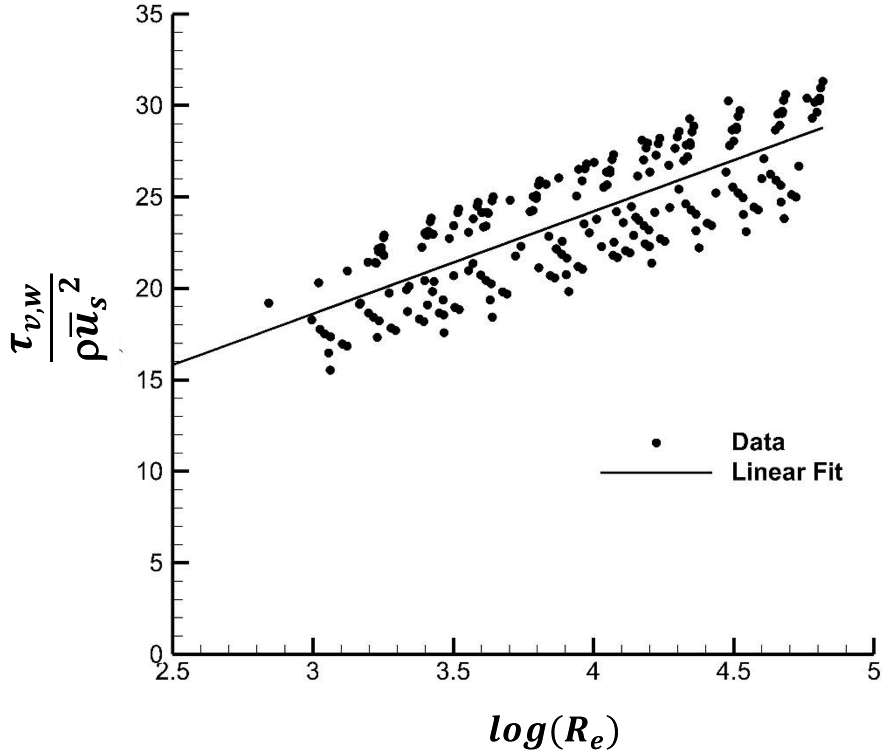


***Figure 3-17*** Wall shear stress data fit

The function of the linear fit is found as;

$$\tau_{v,w} = \rho u_s^2[1.83 + 5.595\log(R_e)] \tag{3-12}$$

The basic idea is to calculate shear stress value on vertical walls by using velocity closest to wall boundary. This method eliminates the need of using wall function to estimate shear stresses on vertical walls and can be applicable to any cross section.

### 3.3.3 Comparison with 2 Dimensional Solution

After defining turbulence and shear stress treatment, comparison of velocity and shear stresses with 2D solution are performed. Several cases are investigated with varying width to depth ratios (*B/H*), step height (*h*), step width (*b*) and pressure gradient. Extreme cases are also investigated to observe the behavior of 1D model by changing step width and step height up to % 80 of total width and height.

Firstly, step width and height are remained constant for all cases. For each cross section which has varying width to depth ratio, half of the total width and height of the channel is defined as step geometry in the channel and comparisons are performed accordingly. Results are shown in Figs. (3-18 ~ 3-25).

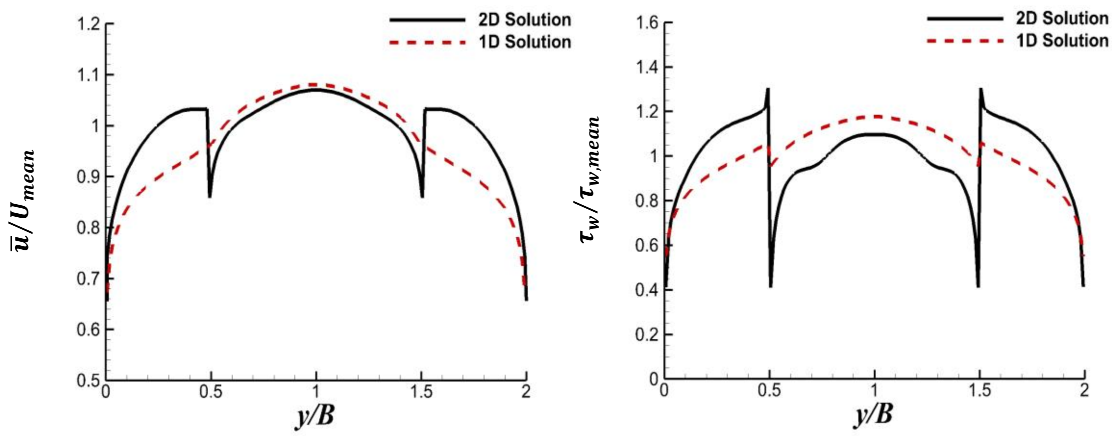


***Figure 3-18*** Velocity and shear stress comparison for *B/H=1, b=0.5B, h=0.5H*

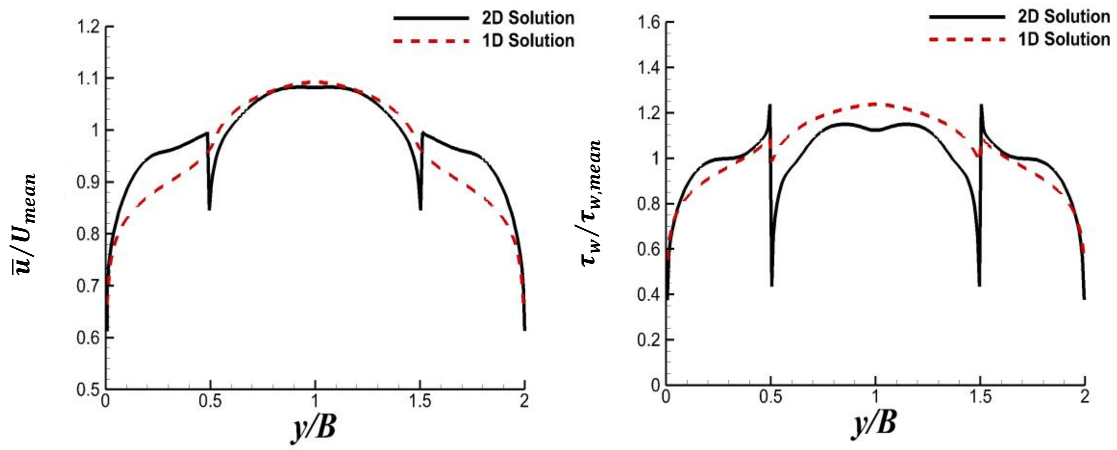


***Figure 3-19*** Velocity and shear stress comparison for *B/H=2, b=0.5B, h=0.5H*

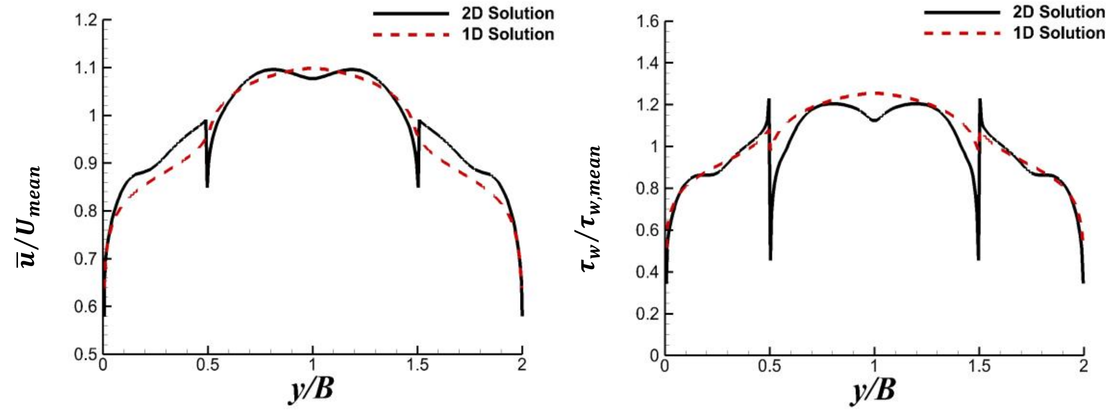


***Figure 3-20*** Velocity and shear stress comparison for *B/H=3, b=0.5B, h=0.5H*

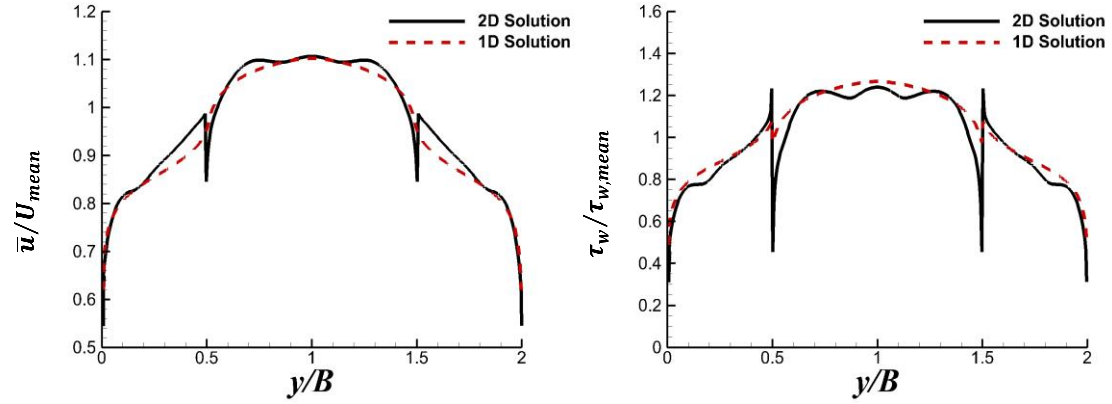


***Figure 3-21*** Velocity and shear stress comparison for *B/H=4, b=0.5B, h=0.5H*

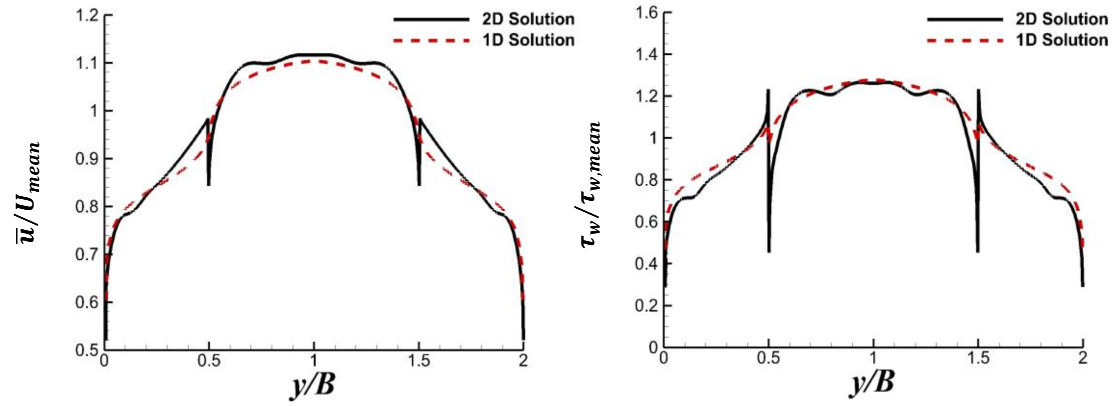


***Figure 3-22*** Velocity and shear stress comparison for *B/H=5, b=0.5B, h=0.5H*

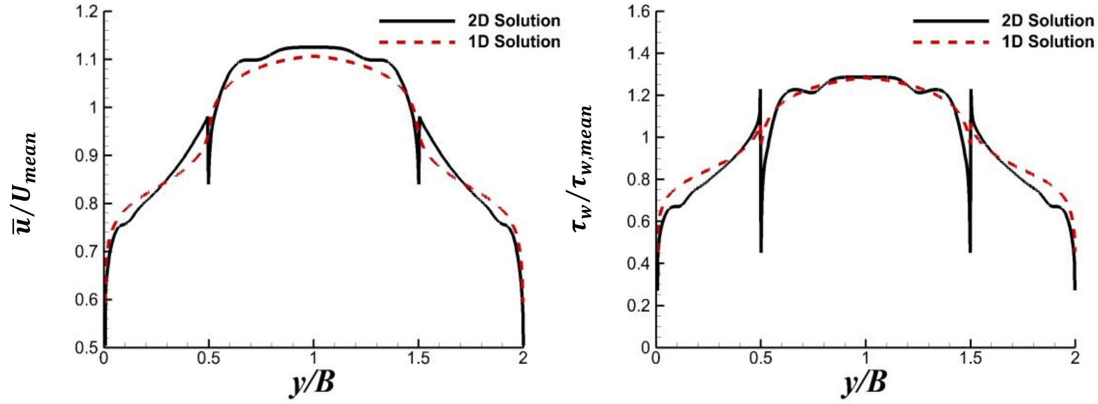


***Figure 3-23*** Velocity and shear stress comparison for *B/H=6, b=0.5B, h=0.5H*

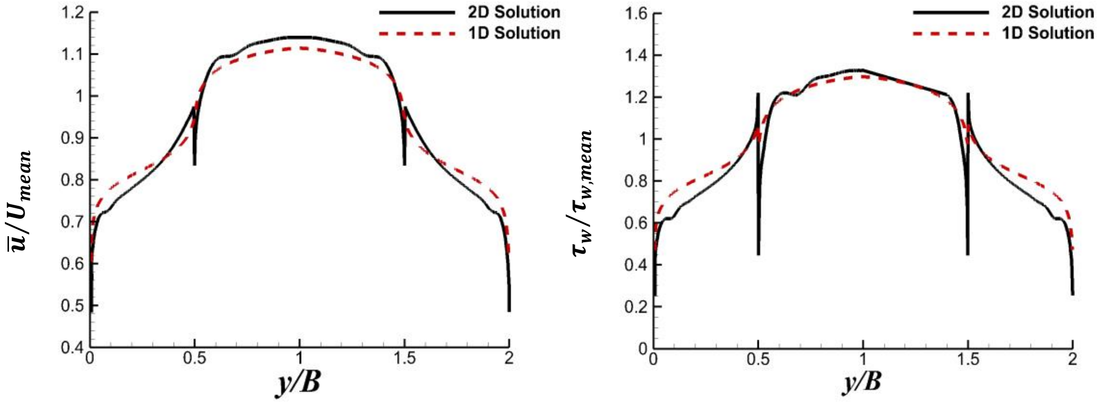


***Figure 3-24*** Velocity and shear stress comparison for *B/H=8, b=0.5B, h=0.5H*

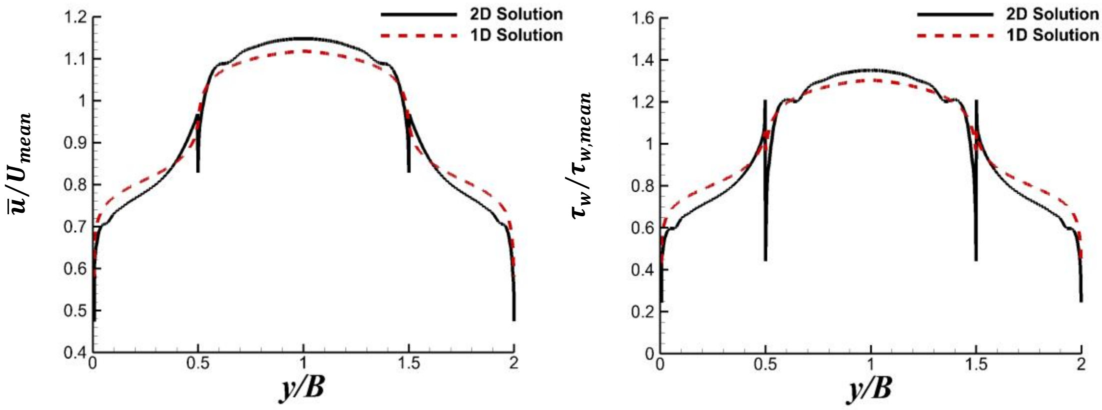


***Figure 3-25*** Velocity and shear stress comparison for *B/H=10, b=0.5B, h=0.5H*

Velocity and shear stress comparison with 2D solution in extreme conditions are performed. Width to depth ratio is remained constant and step height and step width changed. The results are presented for width to depth ratio of 4 and two sets of solutions are presented. Step width is remained constant which is half of total width and step height is changed to % 10,20,40,60 and 80 to total height. Visa versa case is also investigated as step height is remained constant and step width is changed. Comparisons of 1D and 2D solutions are given in Figs. (3-26 ~ 3.35)

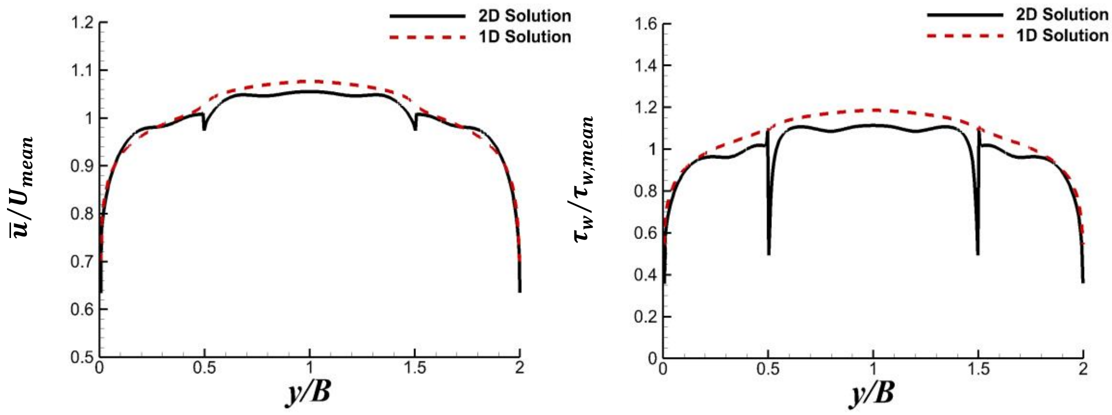


***Figure 3-26*** Velocity and shear stress comparison, *B/H=4, b=0.5B, h=0.1H*

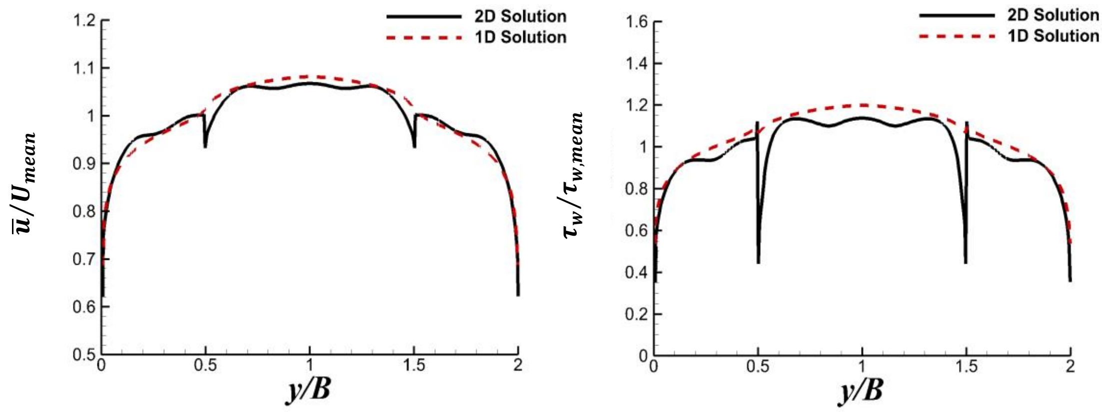


***Figure 3-27*** Velocity and shear stress comparison, *B/H=4, b=0.5B, h=0.2H*

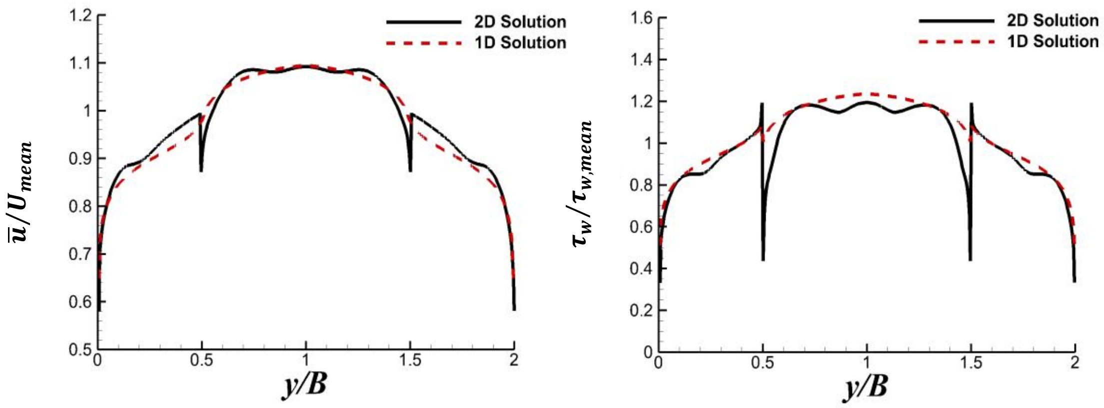


***Figure 3-28*** Velocity and shear stress comparison, *B/H=4, b=0.5B, h=0.4H*

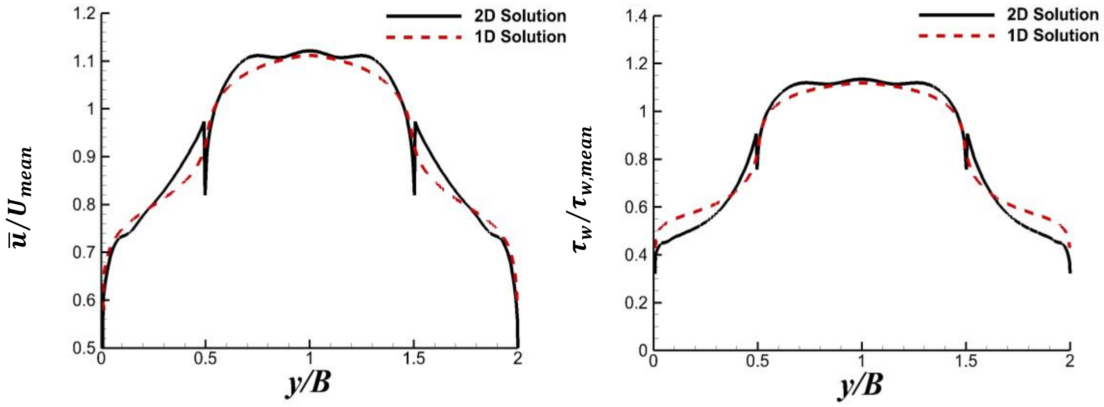


***Figure 3-29*** Velocity and shear stress comparison, *B/H=4, b=0.5B, h=0.6H*

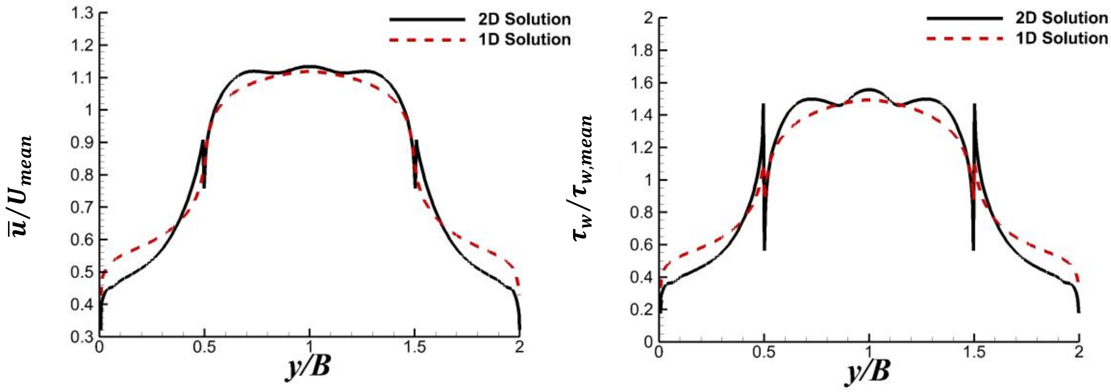


***Figure 3-30*** Velocity and shear stress comparison, *B/H=4, b=0.5B, h=0.8H*

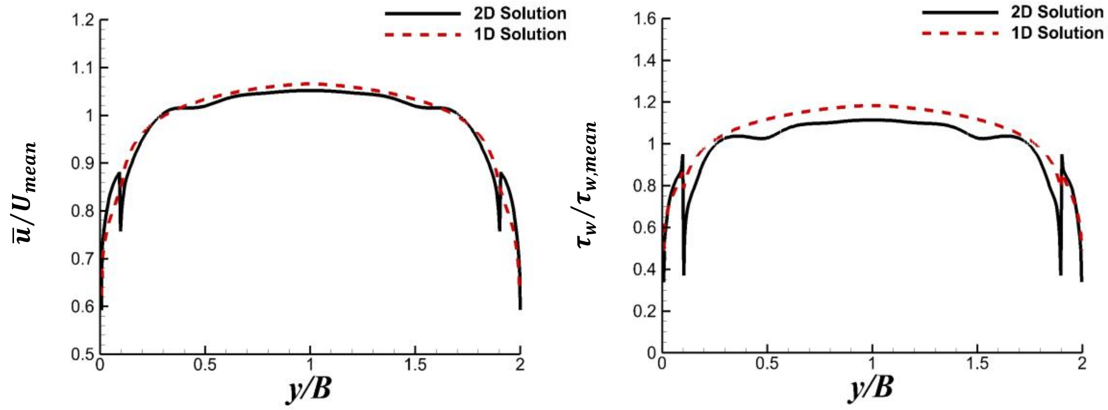


***Figure 3-31*** Velocity and shear stress comparison, *B/H=4, b=0.1B, h=0.5H*

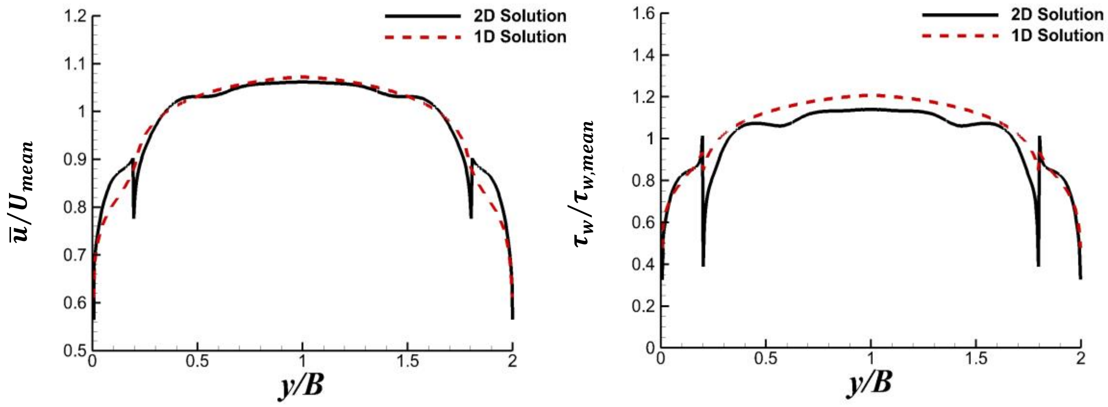


***Figure 3-32*** Velocity and shear stress comparison, *B/H=4, b=0.2B, h=0.5H*

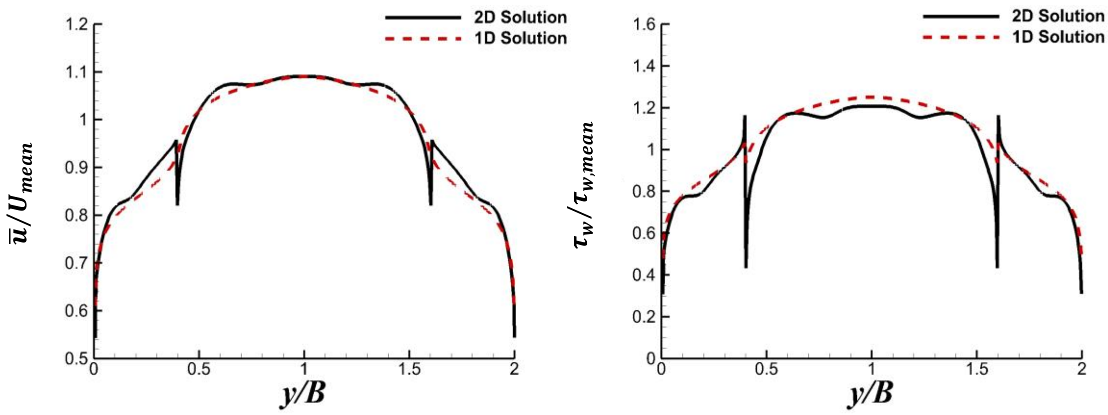


***Figure 3-33*** Velocity and shear stress comparison, *B/H=4, b=0.4B, h=0.5H*

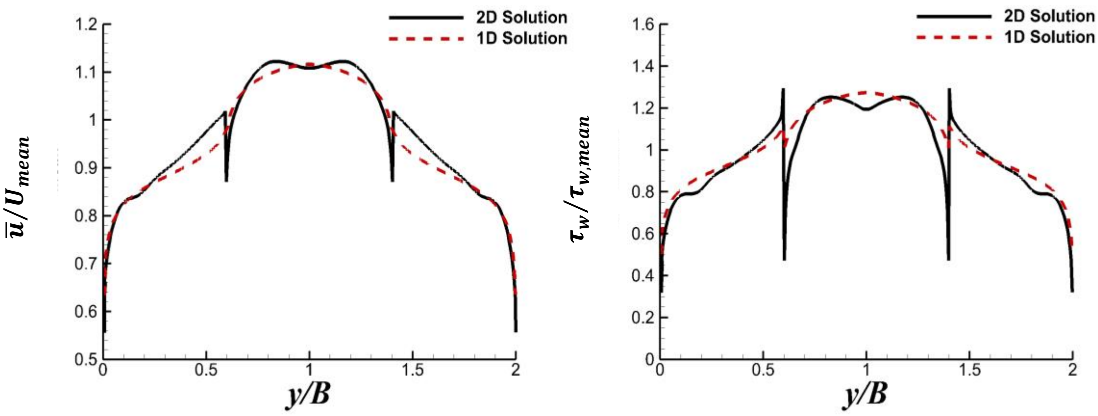


***Figure 3-34*** Velocity and shear stress comparison, *B/H=4, b=0.6B, h=0.5H*

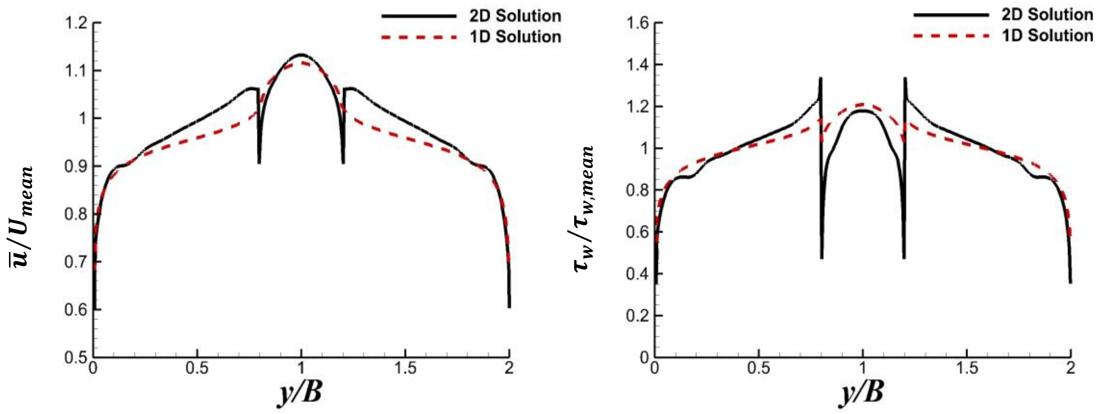


***Figure 3-35*** Velocity and shear stress comparison, *B/H=4, b=0.8B, h=0.5H*

Comparisons for both cases show that 1D model solutions reasonably agree with 2D numerical solutions. Sharp decreases over discontinuity are the result of the depth averaging. Presence of discontinuity creates more turbulence anisotropy and in result this brings more and powerful secondary flows.

One drawback of depth averaged shallow flow model as mentioned before is that the secondary flow effects are not directly represented. In other similar studies (Finnie, Donnell, Letter, & Bernard, 1999) and (Knight, Donald W; Omran, Mazen; Tang, Xiaonan, 2006) modifications are introduced to shallow water model such as corrections by a secondary flow parameter, to correct for the effect of secondary flows in the velocity and boundary shear distributions. In the present study, such modifications are not required since the mixing length for turbulence modelling is obtained from 2D distribution by depth integration.

In narrower domains where width to depth ratios is less than 5, shallow water assumption is not completely satisfied and 1D depth averaged model gives only a good approximation. When shallow water assumption is valid, model is very robust to predict the lateral velocity distribution and wall shear stresses.

In order to validate the model further, comparisons for different pressure gradients are performed. Width to depth ratio of 4 is selected and step width and height is defined as half of the total width and depth. Results are given in Fig. (3-36)

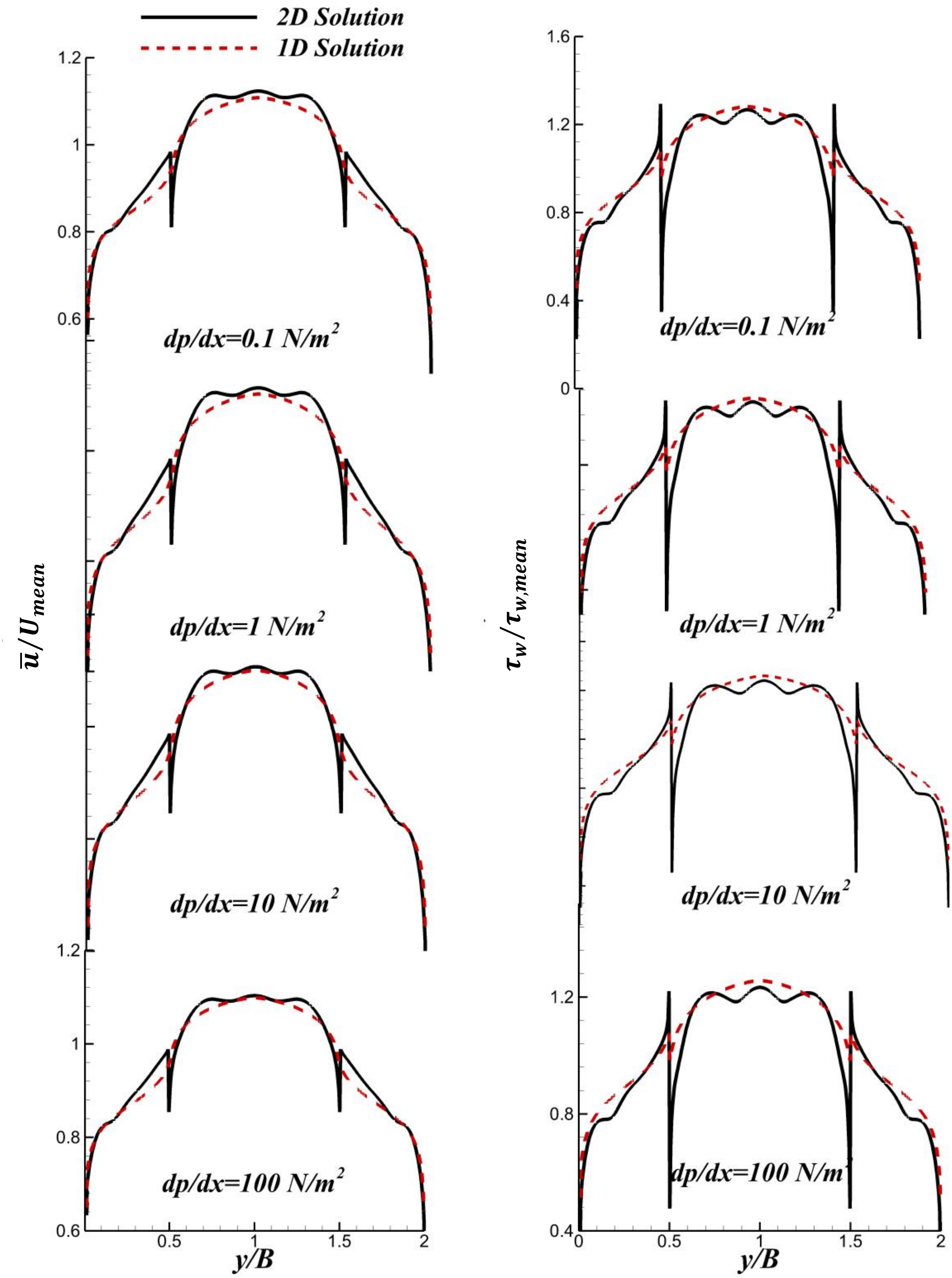


***Figure 3-36*** Velocity, shear stress comparison for different pressure gradients, *B/H=4, b=0.5B, h=0.5H*

Comparisons indicate that 1D depth averaged model gives same result in each pressure gradient and discharge value.

### 3.4 Uniform flow in a periodic compound duct

In both rectangular and compound duct flow, turbulence and bed shear stress models are developed and seen to be working when comparing with 2D solutions. To validate the 1D model further, another geometry with periodic compound duct is considered (Fig. 3-37).

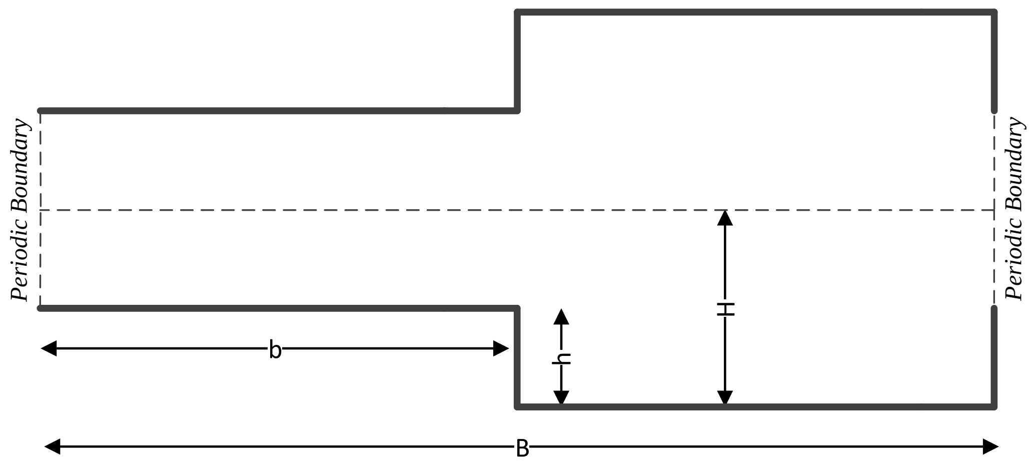


***Figure 3-37:*** Periodic compound duct geometry

Vertical wall boundaries are replaced with periodic boundaries which mean that infinite number of identical channels are placed next to both side of the channel continuously.

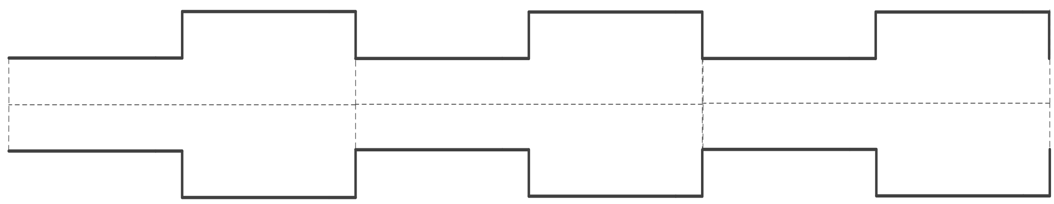

***Figure 3-38*** Infinitely long duct flow in lateral direction

The objective of choosing this geometry is to simulate the bed roughness introduced with changing step height. As channel height ($H$) increases, effect of bed level discontinuity vanishes. By increasing step height enough, gear type shape can be made similar to the roughness in the bed of the channel. Varying step height ($h$), step width ($b$) are used to observe the behavior of the solution.

### 3.4.1 Turbulence Model

Same approach in uniform compound duct flow as described in section 3.3 is applied. Computational grid over 2D domain is formed and mixing length distribution is calculated. When calculating mixing length, horizontal walls are excluded and only vertical walls are taken into account. However, due to the presence of periodic boundaries, there are infinitely many vertical walls as in Fig. (3-38). It is known that, as the point in the domain gets away from the wall boundary, effect of that wall boundary in mixing length calculation vanishes. Making use of this fact, only sufficient number of vertical walls should be taken into account to represent infinitely long channel. Different number of wall boundaries in both side of the channel is considered with $b = H, B = 2H, h = H/2$ and depth averaged mixing length calculated for each case to see the behavior of distribution.

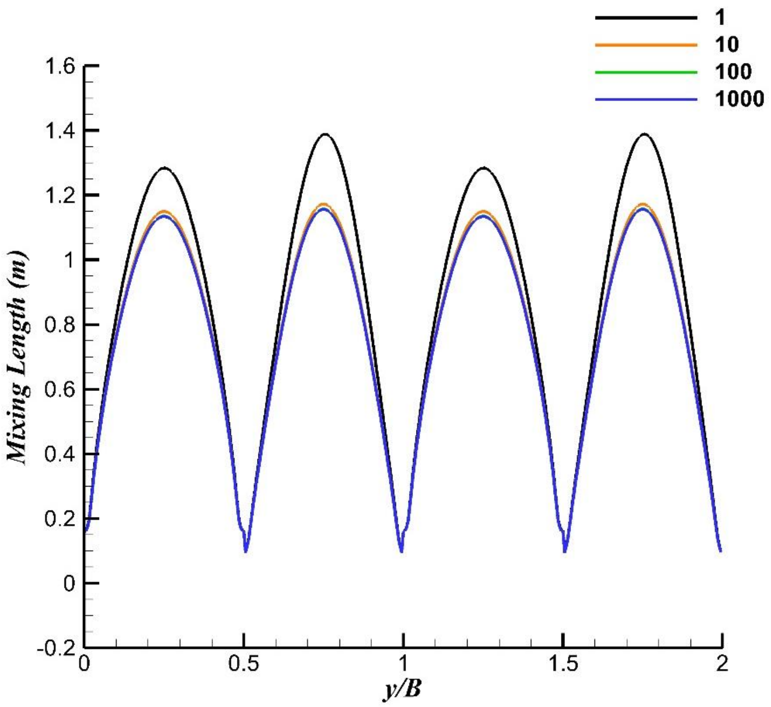


***Figure 3-39*** Effect of vertical wall boundaries in calculation of mixing length in periodic compound duct

Fig. (3-39) states that, 100 channels in both right and left hand side of the channel in calculation of mixing length is sufficient to represent infinitely long duct in lateral direction.

### 3.4.2 Wall shear stress

Wall shear stresses in horizontal extent are treated by using modified empirical function in Eq. (2-20) and vertical shear stress over step is treated by using Eq. (3-13) which was previously defined.

### 3.4.3 Comparison with 2 Dimensional Solution

After defining turbulence and shear stress treatment, comparison of velocity and shear stresses with 2D solution are performed. Several cases are investigated with varying width to depth ratios ($B/H$). For each cross section which has varying width to depth ratio, half of the total width and height of the channel is defined as step geometry and comparisons are performed. Results are shown in Figs. (3-40 ~ 3-47).

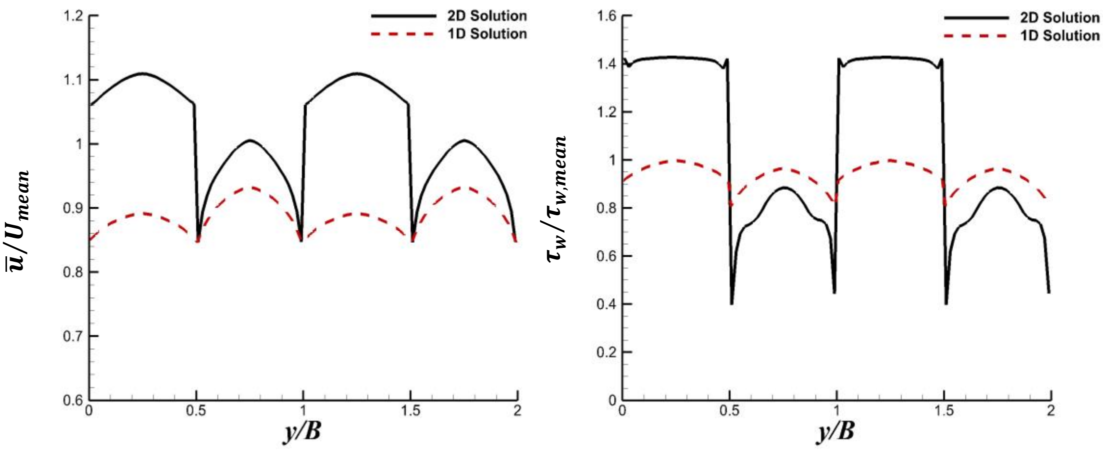


***Figure 3-40*** Velocity and shear stress comparison for *B/H=1, b=0.5B, h=0.5H*

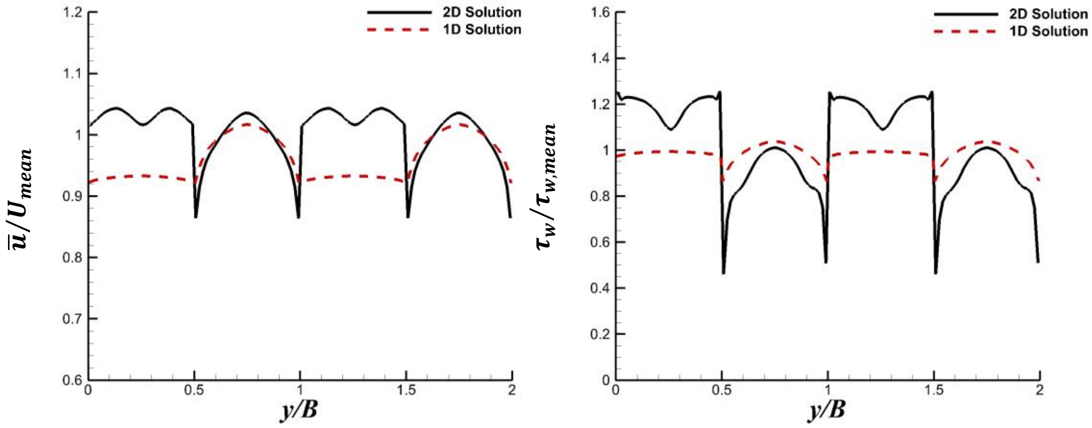


***Figure 3-41*** Velocity and shear stress comparison for *B/H=2, b=0.5B, h=0.5H*

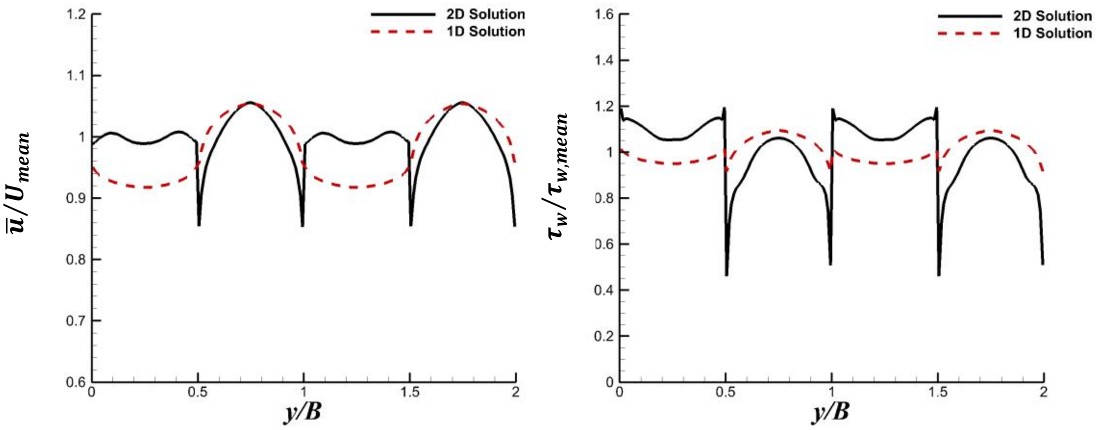


***Figure 3-42*** Velocity and shear stress comparison for *B/H=3, b=0.5B, h=0.5H*

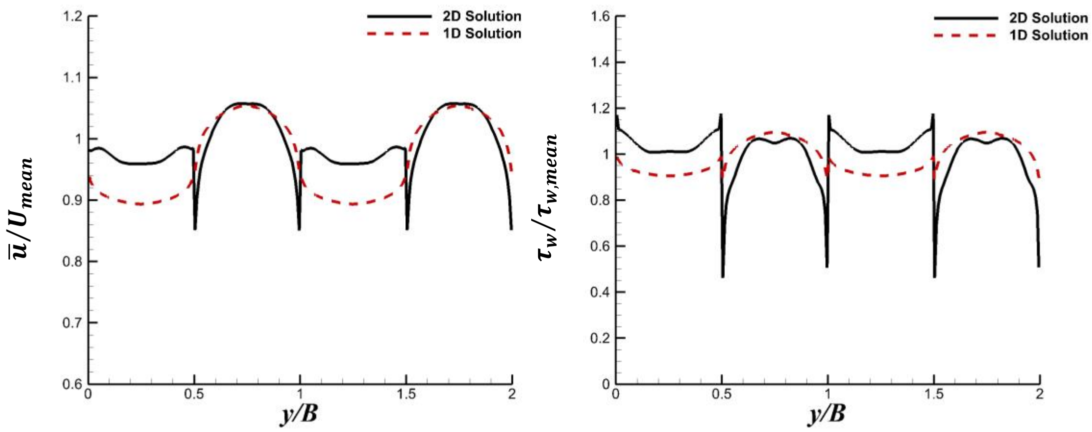


***Figure 3-43*** Velocity and shear stress comparison for *B/H=4, b=0.5B, h=0.5H*

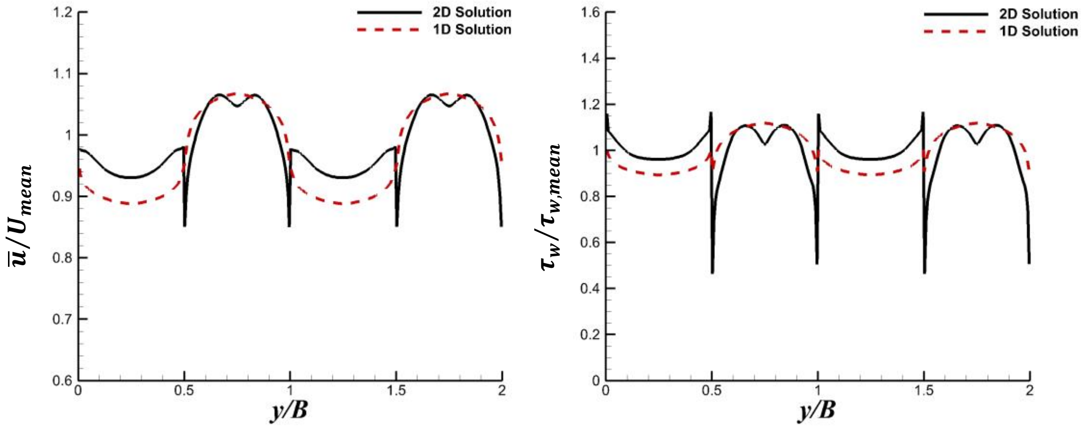


***Figure 3-44*** Velocity and shear stress comparison for *B/H=5, b=0.5B, h=0.5H*

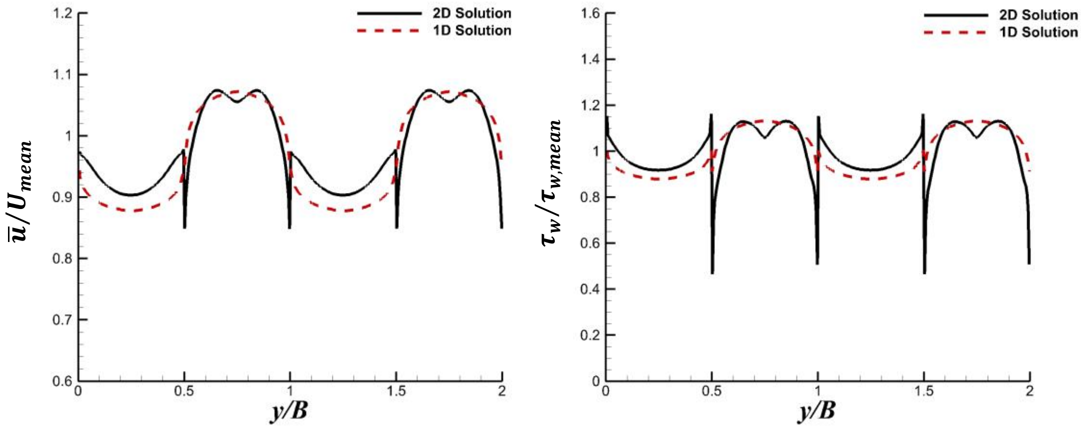


***Figure 3-45*** Velocity and shear stress comparison for *B/H=6, b=0.5B, h=0.5H*

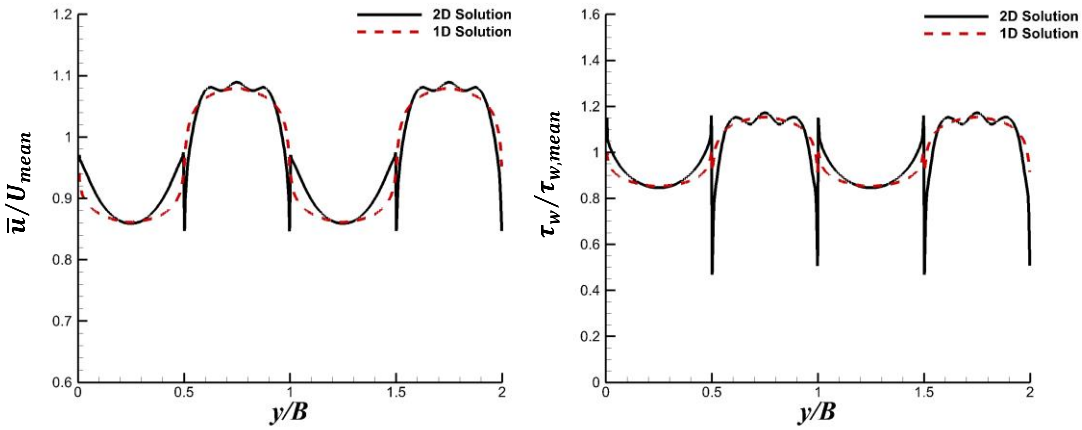


***Figure 3-46*** Velocity and shear stress comparison for *B/H=8, b=0.5B, h=0.5H*

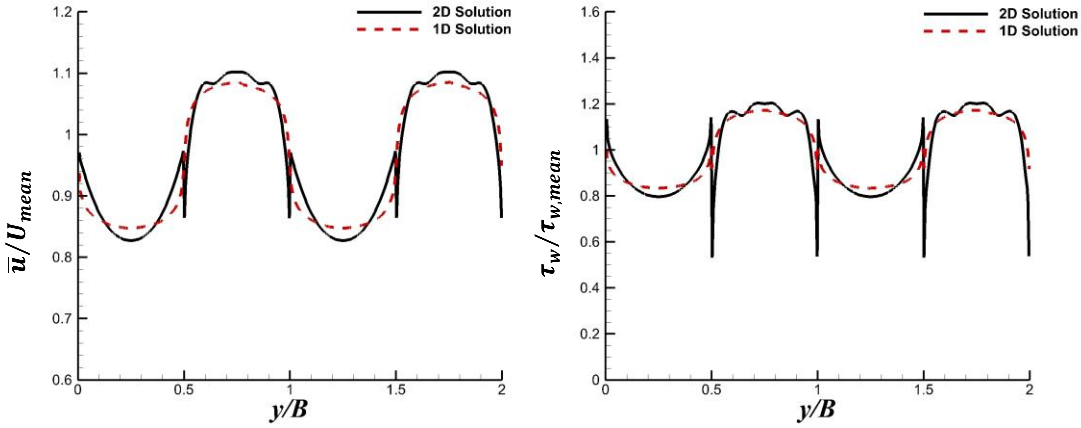


***Figure 3-47*** Velocity and shear stress comparison for *B/H=10, b=0.5B, h=0.5H*

Comparisons clearly states that 1D solution well agree with the 2D solution for large aspect ratios of the cross-section as expected. In narrower regions, where width to depth ratio is less than 5, shallow flow assumption is not fully satisfied, however, 1D model results in approximate prediction of 2D solution.

# CHAPTER 4

# COMPARISON OF 1D MODEL WITH MEASURED DATA

1D model developed in section 3 is applied to several test cases for which measured data is available in the literature. Velocity, shear stress distribution and discharge in numerous channel geometries are compared with 1D model solutions. Firstly, shear stress data in uniform closed duct measured by Patel & Knight (1985) is compared with 1D model. Then, velocity and shear stress distribution data in several symmetric and asymmetric rectangular open channels available in Flood Chanel Facility (FCF), Wallingford, UK are compared with 1D model results. Discharge comparisons are performed with data measured by Knight and Demetriou (1993) in symmetric rectangular channel with varying width to depth ratios. Effect of channel bed slope in symmetric rectangular compound channel is also investigated by comparing 1D model with data available in Lambert & Myers (1998).

## 4.1 Rectangular Duct Flow Comparison

After completing development of the 1D depth averaged model, it is compared to available experimental data in the literature. For turbulent flow in rectangular closed duct Patel & Knight (1985) have measured shear stress distributions for variable width to depth ratios. Comparison of computed values of shear stress by 1D depth averaged model to the experimental data is shown in Fig.4-1.

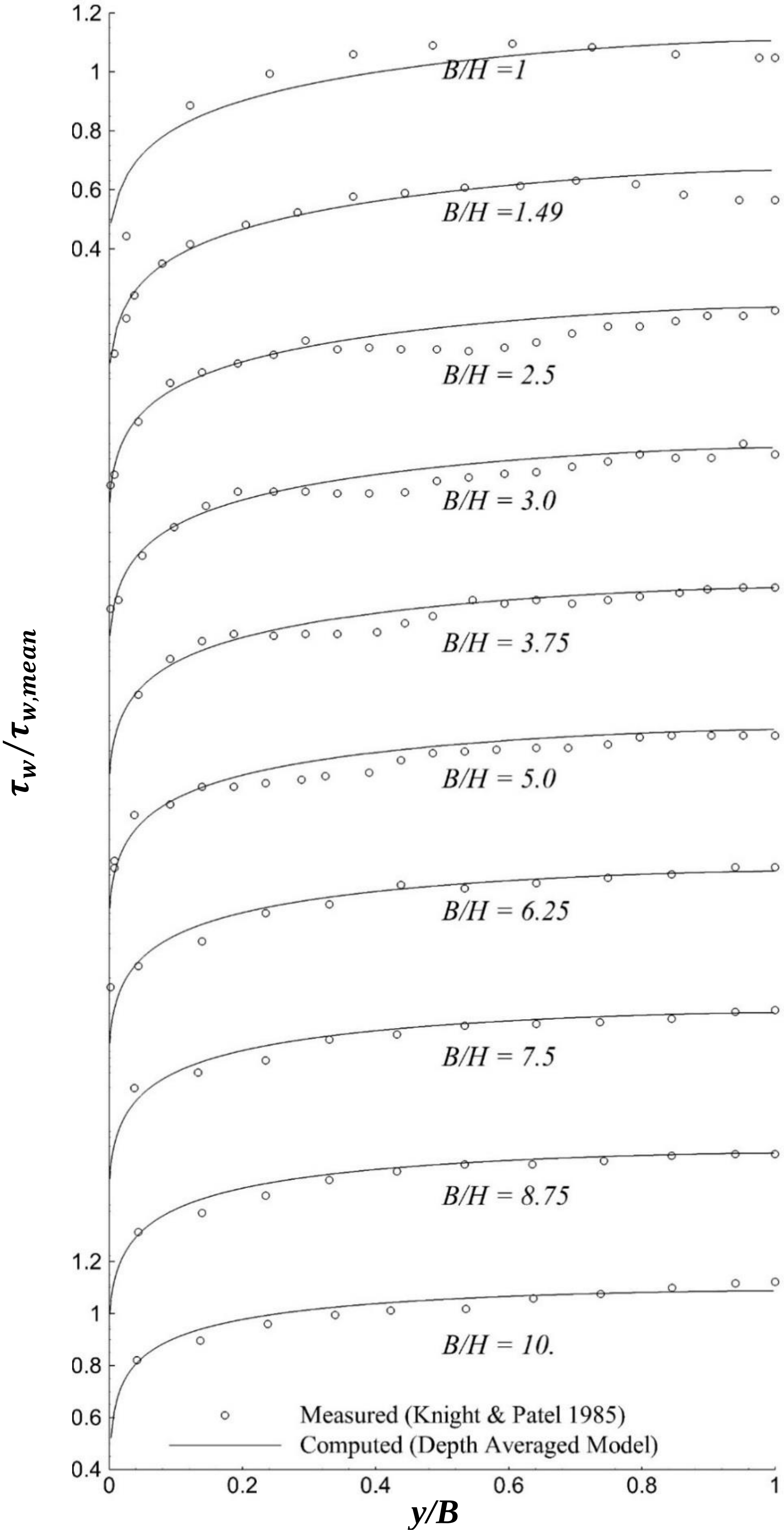


***Figure 4-1*** Comparison of computed and measured wall shear stresses (Patel & Knight, 1985)

Graphs show that 1D depth averaged model agree well with the experimental data, with increasing accuracy at higher aspect ratios.

It can be seen that constructed 1D model works well when compared to 2D solutions. Comparison with 2D solution and experimental data have been conducted and observed that the model is consistent as well as robust for predicting depth averaged velocity, shear stress and discharge in any width to depth ratio. The model will next be applied to uniform flow in open channel.

## 4.2 Open Channel Comparison

1D Model is applied to symmetric and non-symmetric smooth rectangular compound channels at Flood Channel Facility (FCF), Wallingford, UK. Flood Channel facility is a laboratory in Wallingford that founded by SERC. Using results of experiments undertaken by Knight (1970-85), as well as the 74 experiments (1987-89) from the Flood Channel Facility (FCF), documented in 15 volumes (Phase A). There are thus approximately 600 experimental data sets of velocity and bottom shear stress for straight prismatic open channels or ducts with various cross sections and roughness distributions, as well as many data from elsewhere (Flood Channel Facility, 2013).

Several cross sections with varying width to depth ratios are investigated. Five sets of experimental data from FCF are used for comparison. Four of the experiments are symmetric with varying width to depth ratio and one of the experiments has non-symmetric cross section. Depth averaged velocity and shear stress distributions are compared for each case.

Wall boundary with varying flow depth is represented by discretizing it to make similar to step shape. Continuous steps are considered and 1D model developed in section 3 is applied to each step by assuming steps representing wall boundary Fig(4-2). As Δy and Δz gets smaller, representation of wall boundary becomes more precise. By using this approach, any type of cross section including natural channels can be represented.

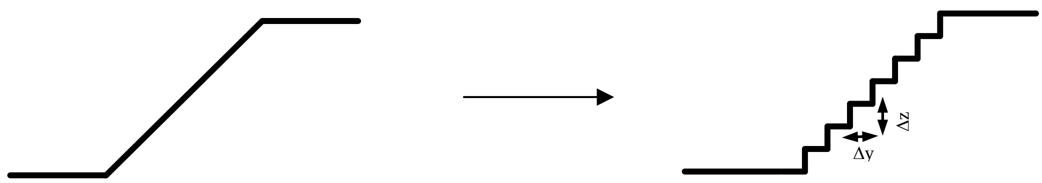


***Figure 4-2*** Treatment of sections with varying flow depths

Channel is considered symmetric around the free surface and symmetry boundary condition is described accordingly. Depth averaged 1D model will be tested with experimental data from the literature.

### 4.2.1 FCF Experiment 1

FCF experiment series 01 is a symmetric rectangular cross section with bed slope of 0.001027. Cross section is given below.

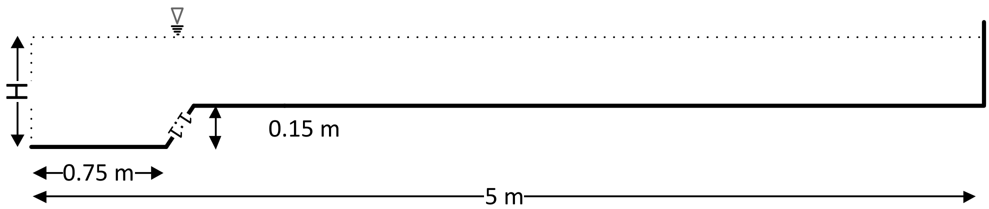


***Figure 4-3*** Cross section for FCF Series 01

Different water depths are used to compare depth averaged velocity and shear stress distribution and results given in Figs. (4-4 ~ 4-8).

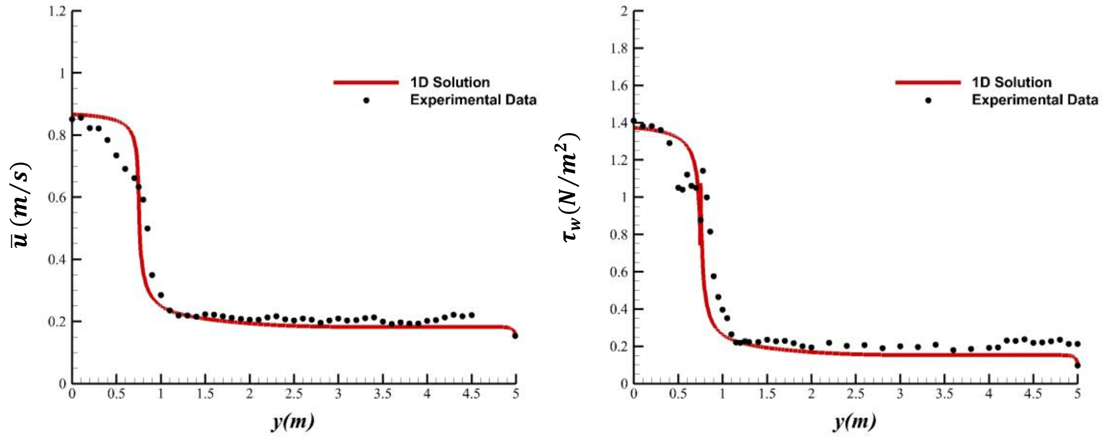


***Figure 4-4*** Comparison between 1D and experimental lateral distributions of $\bar{u}$ and $\tau_w$ for flow depth of H=166 mm in the rectangular compound channel (FCF Series 01).

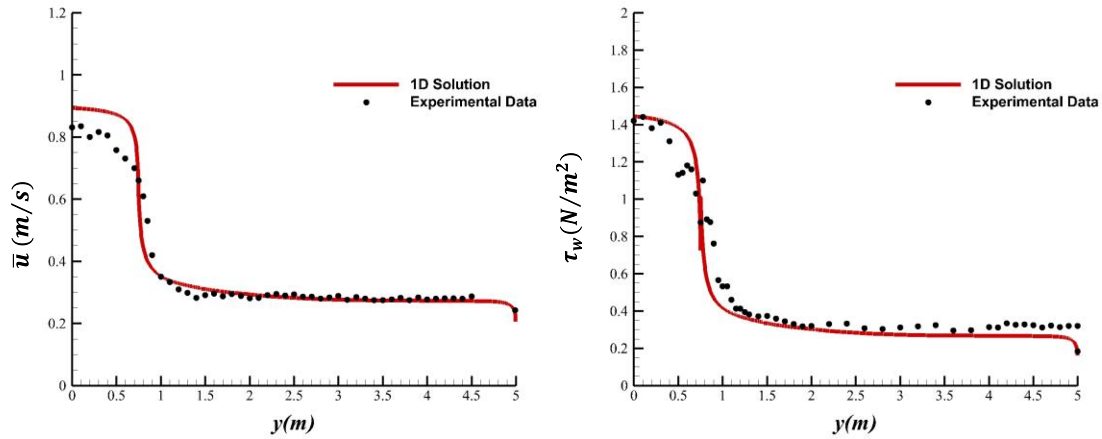


***Figure 4-5*** Comparison between 1D and experimental lateral distributions of $\bar{u}$ and $\tau_w$ for flow depth of H=176 mm in the rectangular compound channel (FCF Series 01).

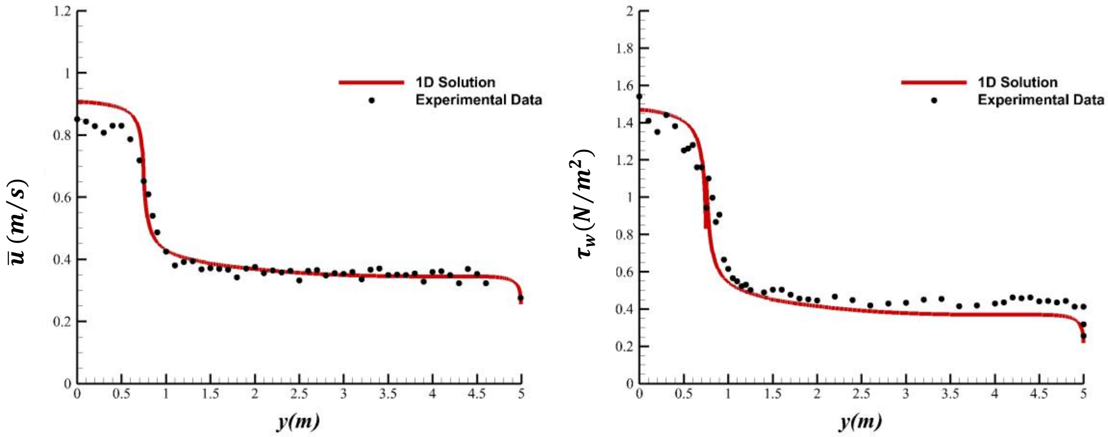


***Figure 4-6*** Comparison between 1D and experimental lateral distributions of $\bar{u}$ and $\tau_w$ for flow depth of H=186 mm in the rectangular compound channel (FCF Series 01).

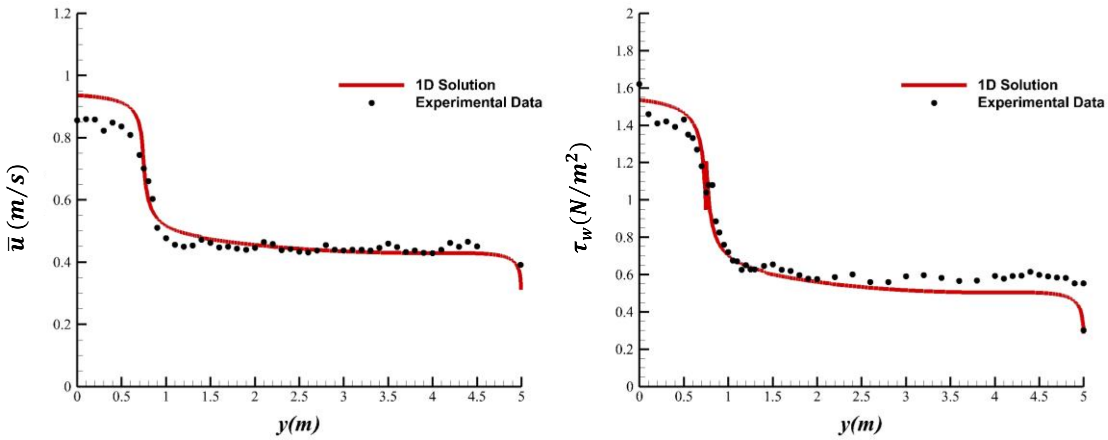


***Figure 4-7*** Comparison between 1D and experimental lateral distributions of $\bar{u}$ and $\tau_w$ for flow depth of H=200 mm in the rectangular compound channel (FCF Series 01).

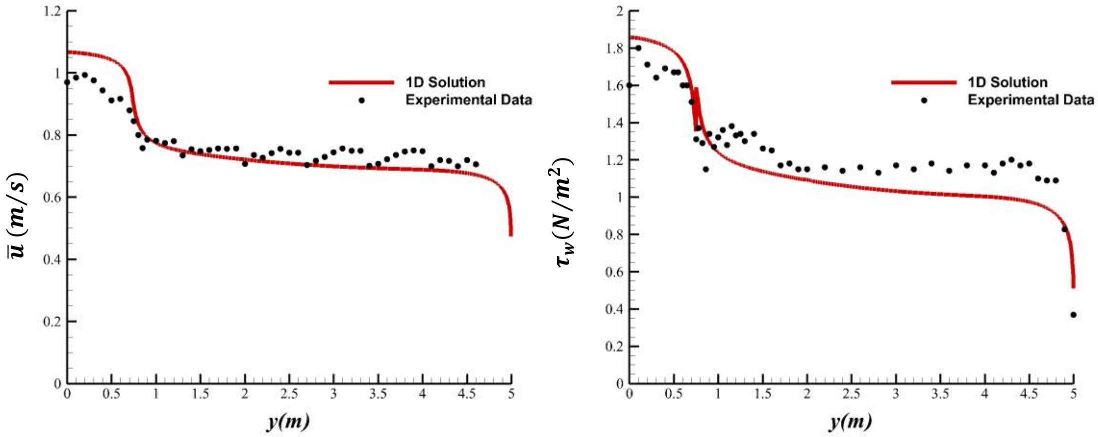


***Figure 4-8*** Comparison between 1D and experimental lateral distributions of $\bar{u}$ and $\tau_w$ for flow depth of H= 250 mm in the rectangular compound channel (FCF Series 01).

### 4.2.2 FCF Experiment 2

FCF experiment series 02 is a symmetric rectangular cross section with bed slope of 0.001027. Cross section is given below.

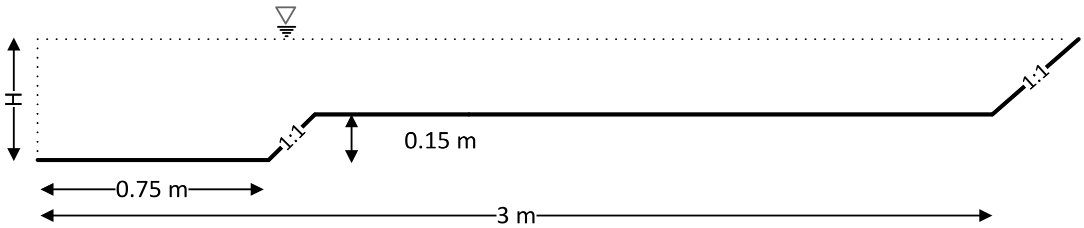


***Figure 4-9*** Cross section for FCF Series 02

Solutions for different water depths are used to compare the depth averaged velocity and shear stress distributions and results given in Figs. (4-10 ~ 4-15).

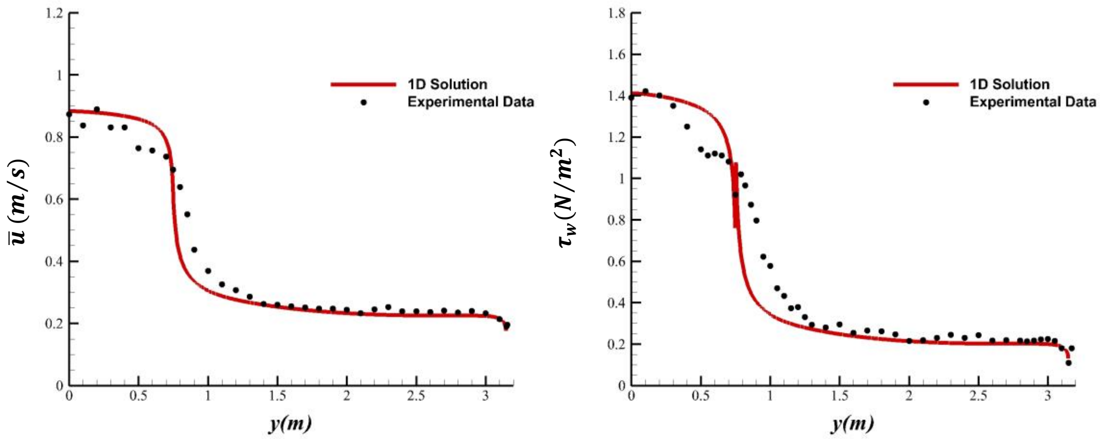


***Figure 4-10*** Comparison between 1D and experimental lateral distributions of $\bar{u}$ and $\tau_w$ for flow depth of H=170 mm in the rectangular compound channel (FCF Series 02).

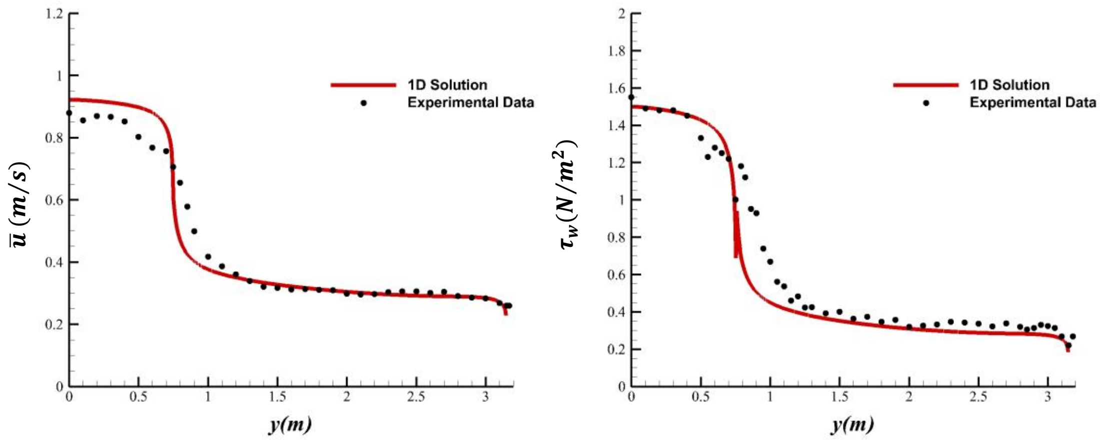


***Figure 4-11*** Comparison between 1D and experimental lateral distributions of $\bar{u}$ and $\tau_w$ for flow depth of H= 178 mm in the rectangular compound channel (FCF Series 02).

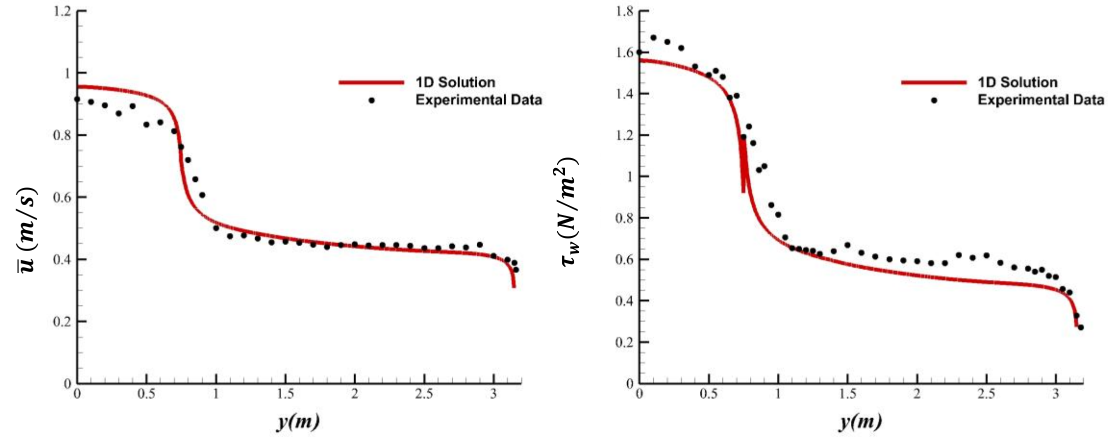


***Figure 4-12*** Comparison between 1D and experimental lateral distributions of $\bar{u}$ and $\tau_w$ for flow depth of H= 198 mm in the rectangular compound channel (FCF Series 02).

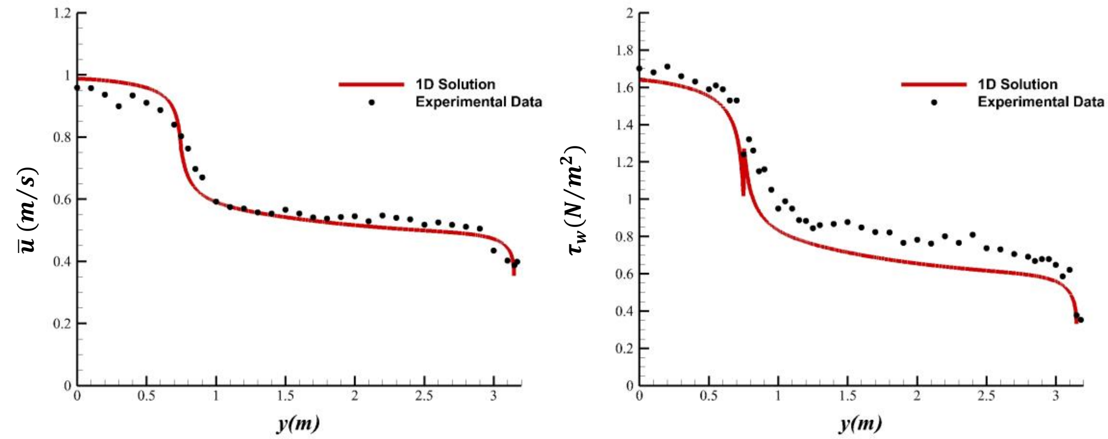


***Figure 4-13*** Comparison between 1D and experimental lateral distributions of $\bar{u}$ and $\tau_w$ for flow depth of H= 210 mm in the rectangular compound channel (FCF Series 02).

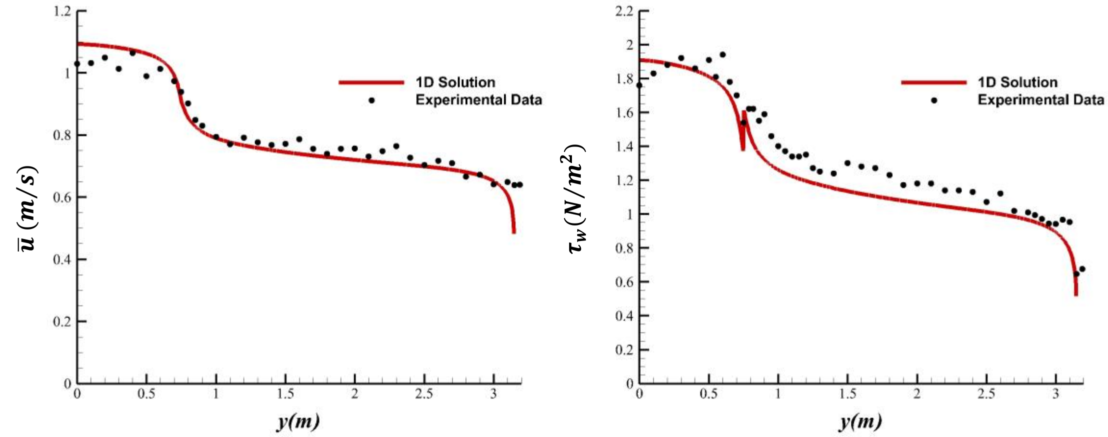


***Figure 4-14*** Comparison between 1D and experimental lateral distributions of $\bar{u}$ and $\tau_w$ for flow depth of H= 250 mm in the rectangular compound channel (FCF Series 02).

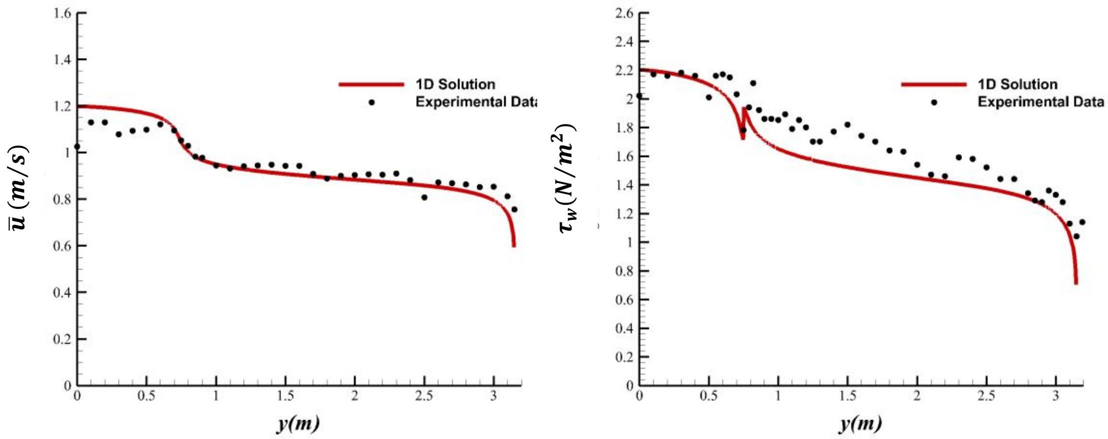


***Figure 4-15*** Comparison between 1D and experimental lateral distributions of $\bar{u}$ and $\tau_w$ for flow depth of H= 290 mm in the rectangular compound channel (FCF Series 02).

### 4.2.3 FCF Experiment 3

FCF experiment series 03 is a symmetric rectangular cross section with bed slope of 0.001027. Cross section is given below.

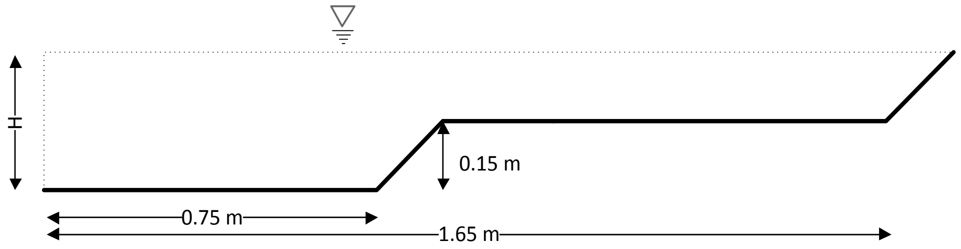


***Figure 4-16*** Cross section for FCF Series 03

Solutions for different water depth are used to compare the depth averaged velocity and shear stress distributions and results given in Figs. (4-17 ~ 4-20).

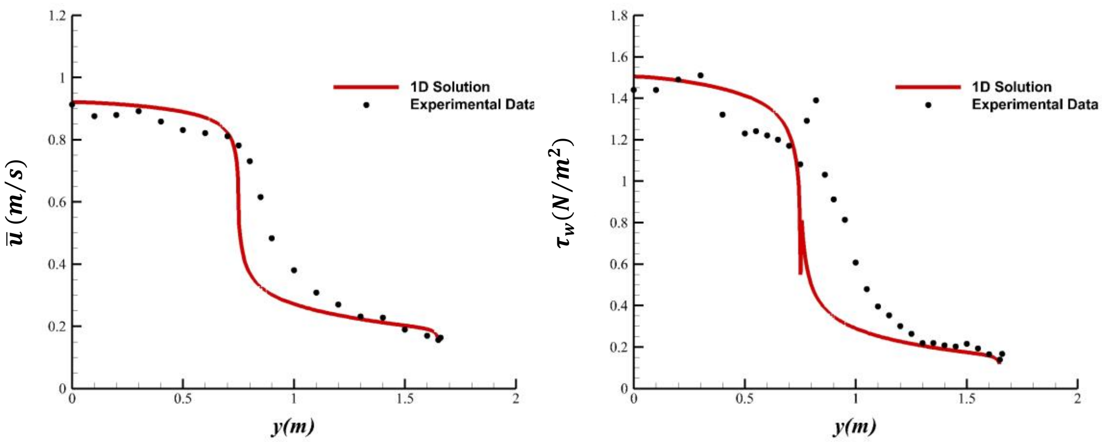


***Figure 4-17*** Comparison between 1D and experimental lateral distributions of $\bar{u}$ and $\tau_w$ for flow depth of H= 170 mm in the rectangular compound channel (FCF Series 03).

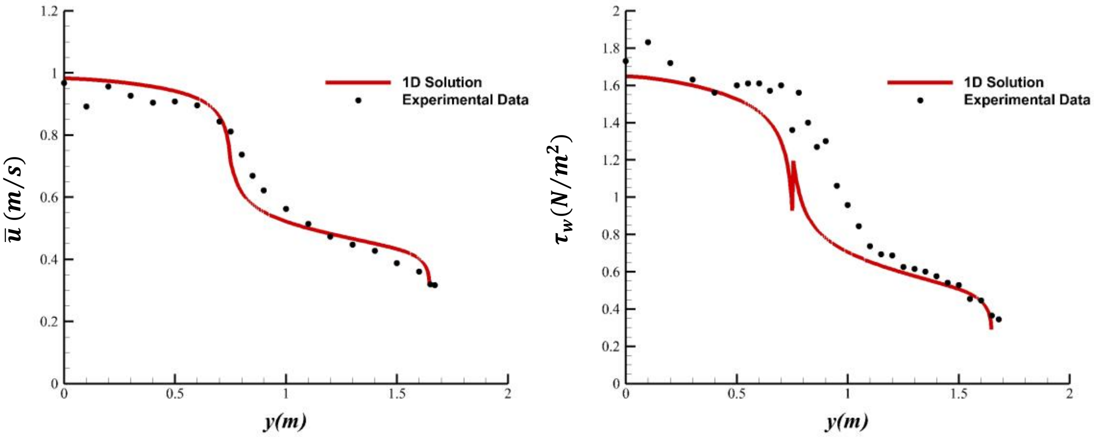


***Figure 4-18*** Comparison between 1D and experimental lateral distributions of $\bar{u}$ and $\tau_w$ for flow depth of H= 200 mm in the rectangular compound channel (FCF Series 03).

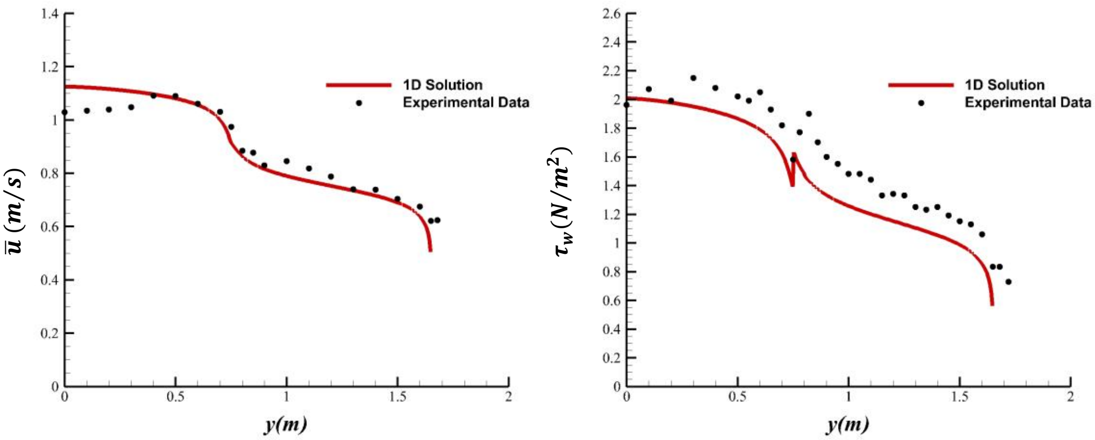


***Figure 4-19*** Comparison between 1D and experimental lateral distributions of $\bar{u}$ and $\tau_w$ for flow depth of H= 250 mm in the rectangular compound channel (FCF Series 03).

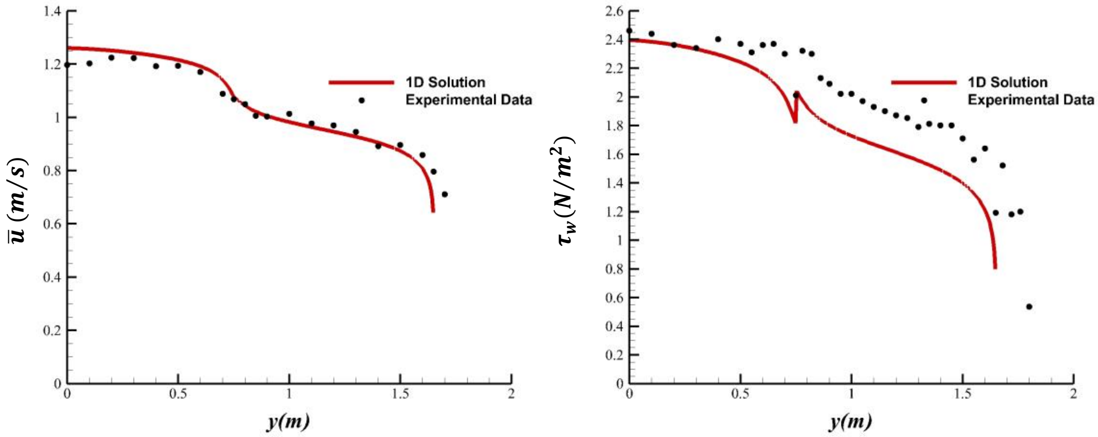


***Figure 4-20*** Comparison between 1D and experimental lateral distributions of $\bar{u}$ and $\tau_w$ for flow depth of H= 300 mm in the rectangular compound channel (FCF Series 03).

### 4.2.4 FCF Experiment 6

FCF experiment series 06 is a non-symmetric rectangular cross section with bed slope of 0.001027. Cross section is given below.

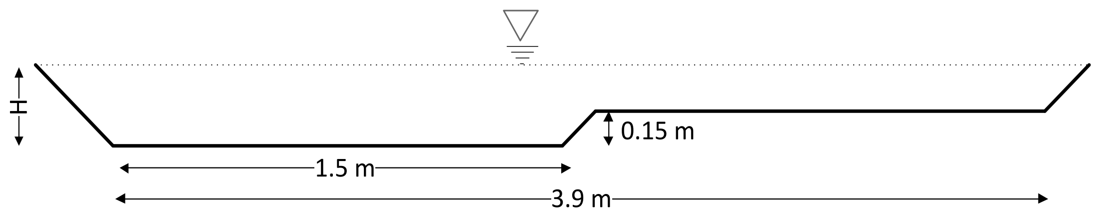


***Figure 4-21*** Cross section for FCF Series 06

Solutions for different water depths are used to compare the depth averaged velocity and shear stress distributions and results given in Figs. (4-22 ~ 4-26).

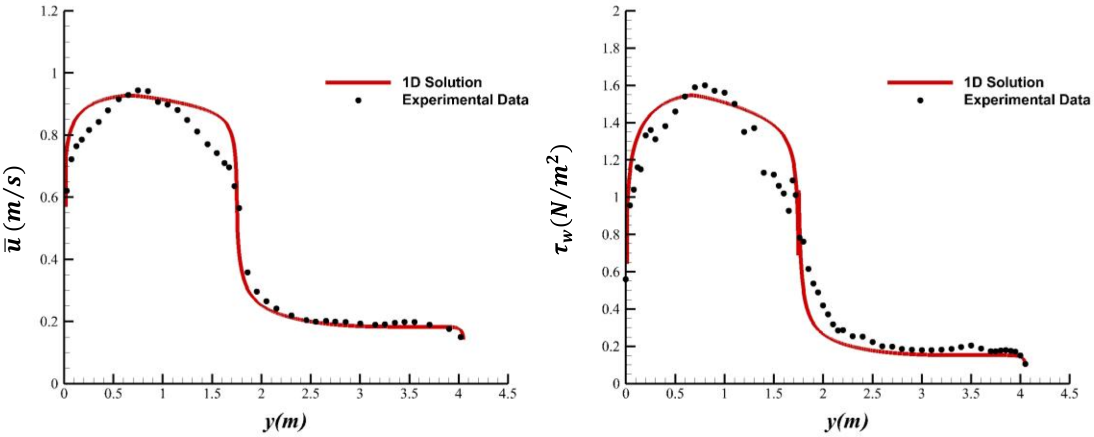


***Figure 4-22*** Comparison between 1D and experimental lateral distributions of $\bar{\boldsymbol{u}}$ and $\tau_w$ for flow depth of H= 165 mm in the rectangular compound channel (FCF Series 06).

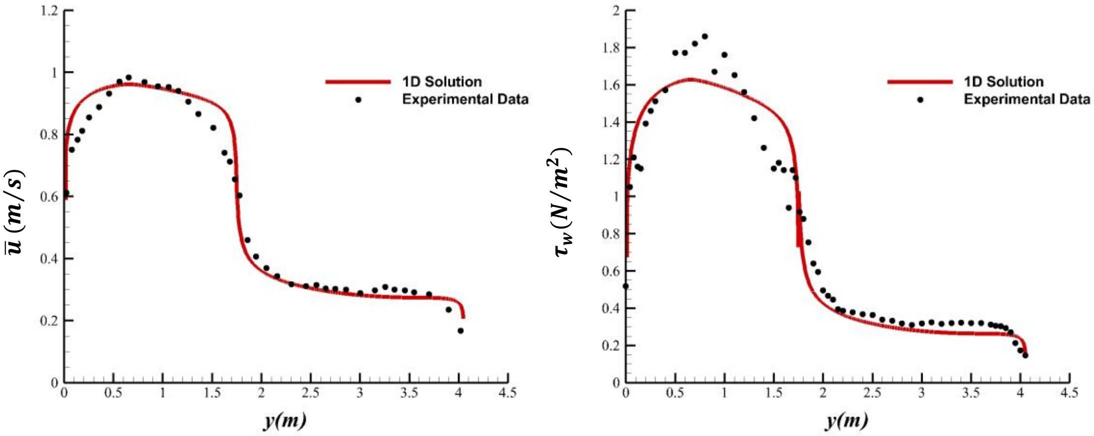


***Figure 4-23*** Comparison between 1D and experimental lateral distributions of $\bar{\boldsymbol{u}}$ and $\tau_w$ for flow depth of H= 175 mm in the rectangular compound channel (FCF Series 06).

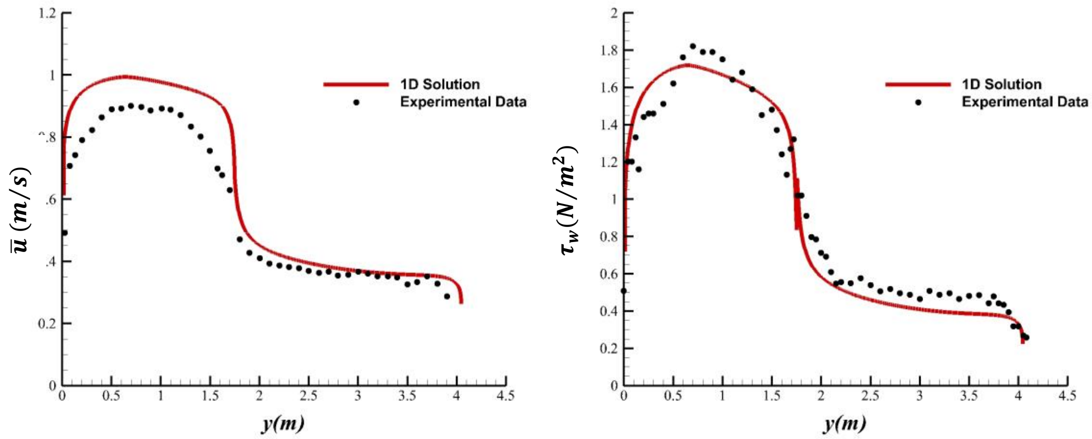


***Figure 4-24*** Comparison between 1D and experimental lateral distributions of $\bar{u}$ and $\tau_w$ for flow depth of H= 190 mm in the rectangular compound channel (FCF Series 06).

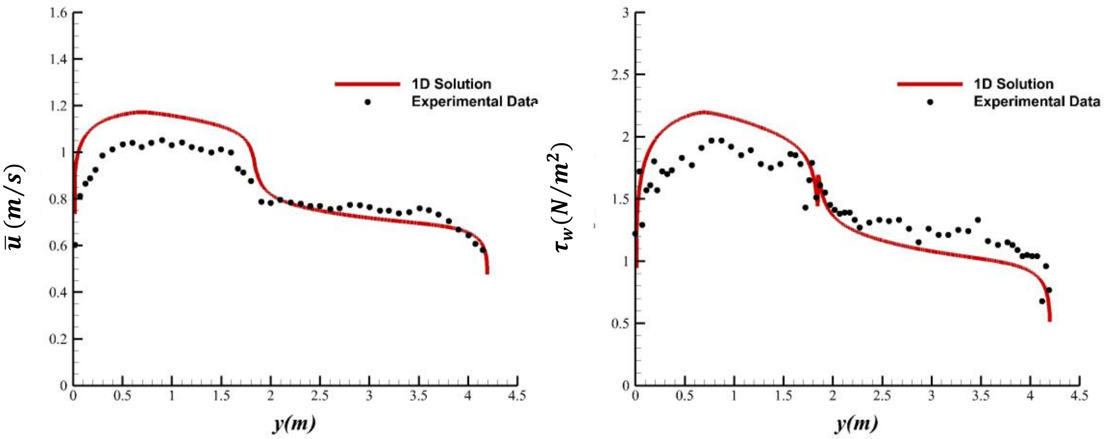


***Figure 4-25*** Comparison between 1D and experimental lateral distributions of $\bar{u}$ and $\tau_w$ for flow depth of H= 250 mm in the rectangular compound channel (FCF Series 06).

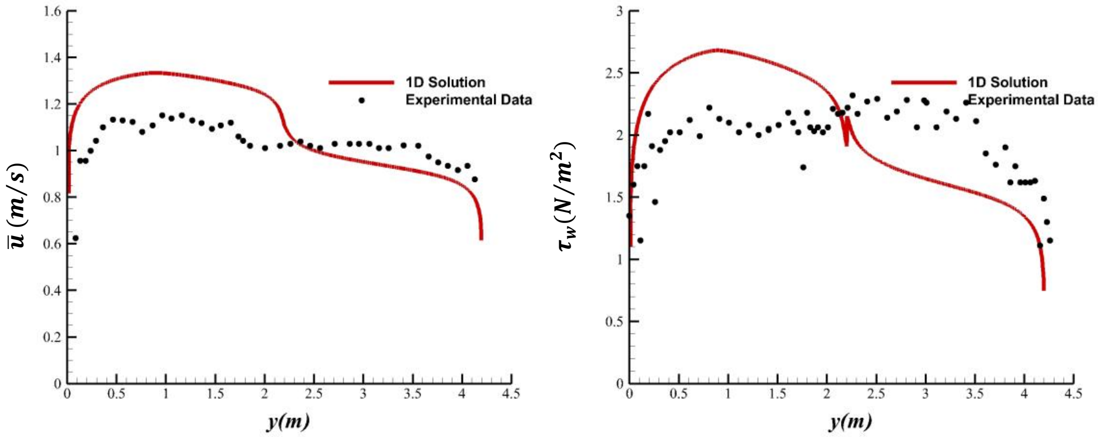


***Figure 4-26*** Comparison between 1D and experimental lateral distributions of $\bar{u}$ and $\tau_w$ for flow depth of H= 300 mm in the rectangular compound channel (FCF Series 06).

### 4.2.5 FCF Experiment 8

FCF experiment series 08 is a symmetric rectangular cross section with bed slope of 0.001027. Cross section is given below.

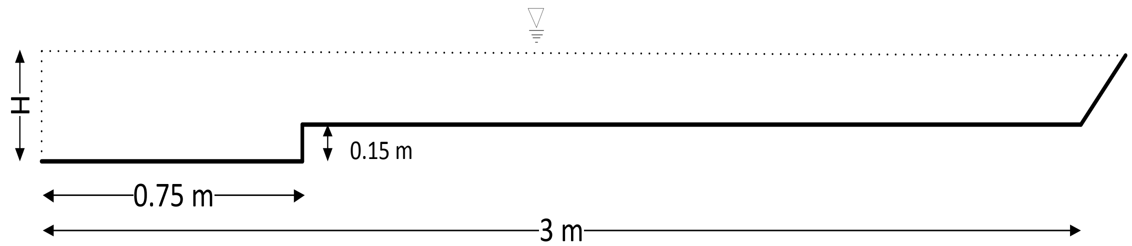


***Figure 4-27*** Cross section for FCF Series 08

Solutions for different water depths are used to compare the depth averaged velocity and shear stress distributions and results given in Figs. (4-28 ~ 4-34).

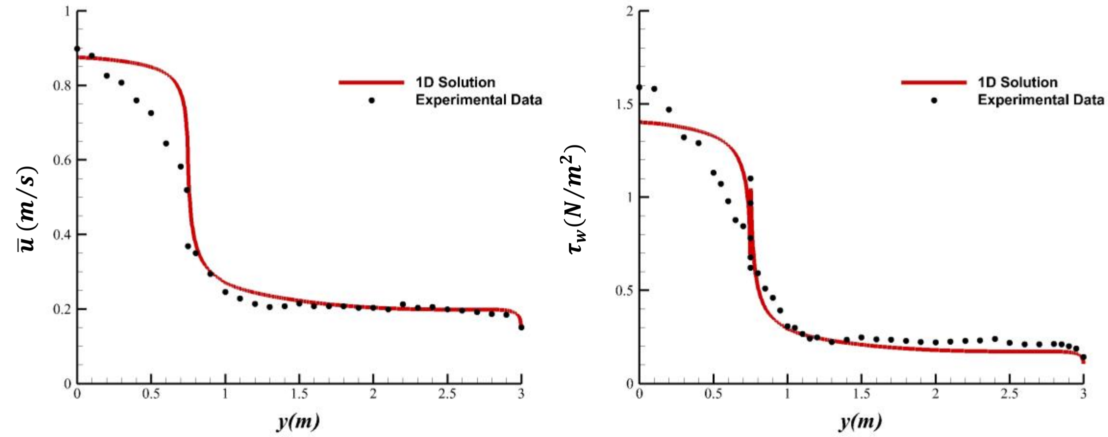


***Figure 4-28*** Comparison between 1D and experimental lateral distributions of $\bar{u}$ and $\tau_w$ for flow depth of H= 167 mm in the rectangular compound channel (FCF Series 08).

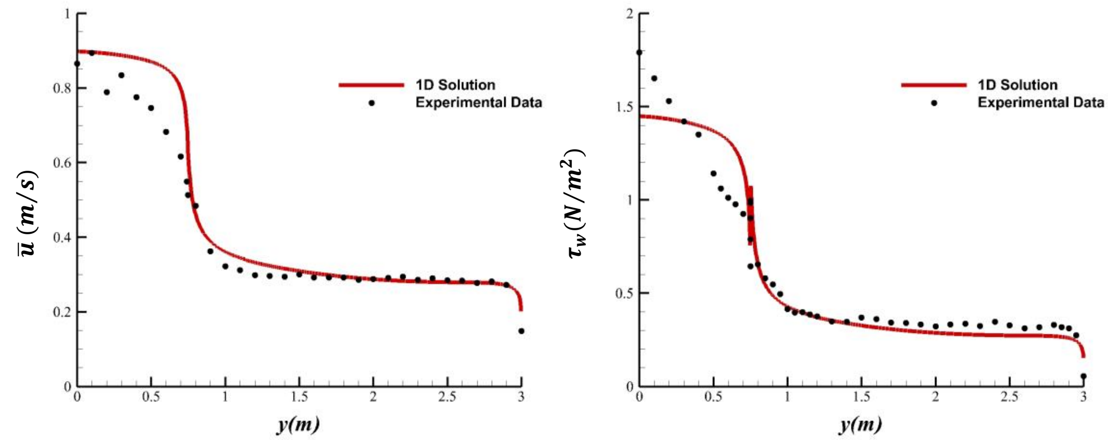


***Figure 4-29*** Comparison between 1D and experimental lateral distributions of $\bar{u}$ and $\tau_w$ for flow depth of 175 mm in the rectangular compound channel (FCF Series 08).

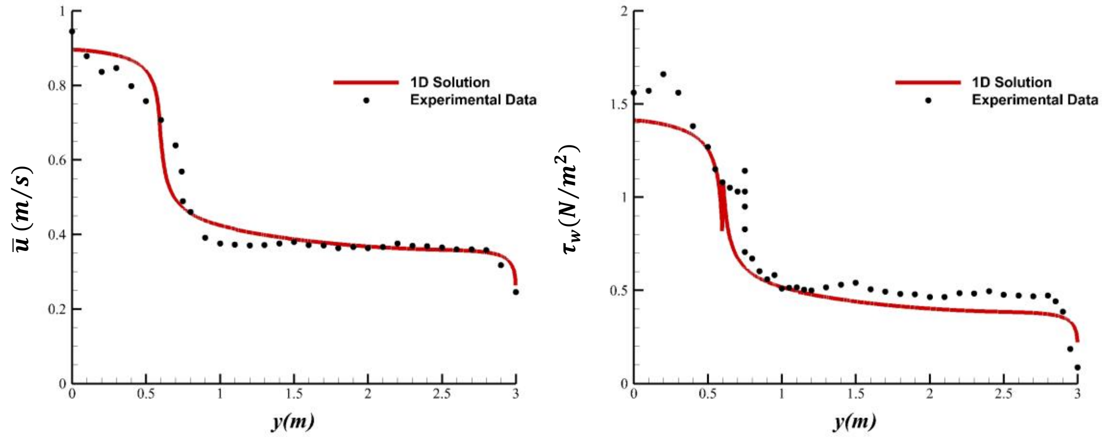


***Figure 4-30*** Comparison between 1D and experimental lateral distributions of $\bar{\boldsymbol{u}}$ and $\tau_w$ for flow depth of H= 188 mm in the rectangular compound channel (FCF Series 08).

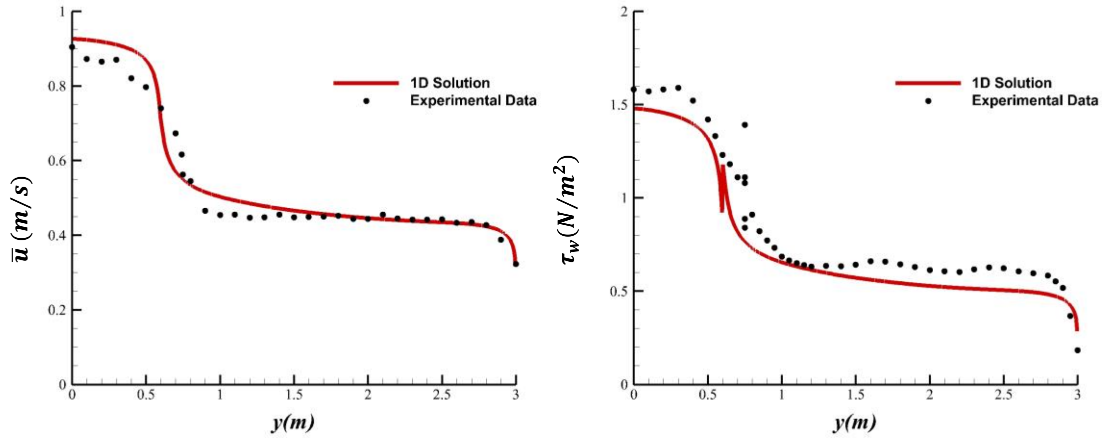


***Figure 4-31*** Comparison between 1D and experimental lateral distributions of $\bar{\boldsymbol{u}}$ and $\tau_w$ for flow depth of H= 200 mm in the rectangular compound channel (FCF Series 08).

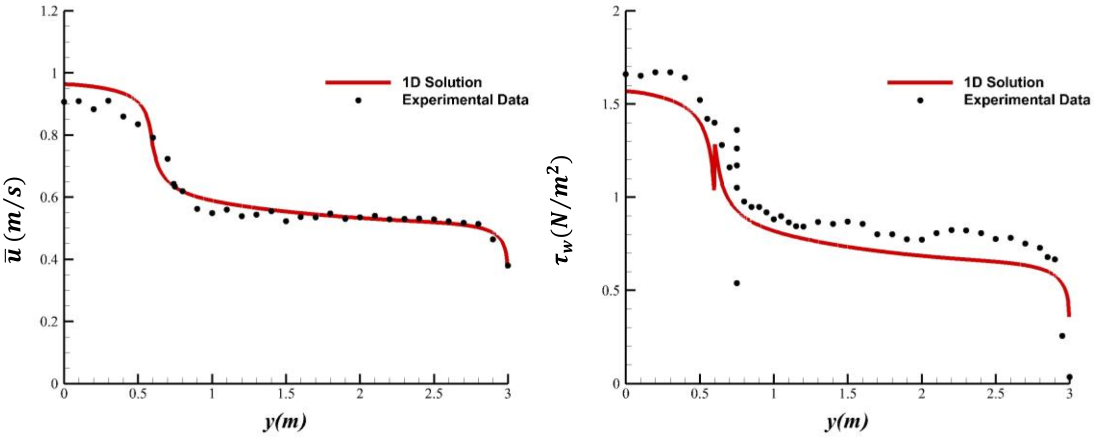


***Figure 4-32*** Comparison between 1D and experimental lateral distributions of $\bar{u}$ and $\tau_w$ for flow depth of H= 215 mm in the rectangular compound channel (FCF Series 08).

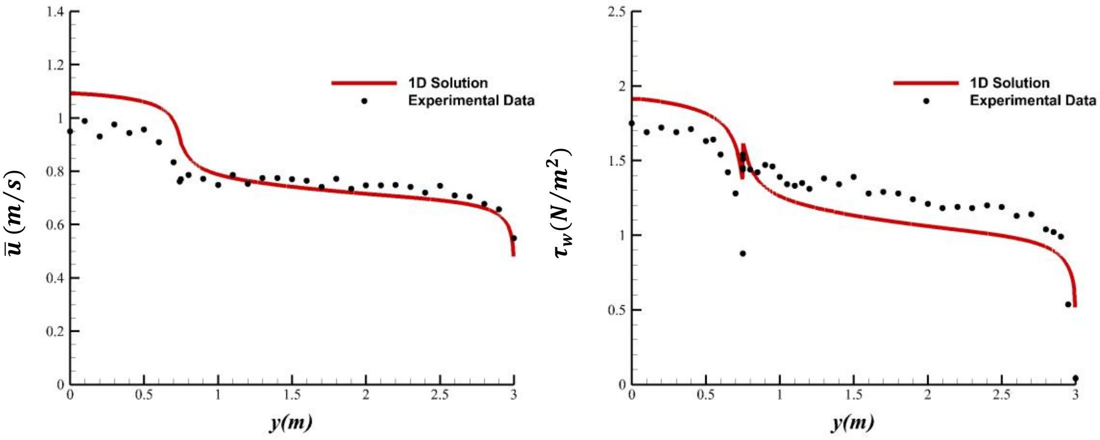


***Figure 4-33*** Comparison between 1D and experimental lateral distributions of $\bar{u}$ and $\tau_w$ for flow depth of H= 250 mm in the rectangular compound channel (FCF Series 08).

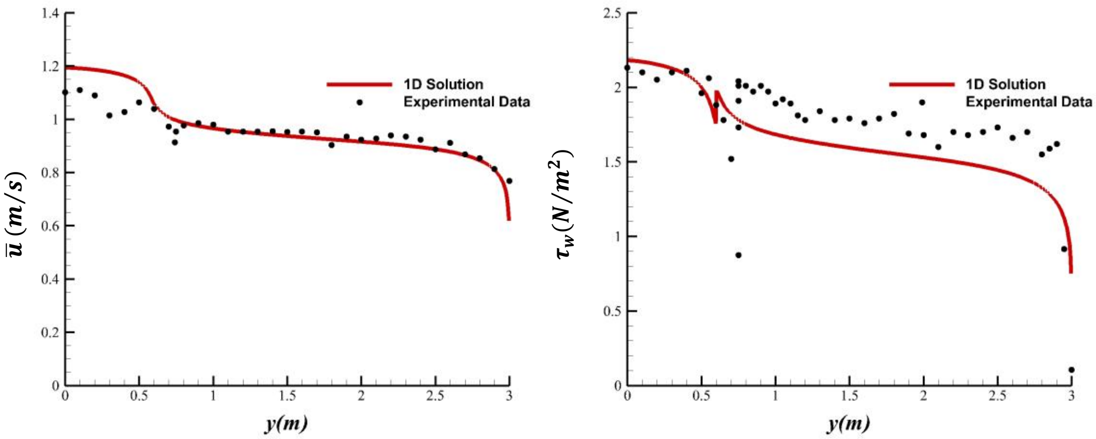


***Figure 4-34*** Comparison between 1D and experimental lateral distributions of $\bar{u}$ and $\tau_W$ for flow depth of H= 300 mm in the rectangular compound channel (FCF Series 08).

Comparisons of velocity and shear stresses of 1D model with experimental data taken from FCF series in several geometries show that 1D model works well in most cases. Differences may be due to inaccuracies in measurement or effect of secondary flows around corners.

## 4.3 Discharge Comparison

Discharge comparison is performed in the main channel and flood plain separately in order to observe 1D model behavior to predict the discharge in the channel. Experimental smooth channel with symmetrical rectangular flood plain (Fig.3-14) data taken from (Knight & Demetriou, 1983) are compared with 1D model. The section mean velocities are used to calculate the discharges in each subarea and were divided by total discharge through the entire cross section. A relative height is defined to observe the relation between the step and the discharge;

$$\text{Relative Height} = (H\text{-}h)/h \tag{4-1}$$

Discharge in the channel geometry is divided into two such as main channel and flood plain and comparisons are done according to parameters listed below.

- $Q_{mc,e}$: Measured discharge in main channel
- $Q_{mc}$ : Calculated discharge in main channel with 2 dimensional model
- $Q_{f,e}$ : Measured discharge in side channel
- $Q_f$ : Calculated discharge in side channel with 2 dimensional model

Relative depth *(H-h)/H* vs. % of total flow is plotted for $B/b$ values of 2, 3, 4 and results are given below for flood plain and main channel.

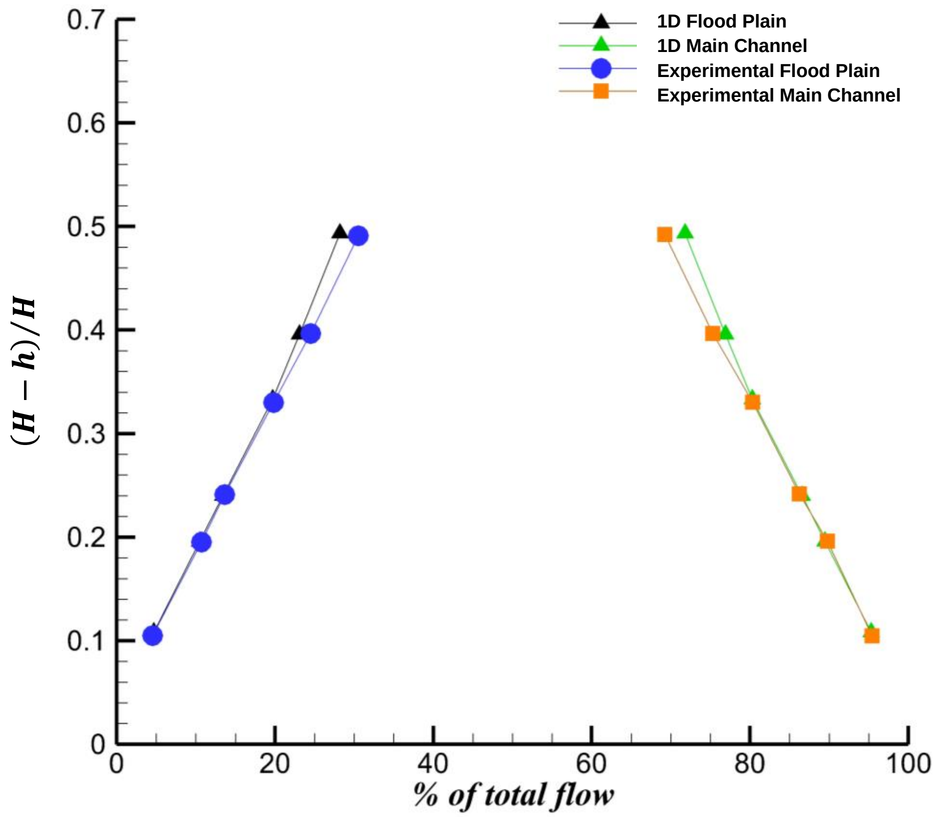


***Figure 4-35*** Percentage of total flow in main channel and flood plains, $B/H = 2$

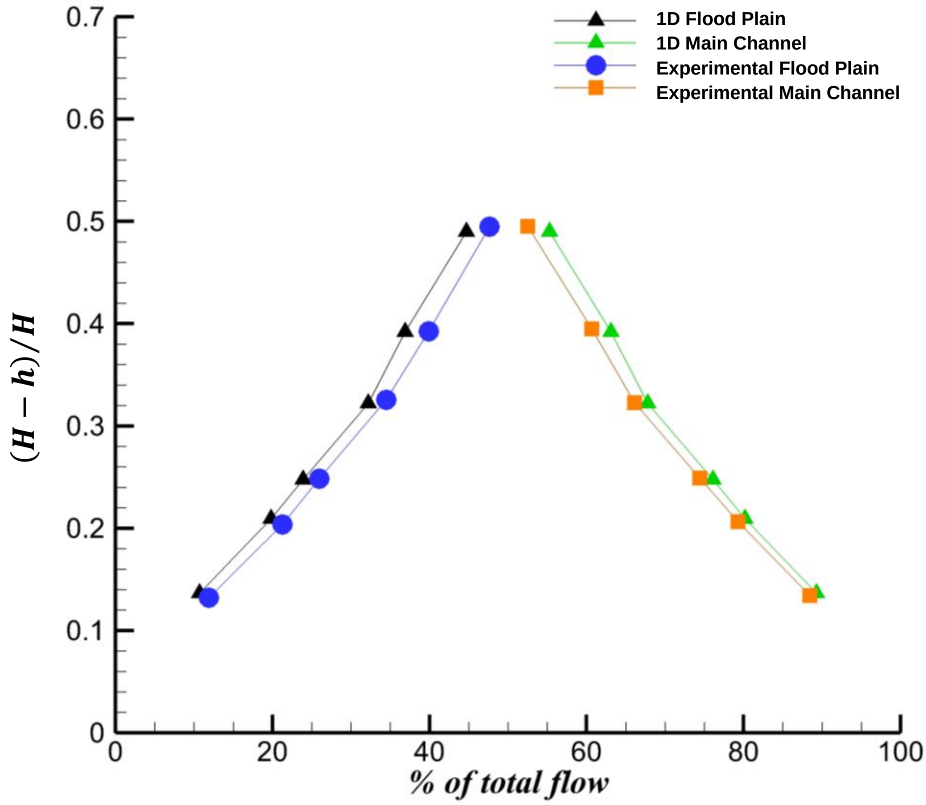


***Figure 4-36*** Percentage of total flow in main channel and flood plains, $B/H = 3$

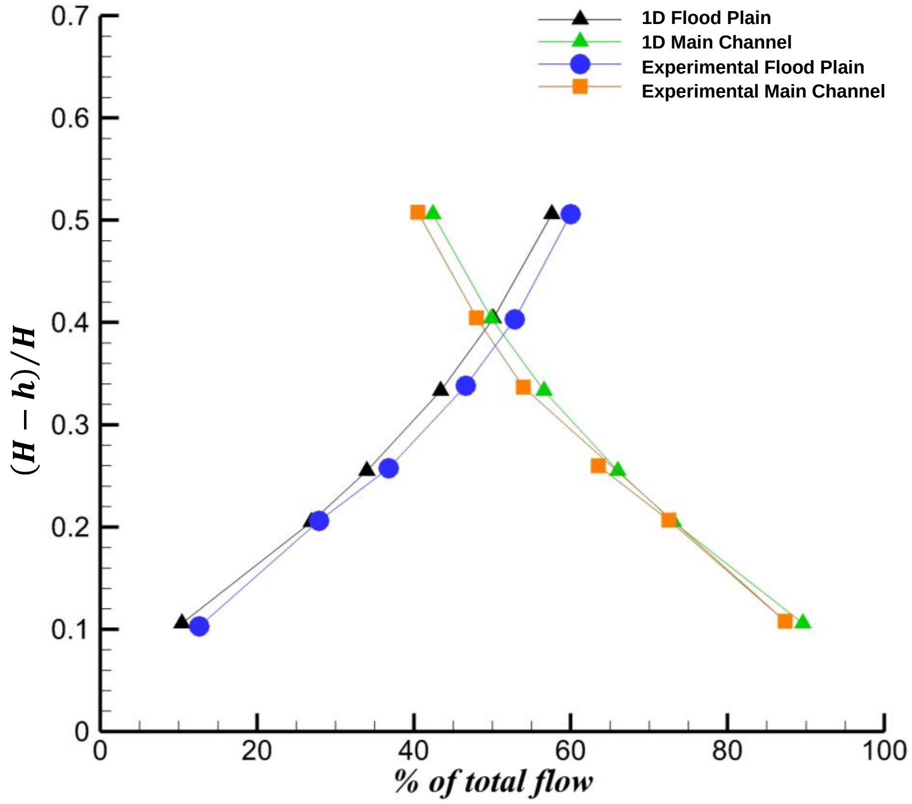


***Figure 4-37*** Percentage of total flow in main channel and flood plains, $B/H = 4$

In all cases, calculated error when comparing measured data with 1D model is not more than 5 percent. This states that 1D model is robust for predicting discharge in flood plain and main channel separately. However, differences in computed and measured values might be inaccuracies in experimental setup, measurement error as well as error in numerical computation of 1D model.

## 4.4 Effect of bed slope

It has been shown using experimental data that 1D model can be applied to straight compound channels. There is also a need to validate the model for different channel bed slopes. For this, model is compared with experimental data taken from Lambert & Myers (1998). There are three different channel geometries given in Fig.(4-38).

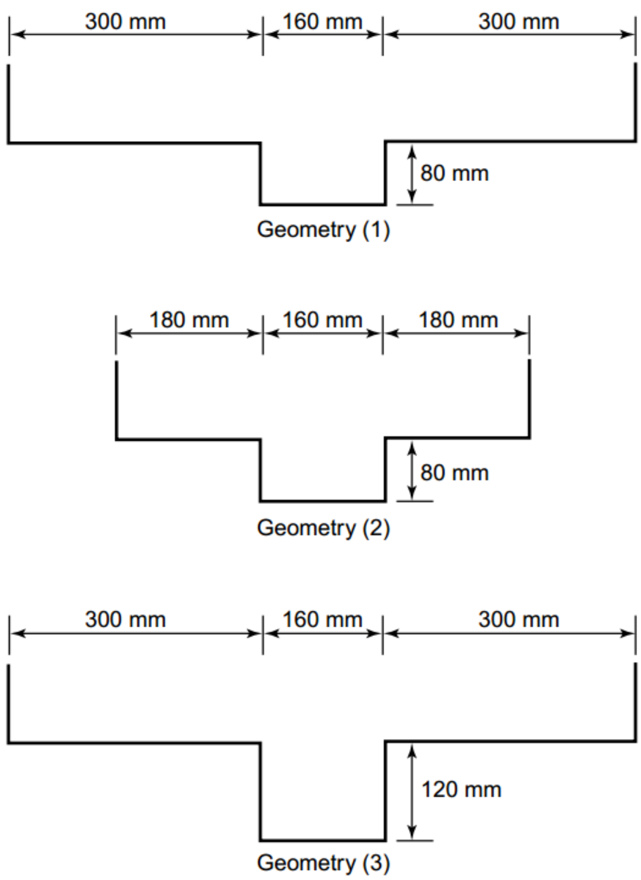


***Figure 4-38*** Three compound channel geometries used in comparison (Lambert & Myers, 1998)

Lambert & Myers (1998) investigated discharge in three compound channel cross-sections, each consisting of a deep main channel section and two adjacent flood-plains with bed slopes ranged from 0.00037 to 0.0019. Same geometries and bed slopes are defined to the 1D model and results are compared with experimental data.

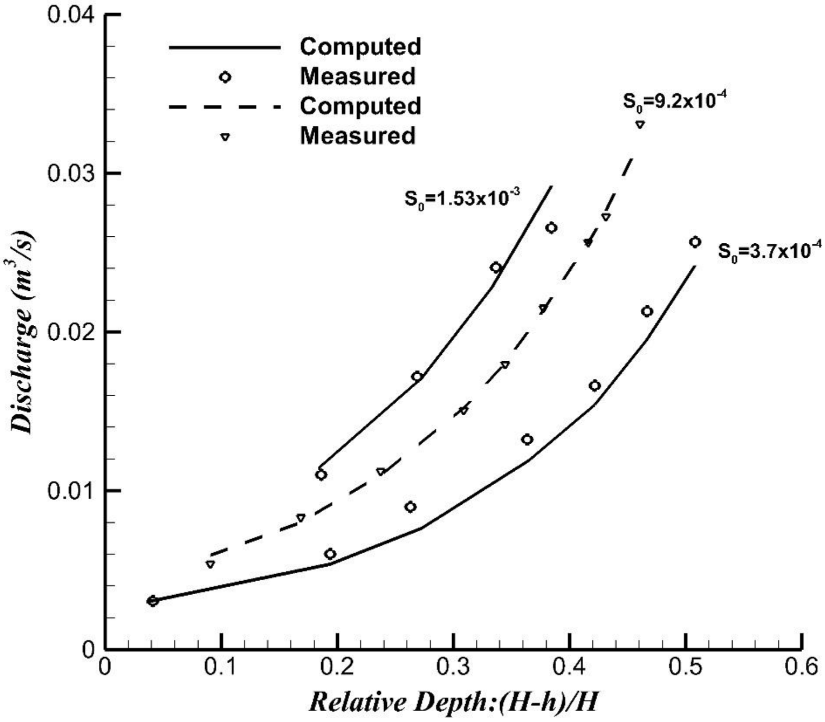


***Figure 4-39*** Comparison of measured discharges, geometry 1

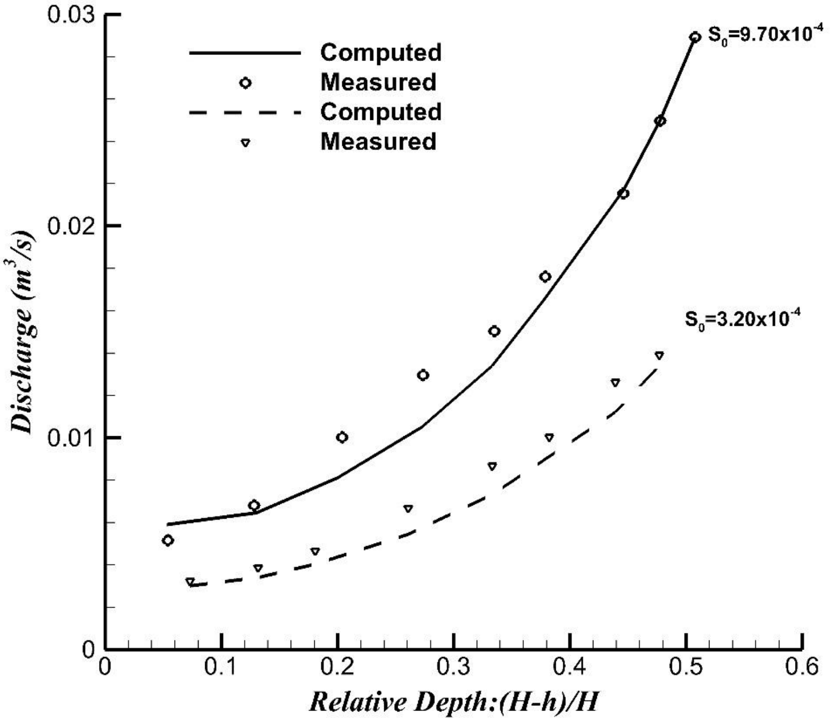


***Figure 4-40*** Comparison of observed discharges, geometry 2

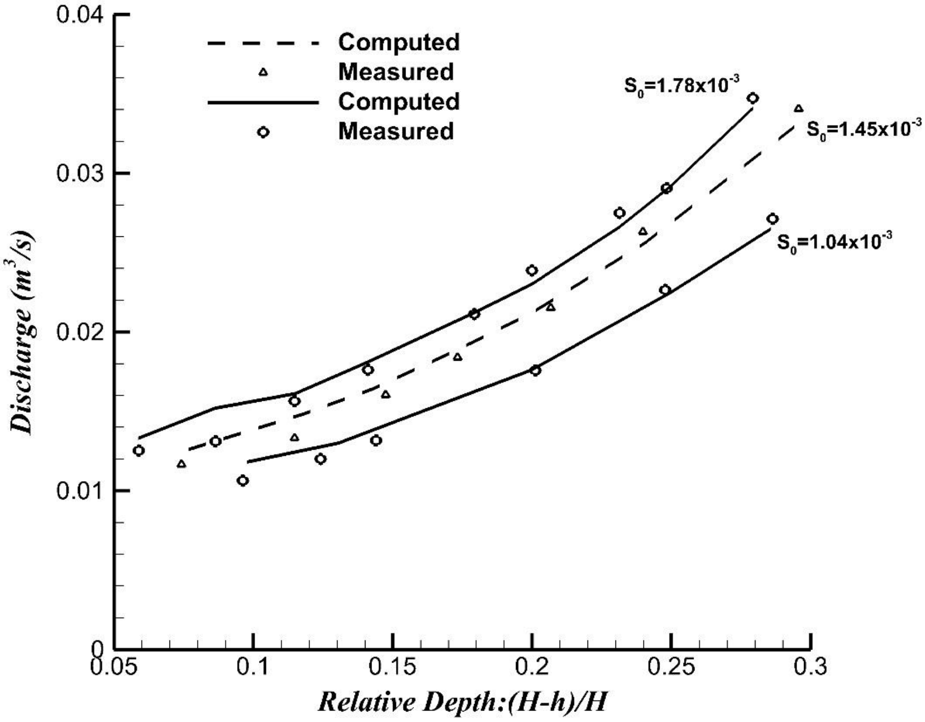


***Figure 4-41*** Comparison of observed discharges, geometry 3

The three figures show that 1D depth averaged model (shown by solid lines) is capable of closely predicting the measured data over all bed slopes examined and for the three different channel geometries.

# CHAPTER 5

# CONCLUSIONS

1D depth averaged shallow water model is developed for steady, uniform channel flow. Turbulence model is formed by volumetric mixing length model using depth averaging over 2-dimensional flow domain. Vertical boundaries were extended to infinity as in the case of parallel plates and horizontal boundaries were discarded in mixing length computations. An empirical formula was developed for the shear stress on the vertical wall boundaries. Wall shear stresses on horizontal boundaries are modelled by using a modified wall function.

Velocity, bottom shear stress and discharge comparisons are performed with 2D solutions and measured data available in the literature. It has been shown that 1D depth averaged model is capable of successfully representing the mean velocity and bed shear stress distributions regardless of the type of the geometry. It has also shown that the 1D model works well at different scales, pressure gradients and different channel bed slopes. However, in narrower domains where width to depth ratio is less than 5, shallow water assumption is not fully satisfied and 1D depth averaged model gives only approximate predictions. When shallow water assumption is valid, model is very robust for predicting lateral velocity distribution, wall shear stress and discharge in any cross section geometry.

Present study introduces a 1D model with mixing length turbulence model for uniform flow in channels of any cross section. The robustness of present model is that it is applicable to any kind of geometry including natural channels. The depth averaged volumetric mixing length is able to introduce some 3D effects into

1D solution and thus provides more accurate prediction over bed level discontinuities.

# REFERENCES


Aydın, I. (2004). International Symposium on Shallow Flows. *Uniform flow computations in natural open channels*, (pp. 299-304).

Aydin, I. (2009). Nonlinear Mixing Length Model for Prediction of Secondary Currents in Uniform Channel Flows. *Journal of Hydraulic Engineering*, pp. 146–153.

Environment, D. W. (2010). DHI Simulation Engine for MOUSE and MIKE 11.

Finnie, J., Donnell, B., Letter, J., & Bernard, R. S. (1999). Secondary flow correction for depth-averaged flow calculations. *Journal of Engineering Mechanics*, 848–863.

*Flood Channel Facility*. (2013). Retrieved from www.flowdata.bham.ac.uk (Last acessed on 09.09.2014)

Knight, D. W., & Demetriou, J. D. (1983). Flood Plain and main channel flow interaction. *Journal of Hydraulic Engineering*, 1073-1092.

Knight, D. W., & Patel, H. S. (1985). Boundary shear in smooth rectangular ducts. *Journal of Hydraulic Engineering*, 29-47.

Knight, D. W., Omran, M., & Tang, X. (2006). Modeling Depth-Averaged Velocity and Boundary Shear in Trapezoidal Channels with Secondary Flows. *Journal of Hydraulic Engineering*, 39–47.

Knight, Donald W; Omran, Mazen; Tang, Xiaonan. (2006). Modeling Depth-Averaged Velocity and Boundary Shear in Trapezoidal Channels with Secondary Flows. *Journal of Hydraulic Engineering*, 39–47.

Kudela, H. (2012). Turbulent flow Modelling.

Lambert, M. F., & Myers, W. R. (1998). Proceedings of the ICE - Water Maritime and Energy. *Estimating the discharge capacity in traight compound channels,* (pp. 84-94).

Launder, B. E., & Ying, W. M. (1972). Secondary flows in ducts of square cross-section. *Journal of Fluid Mechanics*, 289-295.

Monty, J. P. (2005). *Developments In Smooth Wall Turbulent Duct Flows Phd thesis.* Melbourne: The University of Melbourne.

Pierce, F. J., & Zimmerman, B. B. (1973). Wall Shear Stress Inference From Two and Three-Dimensional Turbulent Boundary Layer Velocity Profiles. *Journal of Fluids Engineering*, pp. 1-165.

Sellin, R. J., Ervine, D. A., & Willetts, B. B. (1993). Proceedings of the ICE - Water Maritime and Energy. *Behaviour of meandering two-stage channels,* (pp. 99-111).

Vreugdenhil, C. B. (1994). *Numerical Methods for Shallow-Water Flow.* Netherland: Kluwer Academic Publishers.

Wang, Z. Q., & Cheng, N. S. (2005). Secondary flows over artificial bed strips. *Advances in Water Resources*, 441-450.

Wright, J. (2000, April). The Nation's Responses To Flood Disasters: A Historical Account. Madison, WI.

Yue, W., Lin, C.-L., & Patel, V. C. (2003). *Numerical Investigations Of Turbulent Free Surface Flows Using Level Set Method and Large Eddy Simulation.* IIHR, Hydroscience & Engineering College of Engineering , Iowa City.

## APPENDICES

### A. INTEGRATION OF VOLUMETRIC LENGTH SCALE

Volumetric length scale is calculated by using Eq.(1-10). Surface integral in the denominator must be evaluated over a discretized boundary (Aydin, 2009)

$$\int \frac{dA_r}{r^3} = I = \int \frac{ds\, cos\, \gamma dx cos\beta}{r^3} = \int \frac{\frac{r_0}{r_x}\frac{r_x}{r}\, dxds}{r^3} = r_0 \int_{s_a}^{s_c} \left( \int_{-\infty}^{\infty} \frac{dx}{r^4} \right) ds \tag{A-1}$$

$$I = r_0 \int_{s_a}^{s_c} \left( \int_{-\infty}^{\infty} \frac{dx}{(x^2 + r_x^2)^2} \right) ds = r_0 \int_{s_a}^{s_c} \frac{\pi}{2r_x^3} ds \tag{A-2}$$

$$I = \frac{\pi r_0}{2} \int_{s_a}^{s_c} \frac{ds}{(s^2 + r_0^2)^{3/2}} = \frac{\pi r_0}{2r_0} \left[ \frac{s_c}{\sqrt{s_c^2 + r_0^2}} - \frac{s_a}{\sqrt{s_a^2 + r_0^2}} \right] \tag{A-3}$$

$$s_a = (a^2 - c^2 - e^2)/2c \quad s_c = s_a + e \quad r_0 = \sqrt{a^2 - s_a^2} \tag{A-4}$$

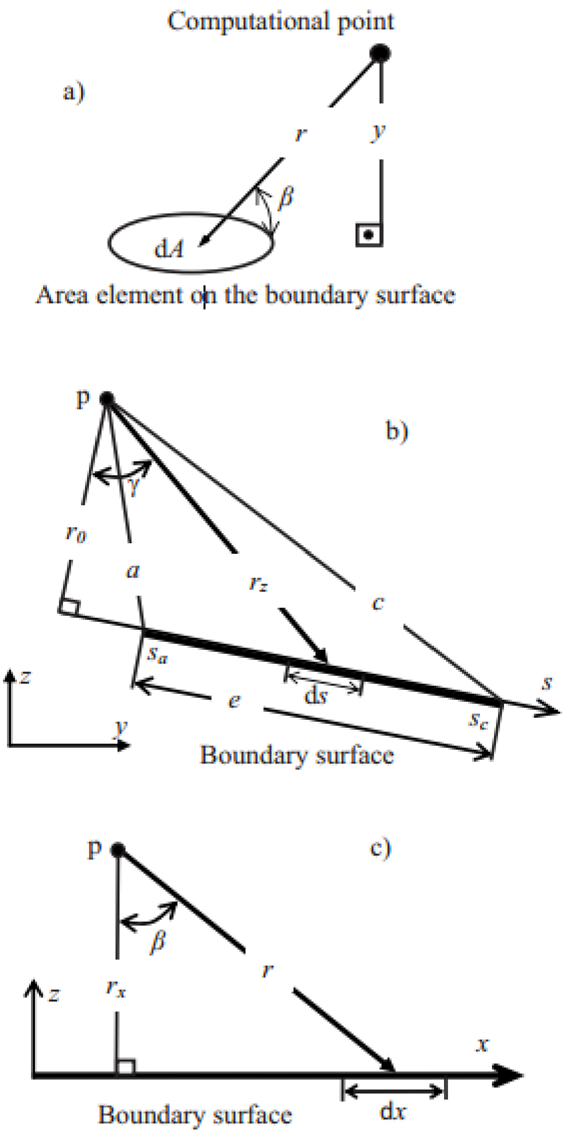


***Figure A-1*** Description of parameters of mixing length: (a) Definition of mixing length; (b) integration on y-z plane; and (c) integration on x-z plane

# B. NUMERICAL SOLUTIONS

## B.1 Numerical Solution of eq.(2-10) in Uniform Duct Flow

Eq.(3-5) forms a tridiagonal matrix and can be solved by using Thomas Algorithm given as;

$$-A_i u_{i+1} + B_i u_i - C_i u_{i-1} = D_i \tag{B-1}$$

Writing terms in Eq.(3-5) according to Eq.(4.1);

$$A_i = \frac{\bar{v}_{e_{i+1}}}{\Delta y} \tag{B-2}$$

$$C_i = \frac{\bar{v}_{e_i}}{\Delta y} \tag{B-3}$$

$$B_i = \frac{\bar{v}_{e_{i+1}}}{\Delta y} + \frac{\bar{v}_{e_i}}{\Delta y} + \frac{C_{f_i}\bar{u}_i}{H}\Delta y \tag{B-4}$$

$$D_i = -C_p \Delta y \tag{B-5}$$

<u>Boundary Conditions:</u>

- At i = 1

$$\frac{\bar{v}_{e_2}}{\Delta y}(\bar{u}_2 - \bar{u}_1) - \bar{v}_{e_1}\frac{d\bar{u}}{dy} = \left[C_p + \frac{C_{f_1}\bar{u}_1\bar{u}_1}{H}\right]\Delta y \tag{B-6}$$

Writing

$$\bar{v}_{e_1}\frac{d\bar{u}}{dy} = \bar{\tau}_w \tag{B-7}$$

And rearranging;

$$\bar{v}_{e_2}(\bar{u}_2 - \bar{u}_1) - \bar{\tau}_w = \left[C_p + \frac{C_{f_1}\bar{u}_1\bar{u}_1}{H}\right]\Delta y \tag{B-8}$$

Collecting similar terms yields;

$$A_1 = \frac{\bar{v}_{e_2}}{\Delta y} \tag{B-9}$$

$$C_1 = 0 \tag{B-10}$$

$$B_1 = \frac{\bar{v}_{e_2}}{\Delta y} + \frac{\bar{\tau}_w}{\bar{u}_1} + \frac{C_{f_1}\bar{u}_1}{H}\Delta y \tag{B-11}$$

$$D_1 = -C_p\Delta y \tag{B-12}$$

- At i = N

$$\bar{u}_N = \bar{u}_{N+1} \tag{B-13}$$

$$\bar{v}_{e_{N+1}}(\bar{u}_{N+1} - \bar{u}_N) - \bar{v}_{e_N}(\bar{u}_N - \bar{u}_{N-1}) = \left[C_p + \frac{C_{f_N}\bar{u}_N\bar{u}_N}{H}\right]\Delta y \tag{B-14}$$

$$-\bar{v}_{e_N}(\bar{u}_N - \bar{u}_{N-1}) = \left[C_p + \frac{C_{f_N}\bar{u}_N\bar{u}_N}{H}\right]\Delta y \tag{B-15}$$

Collecting similar terms;

$$A_N = 0 \tag{B-16}$$

$$C_N = \frac{\bar{v}_{e_N}}{\Delta y} \tag{B-17}$$

$$B_N = \frac{\bar{v}_{e_N}}{\Delta y} + \frac{C_{f_N}\bar{u}_N}{H}\Delta y \tag{B-18}$$

$$D_N = -C_p \Delta y \tag{B-19}$$

## B.2 Numerical Solution of Eq.(2-10) in compound duct flow

- ***<u>Side Channel</u>***

$$0 = C_p(H-h) + \frac{\partial \bar{\tau}_{xy}}{\partial y} - \tau_{xz,b} \tag{B-20}$$

$$\frac{\partial}{\partial y}\left(\bar{v}_e \frac{\partial \bar{u}}{\partial y}\right) = -C_p(H-h) + \tau_{xz,b} \tag{B-21}$$

$$\frac{\partial}{\partial y}\left(\bar{v}_e \frac{\partial \bar{u}}{\partial y}\right) = -C_p(H-h) + C_f \bar{u}^2 \tag{B-22}$$

$$\frac{\partial \bar{\tau}}{\partial y} = C_f \bar{u}^2 - C_p(H-h) \tag{B-23}$$

$$\frac{\bar{\tau}_{i+1} - \bar{\tau}_i}{\Delta y} = C_{f_i}\bar{u}_i\bar{u}_i - C_p(H-h) \tag{B-24}$$

$$\bar{\tau}_{i+1} = \bar{v}_{e_{i+1}} \frac{\bar{u}_{i+1} - \bar{u}_i}{\Delta y}(H-h) \tag{B-25}$$

$$\bar{\tau}_i = \bar{v}_{e_i} \frac{\bar{u}_i - \bar{u}_{i-1}}{\Delta y}(H-h) \tag{B-26}$$

$$\bar{v}_{e_{i+1}} \frac{\bar{u}_{i+1} - \bar{u}_i}{\Delta y}(H - h) - \bar{v}_{e_i} \frac{\bar{u}_i - \bar{u}_{i-1}}{\Delta y}(H - h) = \left[C_{f_i} \bar{u}_i \bar{u}_i - C_p (H - h)\right] \Delta y \tag{B-27}$$

Arranging eq (B.27)

$$\bar{v}_{e_{i+1}} \frac{\bar{u}_{i+1} - \bar{u}_i}{\Delta y} - \bar{v}_{e_i} \frac{\bar{u}_i - \bar{u}_{i-1}}{\Delta y} = \left[\frac{C_{f_i} \bar{u}_i \bar{u}_i}{(H - h)} - C_p\right] \Delta y \tag{B-28}$$

Rearranging;

$$\left(\frac{\bar{v}_{e_{i+1}}}{\Delta y}\right) \bar{u}_{i+1} + \left(-\frac{\bar{v}_{e_{i+1}}}{\Delta y} - \frac{\bar{v}_{e_i}}{\Delta y} - \frac{C_{f_i} \bar{u}_i}{(H - h)} \Delta y\right) \bar{u}_i + \left(\frac{\bar{v}_{e_i}}{\Delta y}\right) \bar{u}_{i-1} = -C_p \Delta y \tag{B-29}$$

- ***Main Channel***

$$0 = C_p H + H \frac{\partial \bar{\tau}_{xy}}{\partial y} - \tau_{xz,b} \tag{B-30}$$

$$H \frac{\partial}{\partial y}\left(\bar{v}_e \frac{\partial u}{\partial y}\right) = -C_p H + \tau_{xz,b} \tag{B-31}$$

$$\frac{\partial}{\partial y}\left(\bar{v}_e \frac{\partial \bar{u}}{\partial y}\right) = -C_p + \frac{C_f \bar{u}^2}{H} \tag{B-32}$$

$$\frac{\partial \bar{\tau}}{\partial y} - \frac{C_f \bar{u}^2}{H} = -C_p \tag{B-33}$$

$$\frac{\bar{\tau}_{i+1} - \bar{\tau}_i}{\Delta y} = -C_p + \frac{C_{f_i} \bar{u}_i \bar{u}_i}{H} \tag{B-34}$$

$$\bar{v}_{e_{i+1}} \frac{\bar{u}_{i+1} - \bar{u}_i}{\Delta y} - \bar{v}_{e_i} \frac{\bar{u}_i - \bar{u}_{i-1}}{\Delta y} = \left[ -C_p + \frac{C_{f_i} \bar{u}_i \bar{u}_i}{H} \right] \Delta y \tag{B-35}$$

$$A_i = \frac{\bar{v}_{e_{i+1}}}{\Delta y} \tag{B-36}$$

$$C_i = \frac{\bar{v}_{e_i}}{\Delta y} \tag{B-37}$$

$$B_i = \frac{\bar{v}_{e_{i+1}}}{\Delta y} + \frac{\bar{v}_{e_i}}{\Delta y} + \frac{C_{f_i} \bar{u}_i}{H} \Delta y \tag{B-38}$$

$$D_i = C_p \Delta y \tag{B-39}$$

- ***<u>Step</u>***

Around step, computational domain is given blow.

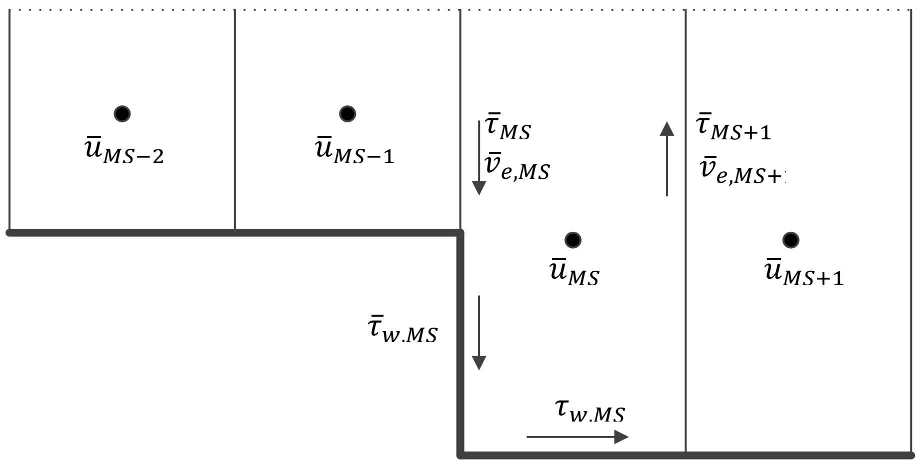


***Figure B-1*** Computational domain on step

Computational cell over step's number is named as *ms*. There are two wall shear stress acting on the cell which are horizontal and vertical as shown in figure. These stresses are included in calculations. Equation 2-15 is written form step node.

$$C_p(H) + \frac{\bar{\tau}_{xy}}{\partial y} - \tau_{xz,b} = 0 \tag{B-40}$$

$$\frac{\partial}{\partial y}\left(\bar{v}_e \frac{\partial \bar{u}}{\partial y}\right) = -C_p(H) + \tau_{xz,b} \tag{B-41}$$

$$\frac{\partial \bar{\tau}}{\partial y} - C_f \bar{u}^2 = -C_p(H) \tag{B-42}$$

$$\frac{\bar{\tau}_{MS+1} - \bar{\tau}_{MS}}{\Delta y} = -C_p(H) + C_{f,MS}\bar{u}_{MS}\bar{u}_{MS} \tag{B-43}$$

$$\bar{\tau}_{MS} = (H-h)\bar{v}_{e_{MS}} \frac{\bar{u}_{MS} - \bar{u}_{MS-1}}{\Delta y} + (h)\bar{\tau}_{w,v} \tag{B-44}$$

$$\bar{\tau}_{MS+1} = (H)\bar{v}_{e_{MS+1}} \frac{\bar{u}_{MS+1} - \bar{u}_{MS}}{\Delta y} \tag{B-45}$$

$$\begin{aligned}(H)\bar{v}_{e_{MS+1}} \frac{\bar{u}_{MS+1} - \bar{u}_{MS}}{\Delta y} - \left[(H-h)\bar{v}_{e_{MS}} \frac{\bar{u}_{MS} - \bar{u}_{MS-1}}{\Delta y} + (h)\bar{\tau}_{w,v}\right] \\ = \Delta y\left[-C_p(H) + C_{f,MS}\bar{u}_{MS}\bar{u}_{MS}\right]\end{aligned} \tag{B-46}$$

$$\begin{aligned}&\left(H\frac{\bar{v}_{e_{MS+1}}}{\Delta y}\right)\bar{u}_{MS+1} \\ &\quad + \left(-H\frac{\bar{v}_{e_{MS+1}}}{\Delta y} - (H-h)\frac{\bar{v}_{e_{MS}}}{\Delta y} - C_{f_{MS}}\bar{u}_{MS}\Delta y \right. \\ &\quad \left. - \frac{(h)\bar{\tau}_{w,v}}{u_{MS}}\right)\bar{u}_{MS} + (H-h)\left(\frac{\bar{v}_{e_{MS}}}{\Delta y}\right)\bar{u}_{MS-1} = -(H)C_p\Delta y\end{aligned} \tag{B-47}$$

$$A_{MS} = H\left(\frac{\bar{v}_{e_{MS+1}}}{\Delta y}\right) \tag{B-48}$$

$$C_{MS} = (H-h)\left(\frac{\bar{v}_{e_{MS}}}{\Delta y}\right) \quad \text{(B-49)}$$

$$B_{MS} = H\left(\frac{\bar{v}_{e_{MS+1}}}{\Delta y}\right) + (H-h)\left(\frac{\bar{v}_{e_{MS}}}{\Delta y}\right) + (h)\frac{\bar{\tau}_{w,v}}{u_{MS}} + C_{f_{MS}}\bar{u}_{MS}\Delta y \quad \text{(B-50)}$$

$$D_{MS} = (H)C_p\Delta y \quad \text{(B-51)}$$

<u>Boundary Conditions</u>

- <u>At i = 1</u>

$$\frac{\bar{v}_{e_2}}{\Delta y}(\bar{u}_2 - \bar{u}_1) - \bar{v}_{e_1}\frac{d\bar{u}}{dy} = \left[-C_p + \frac{C_{f_1}\bar{u}_1\bar{u}_1}{(H-h)}\right] \quad \text{(B-52)}$$

$$\bar{v}_{e_1}\frac{d\bar{u}}{dy} = \bar{\tau}_w \quad \text{(B-53)}$$

$$\bar{v}_{e_2}(\bar{u}_2 - \bar{u}_1) - \bar{\tau}_w = \left[-C_p + \frac{C_{f_1}\bar{u}_1\bar{u}_1}{(H-h)}\right]\Delta y \quad \text{(B-54)}$$

Collecting similar terms yields;

$$A_1 = \frac{\bar{v}_{e_2}}{\Delta y} \quad \text{(B-55)}$$

$$C_1 = 0 \quad \text{(B-56)}$$

$$B_1 = \frac{\bar{v}_{e_2}}{\Delta y} + \frac{\bar{\tau}_w}{u_1} + \frac{C_{f_1}\bar{u}_1}{(H-h)}\Delta y \quad \text{(B-57)}$$

$$D_1 = C_p\Delta y \quad \text{(B-58)}$$

- <u>At i = N</u>

$$\bar{u}_N = \bar{u}_{N+1} \tag{B-59}$$

$$\bar{v}_{e_{N+1}}(\bar{u}_{N+1} - \bar{u}_N) - \bar{v}_{e_N}(\bar{u}_N - \bar{u}_{N-1}) = \left[-C_p + \frac{C_{f_N}\bar{u}_N\bar{u}_N}{(H-h)}\right]\Delta y \tag{B-60}$$

$$-\bar{v}_{e_N}(\bar{u}_N - \bar{u}_{N-1}) = \left[-C_p + \frac{C_{f_N}\bar{u}_N\bar{u}_N}{(H-h)}\right]\Delta y \tag{B-61}$$

Collecting similar terms;

$$A_N = 0 \tag{B-62}$$

$$C_N = \frac{\bar{v}_{e_N}}{\Delta y} \tag{B-63}$$

$$B_N = \frac{\bar{v}_{e_N}}{\Delta y} + \frac{C_{f_N}\bar{u}_N}{(H)}\Delta y \tag{B-64}$$

$$D_N = C_p \Delta y \tag{B-65}$$

## B.3 Numerical Solution of Eq.(2-10) in periodic compound duct flow

Discretization of Eq.(2-10) for side channel, main channel and discontinuity (step) will be same as in appendix (1-3). However, periodic boundaries need special treatment.

In two periodic boundaries, conditions must be exactly the same.

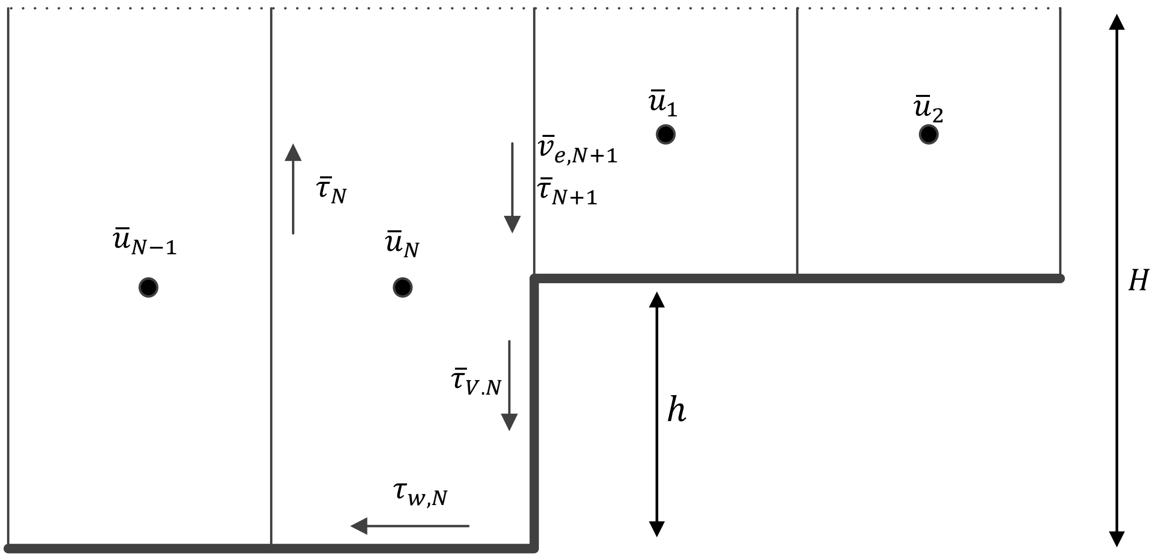


***Figure B-2*** Computational domain in the periodic boundary

- <u>At i = 1</u>

$$0 = C_p(H-h) + \frac{\partial \overline{\tau_{xy}}}{\partial y} - \tau_{xz,b} \tag{B-66}$$

$$\frac{\partial}{\partial y}\left(\bar{v}_e \frac{\partial \bar{u}}{\partial y}\right) = -C_p(H-h) + \tau_{xz,b} \tag{B-67}$$

$$\frac{\partial \bar{\tau}}{\partial y} = -C_p(H-h) + \tau_{xz,b} \tag{B-68}$$

$$\frac{\bar{\tau}_2 - \bar{\tau}_1}{\Delta y} = -C_p(H-h) + \tau_{xz,b} \tag{B-69}$$

$$\bar{\tau}_2 = \bar{v}_{e_2} \frac{\bar{u}_2 - \bar{u}_1}{\Delta y}(H-h) \tag{B-70}$$

$$\bar{\tau}_1 = \bar{v}_{e_1}\frac{\bar{u}_1 - \bar{u}_0}{\Delta y}(H-h) + \bar{\tau}_{V,N}(h) \quad \text{(B-71)}$$

$$\begin{aligned}\bar{v}_{e_2}\frac{\bar{u}_2 - \bar{u}_1}{\Delta y}(H-h) - \bar{v}_{e_1}\frac{\bar{u}_1 - \bar{u}_0}{\Delta y}(H-h) - \bar{\tau}_{V,N}(h) \\ = \left[-C_p(H-h) + C_{f_1}\bar{u}_1\bar{u}_1\right]\Delta y\end{aligned} \quad \text{(B-72)}$$

$$\begin{aligned}&\left((H-h)\frac{\bar{v}_{e_2}}{\Delta y}\right)\bar{u}_2 \\ &\quad + \left(-\frac{\bar{v}_{e_2}}{\Delta y}(H-h) - \frac{\bar{v}_{e_1}}{\Delta y}(H-h) - C_{f_1}\bar{u}_1\Delta y \right. \\ &\quad \left. - \frac{\bar{\tau}_{V,N}(h)}{u_1}\right)\bar{u}_1 + \left((H-h)\frac{\bar{v}_{e_1}}{\Delta y}\right)\bar{u}_0 = -C_p(H-h)\Delta y\end{aligned} \quad \text{(B-73)}$$

Since .

$$\bar{u}_0 = \bar{u}_N$$

$$A_1 = \left((H-h)\frac{\bar{v}_{e_2}}{\Delta y}\right) \quad \text{(B-74)}$$

$$C_1 = (H-h)\frac{\bar{v}_{e_1}}{\Delta y} \quad \text{(B-75)}$$

$$B_1 = \frac{\bar{v}_{e_2}}{\Delta y}(H-h) + \frac{\bar{v}_{e_1}}{\Delta y}(H-h) + C_{f_1}\bar{u}_1\Delta y + \frac{\bar{\tau}_{V,N}(h)}{u_1} \quad \text{(B-76)}$$

$$D_1 = C_p\Delta y(H-h) \quad \text{(B-77)}$$

<u>At i = N</u>

$$C_p(H) + \frac{\partial\overline{\tau_{xy}}}{\partial y} - \tau_{xz,b} \quad \text{(B-78)}$$

$$\frac{\partial}{\partial y}\left(\bar{v}_e\frac{\partial\bar{u}}{\partial y}\right) = -C_p(H) + \tau_{xz,b} \quad \text{(B-79)}$$

$$\frac{\partial \bar{\tau}}{\partial y} - C_f \bar{u}^2 = -C_p(H) \tag{B-80}$$

$$\frac{\bar{\tau}_{N+1} - \bar{\tau}_N}{\Delta y} = -C_p(H) + C_{f,N}\bar{u}_N\bar{u}_N \tag{B-81}$$

$$\bar{\tau}_{N+1} = (H-h)\bar{v}_{e_{N+1}}\frac{\bar{u}_{N+1} - \bar{u}_N}{\Delta y} + (h)\bar{\tau}_{V,N} \tag{B-82}$$

$$\bar{\tau}_N = (h)\bar{v}_{e_N}\frac{\bar{u}_N - \bar{u}_{N-1}}{\Delta y} \tag{B-83}$$

$$\begin{aligned}(H-h)\bar{v}_{e_{N+1}}\frac{\bar{u}_{N+1} - \bar{u}_N}{\Delta y} + (h)\bar{\tau}_{V,N} - \left[(H)\bar{v}_{e_N}\frac{\bar{u}_N - \bar{u}_{N-1}}{\Delta y}\right] \\ = \Delta y\left[-C_p(H) + C_{f,N}\bar{u}_N\bar{u}_N\right]\end{aligned} \tag{B-84}$$

$$\begin{aligned}&\left((H-h)\frac{\bar{v}_{e_{N+1}}}{\Delta y}\right)\bar{u}_{N+1} \\ &\quad + \left(-H\frac{\bar{v}_{e_N}}{\Delta y} - (H-h)\frac{\bar{v}_{e_{N+1}}}{\Delta y} - C_{f_N}\bar{u}_N\Delta y + \frac{(h)\bar{\tau}_{V,N}}{u_N}\right)\bar{u}_N \\ &\quad + (H)\left(\frac{\bar{v}_{e_N}}{\Delta y}\right)\bar{u}_{N-1} = -(H)C_p\Delta y\end{aligned} \tag{B-85}$$

Since $\bar{u}_{N+1} = \bar{u}_1$ and $\bar{v}_{e_{N+1}} = \bar{v}_{e_1}$

Collecting similar terms;

$$A_N = (H-h)\left(\frac{\bar{v}_{e_1}}{\Delta y}\right) \tag{B-86}$$

$$C_N = (H)\left(\frac{\bar{v}_{e_N}}{\Delta y}\right) \tag{B-87}$$

$$B_N = \left(H\frac{\bar{v}_{e_N}}{\Delta y} + (H-h)\frac{\bar{v}_{e_1}}{\Delta y} + C_{f_N}\bar{u}_N\Delta y - \frac{(h)\bar{\tau}_{V,N}}{u_N}\right) \tag{B-88}$$

$$D_N = (H)C_p\Delta y \tag{B-89}$$